NASA/TM—2007–215073

A One-Piece Lunar Regolith Bag Garage Prototype

G.A. Smithers, M.K. Nehls, M.A. Hovater, S.W. Evans
Marshall Space Flight Center, Marshall Space Flight Center, AL

J.S. Miller
Qualis Corporation, Huntsville, AL

R.M. Broughton, Jr., D. Beale, F. Kilinc-Balci
Auburn University, Auburn, AL

September 2007

The NASA STI Program…in Profile

Since its founding, NASA has been dedicated to the advancement of aeronautics and space science. The NASA Scientific and Technical Information (STI) Program Office plays a key part in helping NASA maintain this important role.

The NASA STI program operates under the auspices of the Agency Chief Information Officer. It collects, organizes, provides for archiving, and disseminates NASA's STI. The NASA STI program provides access to the NASA Aeronautics and Space Database and its public interface, the NASA Technical Report Server, thus providing one of the largest collections of aeronautical and space science STI in the world. Results are published in both non-NASA channels and by NASA in the NASA STI Report Series, which includes the following report types:

- TECHNICAL PUBLICATION. Reports of completed research or a major significant phase of research that present the results of NASA programs and include extensive data or theoretical analysis. Includes compilations of significant scientific and technical data and information deemed to be of continuing reference value. NASA's counterpart of peer-reviewed formal professional papers but has less stringent limitations on manuscript length and extent of graphic presentations.

- TECHNICAL MEMORANDUM. Scientific and technical findings that are preliminary or of specialized interest, e.g., quick release reports, working papers, and bibliographies that contain minimal annotation. Does not contain extensive analysis.

- CONTRACTOR REPORT. Scientific and technical findings by NASA-sponsored contractors and grantees.

- CONFERENCE PUBLICATION. Collected papers from scientific and technical conferences, symposia, seminars, or other meetings sponsored or cosponsored by NASA.

- SPECIAL PUBLICATION. Scientific, technical, or historical information from NASA programs, projects, and missions, often concerned with subjects having substantial public interest.

- TECHNICAL TRANSLATION. English-language translations of foreign scientific and technical material pertinent to NASA's mission.

Specialized services also include creating custom thesauri, building customized databases, and organizing and publishing research results.

For more information about the NASA STI program, see the following:

- Access the NASA STI program home page at <http://www.sti.nasa.gov>

- E-mail your question via the Internet to <help@sti.nasa.gov>

- Fax your question to the NASA STI Help Desk at 301–621–0134

- Phone the NASA STI Help Desk at 301–621–0390

- Write to:
  NASA STI Help Desk
  NASA Center for AeroSpace Information
  7115 Standard Drive
  Hanover, MD 21076–1320

NASA/TM—2007–215073

A One-Piece Lunar Regolith Bag Garage Prototype

G.A. Smithers, M.K. Nehls, M.A. Hovater, S.W. Evans
Marshall Space Flight Center, Marshall Space Flight Center, AL

J.S. Miller
Qualis Corporation, Huntsville, AL

R.M. Broughton, Jr., D. Beale, F. Kilinc-Balci
Auburn University, Auburn, AL

National Aeronautics and
Space Administration

Marshall Space Flight Center • MSFC, Alabama 35812

September 2007

Acknowledgments

In addition to the authors, a number of other people contributed to this work. They include David Hoppe, Don McQueen, Robert Hoffman, Kevin Burk, Joe Minow, Charley Meyers, Mark Kearney, David Smitherman, and Mark D'Agostino, NASA Marshall Space Flight Center. Also contributing to this work were Steve Kennamer, Shirley Abercrombie, and Bill Major, Teledyne Brown Engineering, William Seymour, BD Systems, Chuck Semmel, Qualis Corporation, and Max Cichon, David Branscomb, Melody George, Hassan Kocer, Mandeep Singh, Manoj Rajagopalan, and Jeff Thompson, Auburn University.

The "lunar garage team" extends sincere appreciation to those who made this work possible: the project managers and systems engineers (past and present) and the Contracting Officer and Contracting Officer's Technical Representative who manage the Cooperative Agreement with Auburn University. They are: Julie Bassler, Melanie Bodiford, Carole McLemore, Nathan Brown, Janet Strong, Mike Fiske, Kevin McCarley, Glen Alexander, and Jenenne Suttle.

The MSFC team, which included members from the Engineering Directorate's Instrument and Payload Systems Department, Spacecraft and Vehicle Systems Department, and Materials and Processes Space Environmental Effects Team, and Non-metals Process Engineering Team, partnered with Auburn University's Department of Polymer and Fiber Engineering and Department of Mechanical Engineering to conduct this work.

The authors gratefully acknowledge the suppliers who have bid on projects, worked with us and/or supplied fabric samples: ILC Dover, Lincoln Textiles, Hexcel, W. L. Gore, Fabric Development Ltd., 3M, Kappler, Inc., Techsphere, American and Efird, and W. R. Grace.

TRADEMARKS

Available from:

NASA Center for AeroSpace Information
7115 Standard Drive
Hanover, MD 21076–1320
301–621–0390

This report is also available in electronic form at
<https://www2.sti.nasa.gov>

TABLE OF CONTENTS

LIST OF FIGURES

LIST OF FIGURES (Continued)

LIST OF FIGURES (Continued)

LIST OF FIGURES (Continued)

LIST OF FIGURES (Continued)

LIST OF FIGURES (Continued)

LIST OF TABLES

LIST OF ACRONYMS AND SYMBOLS

ASTM	American Society for Testing and Materials
CAD	computer-aided design
CO_2	carbon dioxide
^{60}CO	cobalt-60
CRE	constant rate of extension
CSI	Custom Scientific Instruments
CV	coefficient of variation
EPR	ethylene propylene rubber
F	filling
fpi	filling per inch
GN_2	gaseous Nitrogen
GCR	galactic cosmic ray
ISFR	In Situ Fabrication and Repair
ITS	Integrated Tiger Series
JSC	Johnson Space Center
LCP	liquid crystal polymer
LN_2	liquid Nitrogen
MCP	MSFC Call for Proposals
MIT	Massachusetts Institute of Technology
MLGG	micro light gas gun

LIST OF ACRONYMS AND SYMBOLS (Continued)

MSFC	Marshall Space Flight Center
NEC	National Electronics Corporation
PBO	poly (p-phenylene-2, 6-benzobisoxazole)
PPTA	poly (p-phenylene terepthalamide)
PTFE	polytetrafluoroethylene
SEEF	Space Environmental Effects Facility
SPE	solar particle event
SPHC	smooth particle hydrodynamic code
SRIM	stopping range of ion matters
TEFC	totally enclosed fan cooled
TPI	threads per inch
UHMW	ultrahigh molecular weight
UV	ultraviolet
VUV	vacuum ultraviolet
W	warp
wpi	warp per inch

TECHNICAL MEMORANDUM

A ONE-PIECE LUNAR REGOLITH BAG GARAGE PROTOTYPE

1. BACKGROUND

The task entitled "A One-Piece Lunar Regolith Bag Garage Prototype" resulted from a proposal responding to SY10 (16-05) Marshall Space Flight Center (MSFC) call for proposals (MCP) issued by the Technology and Capability Development Projects Office. The original proposal (entitled, "A One-Piece Lunar Regolith Bag Habitat Prototype") presented a plan for construction of a lunar habitat using connected lunar regolith bags (a regolith bag being the lunar counterpart to a sandbag on Earth). The Project Office (In Situ Fabrication and Repair (ISFR) Habitat Structures Technology) had already considered construction of a habitat with individual regolith bags or with a long, continuous tube bag. However, these earlier concepts could be structurally unstable, in the case of individual bags, and the continuous tube bag required unacceptable barbed wire between layers and could result in handling issues during assembly on the Moon. Therefore, a one-piece concept was proposed that consisted of lightweight, connected fabric bags or pockets (referred to as the "fabric form") to be launched from Earth and landed on the Moon where they would be filled with raw lunar regolith, and resemble a type of "log house." It was anticipated that such a structure would have considerably greater stability than stacked individual bags.

The originally planned habitat was to become a pressurized structure. However, when the contract was awarded, the Project Office was in a dynamic state, and the task was reduced in funding and in period of performance. This changed the task scope and it became the "Lunar Regolith Bag Prototype Structure," and subsequently the "Lunar Garage Prototype," an unpressurized structure. Structural tests of the prototype would be dropped (the structure would be a demonstration article), and a materials testing program would be added. The technology development plan created by the Project Office dictated that early-on missions were to be conducted by robots, and this became an important consideration.

While sandbagging has been a technique on Earth for centuries, the concept of lunar regolith bags has also received attention in recent years. After all, if NASA is to colonize the Moon and explore the Universe, using the native materials of planets of residence will become necessary. Among previous work in this area are: a 1990 report entitled "Lunar Regolith Bagging System" (a study by Georgia Institute of Technology in cooperation with NASA and Universities Space Research Association);[1] an August 2005 report entitled "Regolithbag Report" by Regina Pope (MSFC, Qualis Corporation);[2] an October 2005 report, "Regolith Bag Structures Analysis" by Mark Kearney and Charles Meyers (NASA MSFC Dynamics, Loads, and Strength Branch;[3] a November 2005 report, "Preliminary Regolith Bag Lunar Habitat Thermal Study and Deliverable" by Greg Schunk (NASA MSFC Spacecraft Thermal Team).[4]

Prior to this task, Dr. Raj Kaul and Gweneth Smithers (NASA MSFC Nonmetals Engineering Branch) had conducted a literature review/trade study on material candidates for lunar regolith bag structures ("Bagging Material Trade Study for Lunar Sandbag Habitat," June 2005).[5] This literature review concluded that a lunar regolith bag structure would likely be constructed not from one type of fabric, but from a combination of fabrics, or a blended fiber, and would likely employ coated material(s).

At task initiation, it was stated that the proposing team understood that the Project Office expected the following: ultraviolet radiation, ionizing radiation, and hypervelocity impact testing of Vectran™ (a Celanese Acetate product), Nextel™ (a 3M Company product), and Gore-Tex™ (a W. L. Gore and Associates product) fabrics; design, construction, and delivery of a regolith bag prototype structure; and a final report. However, the task team felt that, even though the task had been reduced from the original scope and funding, it was important to include more than what was required: the materials testing program should be expanded to include not only radiation and impact testing but also density and geometry, tensile strength, flex/fold endurance, abrasion resistance, and, wherever possible, ambient, cold, and hot environments. The list of material candidates to be evaluated was also extended to include Zylon™ (a Toyobo Company product), Kevlar™, and Nomex™ (both DuPont Company products).

The goals of the task were:

(1) To learn, through materials testing, which materials are suitable for use in construction of a one-piece regolith bag form to be launched from Earth, landed on the Moon, filled with raw lunar regolith, and used as a functional structure (materials chosen from a previous literature review to be tested in conjunction with official lunar regolith simulant).

(2) To successfully design, develop, and construct a large one-piece regolith bag form and fill it with sand (and perhaps, fill some sections with official lunar regolith simulant).

(3) To assess this first one-piece regolith bag prototype structure for structural integrity and manufacturability.

The Project Office provided "Environmental Design Requirements and Assumptions" (see appendix). Attempts to simulate these conditions fell far short of lunar condition assumptions. While the requirements and assumptions specified only cold temperatures, warmer than ambient conditions were included because of the uncertainty of future mission sites/conditions.

Before the Apollo missions there were attempts to better understand the Moon. But after the Apollo missions, considerable factual information became available about lunar environmental conditions and the chemical and physical characterization of the lunar regolith. Minow and Altstatt in "Lunar Radiation Environments for Characterization of ISFR/Habitat Structures Materials"[6] state: "Habitat Structures goals are to provide an environment safe from hazards of the lunar environment including the lack of atmosphere, extremes of temperature, space radiation effects, and micro-meteorite impacts while supporting physiological needs of the inhabitants. Selection criteria for candidate habitat materials include the ability of material properties to meet design requirements after long term exposure to space radiation environments and shielding properties of the materials to protect the inhabitants from galactic

cosmic rays and solar energetic particles." Although the task's original pressurized habitat plan became an unpressurized garage plan, most of these concerns still applied, especially since it is possible that the garage might eventually evolve into a habitat. The "Lunar Sourcebook" edited by Heiken, Vaniman, and French)[7] and the Minow and Altstatt document[6] (for radiation testing) were major sources that guided consideration of material candidates for the literature review, the materials testing program, and the prototype design.

Fabrics constructed with intermittent "pockets" in them, much like the ones in figure 1, have been used as forms for concrete erosion control structures on stream banks, and this concept served as inspiration for the connected regolith bag proposal; it was hoped that the same concept could also provide stability within the context of a lunar structure.

Figure 1. A concrete-filled, woven double cloth used for erosion control on stream banks.

2. MATERIALS TESTING PROGRAM

The following six candidate fabric materials were selected for testing:

- Vectran – a polyester-based liquid crystal polymer, (LCP) fiber
- Nextel – a refractory aluminoborosilicate (ceramic) fiber
- Gore PTFE Fabric – an expanded polytetrafluoroethylene (PTFE) fiber
- Nomex – a meta-aramid or poly(metaphenyleneisophthalamide) fiber
- Twaron™ (a Teijin Group product) – a polyparaphenylene terepthalamide (PPTA) fiber (this was used instead of Kevlar, which has a similar chemistry and properties)
- Zylon – a fiber consisting of rigid rod chain molecules of poly (p-phenylene-2, 6-benzobisoxazole) (PBO).

2.1 Determination of Fabric Structural Properties

Woven fabrics were selected from manufacturers based on similarity of construction parameters from among those materials that were readily available (without custom manufacturing, which would have been prohibitively expensive in terms of both money and time). Similarity in construction parameters was necessary to enable a valid "apples and apples" comparison of different materials subjected to the same testing. The main structural properties of candidate fabrics are listed in table 1 and illustrated in figures 2 through 4. The construction was determined by examination of a magnified image of the fabrics. Fabric areal weight was determined by cutting a piece of fabric, measuring its dimensions and weighing it. Nomex fabric has the finest yarns in the group, while Nextel fabric has the coarsest yarns. Zylon fabric has the lowest number of warp and filling yarns per inch, while Gore-PTFE has the tightest structure. As expected, these measurements agreed with those provided by the manufacturers. Material densities of the fibers were obtained from the manufacturers[8–13] and are shown in table 1. One sample per fabric was examined and determination of all fabric structural properties was performed at Auburn University Department of Polymer and Fiber Engineering.

2.2 Tensile Testing

2.2.1 Yarn Tensile Testing

All tensile tests were performed at Auburn University Department of Polymer and Fiber Engineering. Tensile properties of the yarns were obtained according to American Standard for Testing and Materials (ASTM) D-2256, "Standard Test Method for Tensile Properties of Yarns by Single-Strand

Table 1. Structural properties of fabric samples.

Fabric	Source	Type/ Style	Weave (Pattern)	Yarn Count Warp/Filling (denier)	TPI (W/F)*	Density (g/cm^3)	Areal Density (oz/sq yd)	Thickness (mm)
Nextel	3 M	312-AF10	1/4 Satin	600/600	46/46	2.7	7.1	0.33
Nomex	Fabric Development Inc.	503	Plain	200/200	54/54	1.38	2.9	0.19
Gore PTFE Fabric	W.L. Gore	VG0181	1/3 Satin	400/400	88/84	2.17	10.0	0.30
Twaron	Lincoln Textiles	2040-3531	Plain	500/500	48/46	1.45	6.5	0.36
Vectran	ILC Dover	HS	Plain	400/400	54/54	1.4	6.0	0.31
Zylon	Hexcel	530	Plain	500/500	30/30	1.55	4.0	0.25

*Threads per inch (TPI)
Warp/filling (W/F)

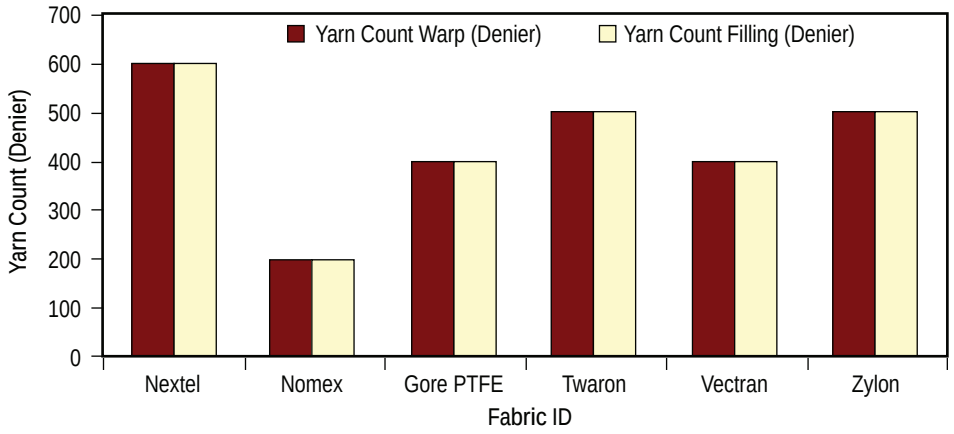

Figure 2. Yarn counts of the samples.

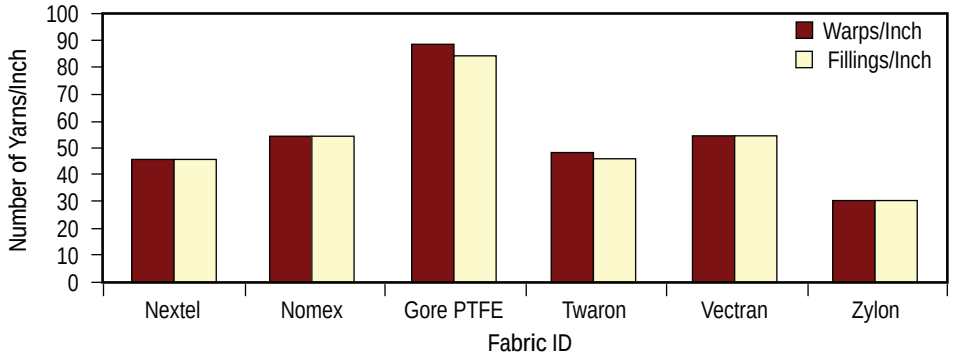

Figure 3. Number of warps and fillings of the samples.

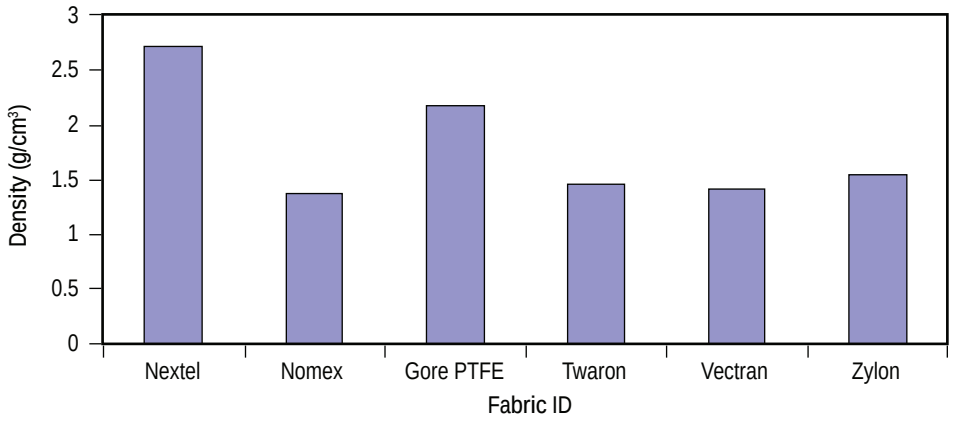

Figure 4. Density of the fibers used in the fabric samples.

Method"[14] at laboratory conditions (70 ºF and 65 percent humidity). In this test, the yarn sample is clamped in a tensile testing machine (Instron Model 1122) and a force is applied to the sample until it breaks. Values for the breaking force and elongation of the samples are obtained from a computer interfaced with the testing machine. Yarn samples (10 in each direction) were removed from the candidate fabrics to test for tensile strength and elongation values. Calculated values were found by dividing the fabric tensile strength (also obtained by testing) by the number of yarns in the tested area (see table 2). Conversion efficiency (in percent) is found by dividing the calculated yarn tensile strength by the meas-ured yarn tensile strength and shows the comparison of pulled-out yarn strength to yarn strength obtained from testing the fabric. Ten yarn samples of each fabric type were tested for yarn strength. The yarn strength values are not normalized for yarn size and are reported in kN/yarn in table 2 and figures 5 and 6.

Table 2. Tensile properties of yarns.

Fabric TM	Measured Yarn Tensile Strength (kN) (W)	Calculated Yarn Strength (kN) (Measured Fabric Strength/wpi)* (W)	Conversion **Efficiency (%)** Calculated/ Measured (W)	Measured Yarn Tensile Strength (kN) (F)	Calculated Yarn Strength (kN) (Measured Fabric Strength/fpi)** (F)	Conversion **Efficiency (%)** Calculated/ Measured (F)
Nextel	0.0081	0.017	208	0.0109	0.017	152
Nomex	0.0094	0.0084	89	0.0083	0.0082	98
Gore PTFE	0.0165	0.015	92	0.015	0.016	109
Twaron	0.072	0.044	61	0.097	0.100	104
Vectran	0.084	0.042	50	0.112	0.080	72
Zylon	0.133	0.089	66	0.148	0.126	85

*warp per inch (wpi)
**filling per inch (fpi)

Figures 5 and 6 illustrate the tensile strength values obtained by the single strand method as compared to the calculated values for both warp and filling yarns. Zylon yarns exhibit the highest strength, while Nextel and Nomex yarns exhibit the lowest strength values in both directions. The highest conversion efficiency is obtained in Nextel yarns while the lowest efficiency is obtained in Vectran yarns.

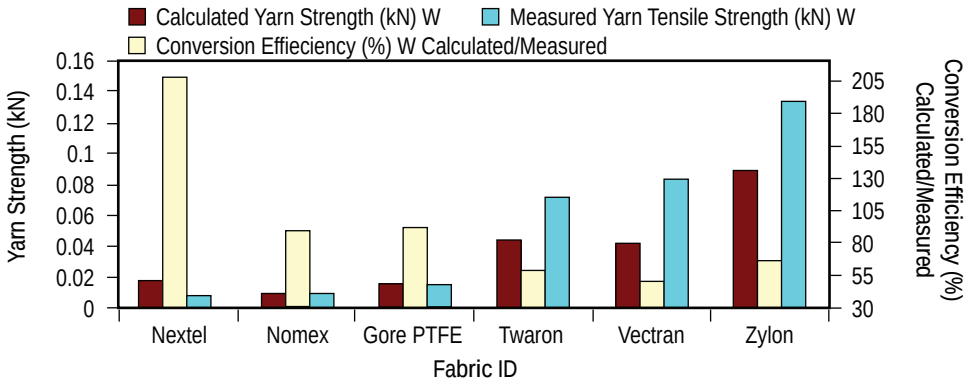

Figure 5. Tensile strength of warp yarns (kN) as compared to calculated values.

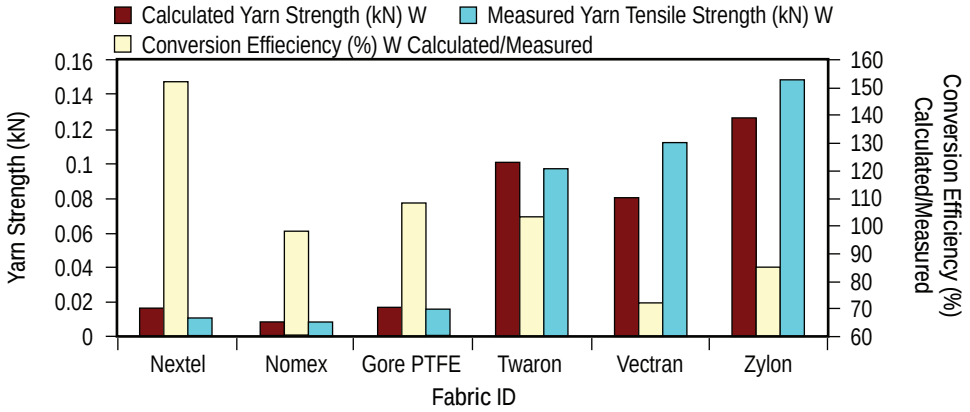

Figure 6. Tensile strength of filling yarns (kN) as compared to calculated values.

It should be added here that, since Nextel yarns are very brittle and the yarn structure is very loose, when the yarns were being mounted for the tensile test, some of the fibers were already lost from the yarn structure. In addition to that, during the yarn tensile test of Nextel and Zylon yarns, many yarn breakages were observed in the testing machine jaw clamps—probably due to damage in the clamps.

Measured values (from these tests) and values reported by manufacturers[8–13] for tensile strength (MPa) and elongation (percent) of the warp and filling yarns are listed in the tables 3 and 4 and are illustrated in figures 7 through 10.

Tensile strength values given in MPa in table 3 are calculated by dividing the tensile values obtained by single strand method in kN/inch by the area.

$$\sigma(MPa) = \frac{F(kN/inch)\times 10^{3}}{No\ of\ yarns/inch \times \dfrac{Yarn\ Denier}{9{,}000 \times Density}} \times 10^{-6}$$

Table 3. Yarn tensile strength values (MPa) as compared to reported values.

Fabric TM	Measured Yarn Tensile Strength (MPa) (W)	Reported Yarn Tensile Strength (MPa) (W)	Measured/ Reported Yarn Strength **(%) (W)**	Measured Yarn Tensile Strength (MPa) (F)	Reported Yarn Tensile Strength (MPa) (F)	Measured/ Reported Yarn Tensile Strength **(%) (F)**
Nextel	324	450	72	446	550	81
Nomex	559	550	102	497	550	90
Gore PTFE	830	810	102	732	810	90
Twaron	1,879	3,000	63	2,532	3,000	84
Vectran	2,646	2,800	95	3,528	2,800	126
Zylon	2,483	5,800	43	4,129	5,800	71

Table 4. Elongation of warp and filling yarns (kN) as compared to reported values.

Fabric	Measured Yarn Elongation **(%) (W)**	Reported Yarn Elongation **(%) (W)**	Measured Yarn Elongation **(%) (F)**	Reported Yarn Elongation **(%) (F)**	Measured/ Reported Yarn Elongation **(%) (W)**	Measured/ Reported Yarn Elongation **(%) (F)**
Nextel	1.1	1.2	1.3	1.2	91.8	109.6
Nomex	29.8	22	29.1	22	135.4	132.2
Gore PTFE	8.6	15	6.9	15	57.2	45.8
Twaron	8.2	2	3.8	2	408.4	188.9
Vectran	7.6	3.3	5.3	3.3	228.97	159.8
Zylon	4.8	2	4.1	2	237.7	204.1

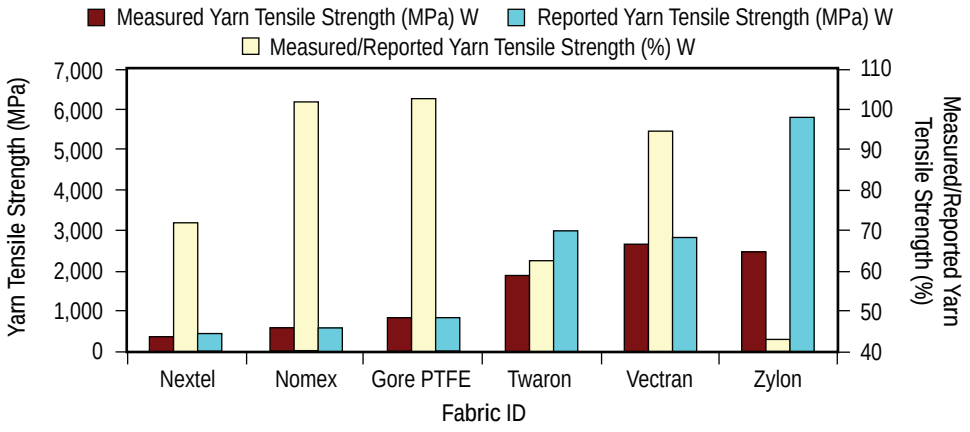

Figure 7. Tensile strength of warp yarns (MPa) as compared to reported values.

Figures 9 and 10 show that Nomex yarns have the highest elongation values while Nextel has the lowest. Except for Nextel and Gore PTFE fabrics, higher elongation values were obtained in tensile tests compared to the reported values in both directions.

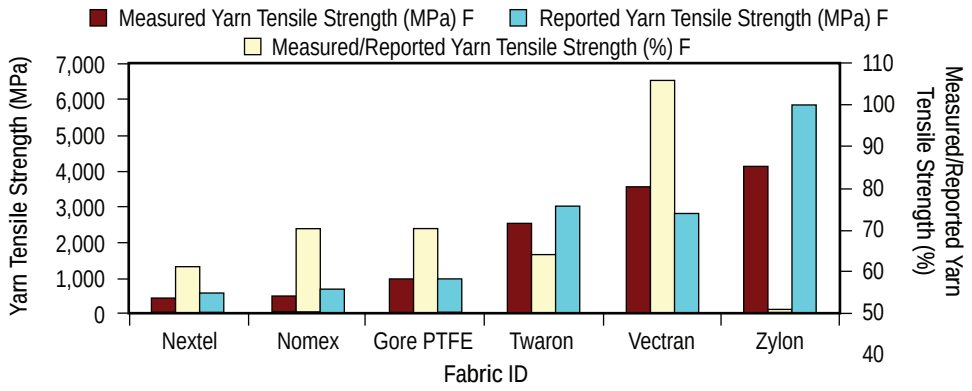

Figure 8. Tensile strength of filling yarns (MPa) as compared to reported values.

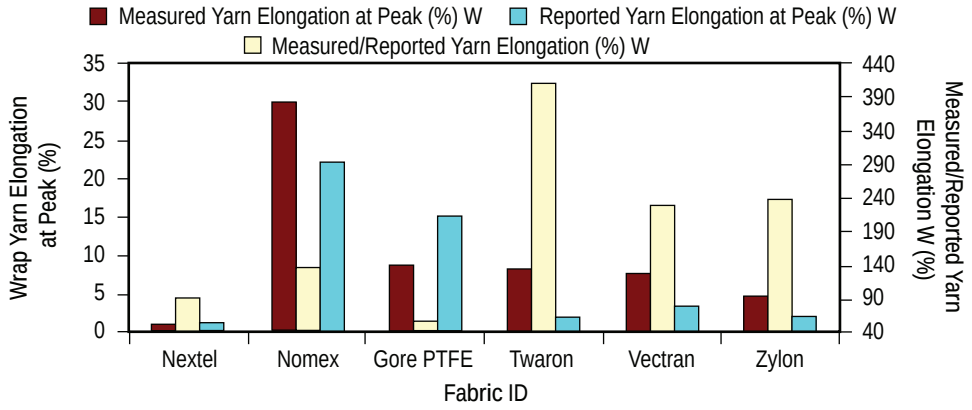

Figure 9. Tensile elongation of warp yarns (percent) as compared to reported values.

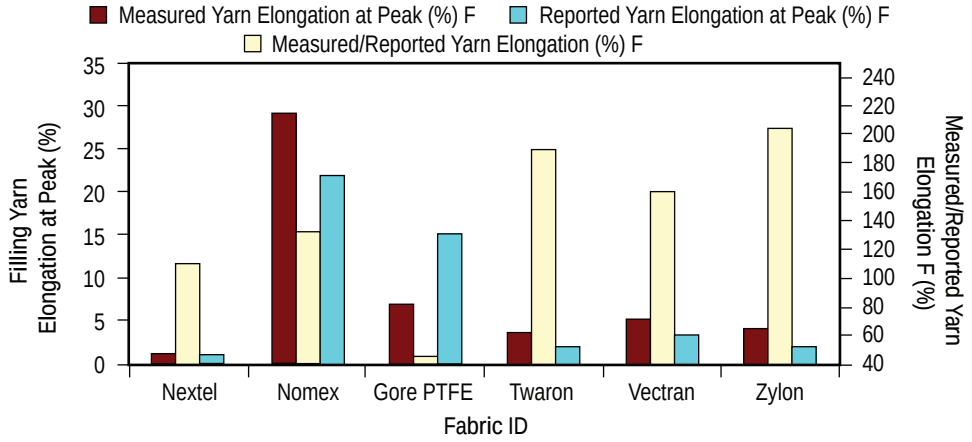

Figure 10. Tensile elongation of filling yarns (percent) as compared to reported values.

2.2.2 Fabric Tensile Testing

2.2.2.1 General Procedures. Tensile properties of the fabrics were obtained according to the ASTM D-5035[14] strip test at ambient conditions. Five fabric samples of each fabric type were tested for tensile strength. In this test, the fabric sample is clamped in a tensile testing machine (Instron-4505) and a force is applied to the sample until it breaks. Values for the breaking force and elongation of the test sample are obtained from a computer interfaced with the testing machine. Since the fabrics used in this study are high strength textile materials, special modifications were made to prevent the fabrics from slipping in the clamps or being damaged as a result of being gripped in the jaws. Measurements employed a constant rate of extension (CRE) type mechanism. Each clamp face is a 2-inch square. Each sample was cut 2 inches wide and 14 inches long both in warp (machine) and filling (cross) direction (see fig. 11). The machine was set at a 6-inch/min crosshead speed. To minimize slippage, manual clamps were used instead of automatic clamps. Pneumatic clamps are limited by the pressure of the fluid and have questionable performance at both high and low temperatures.

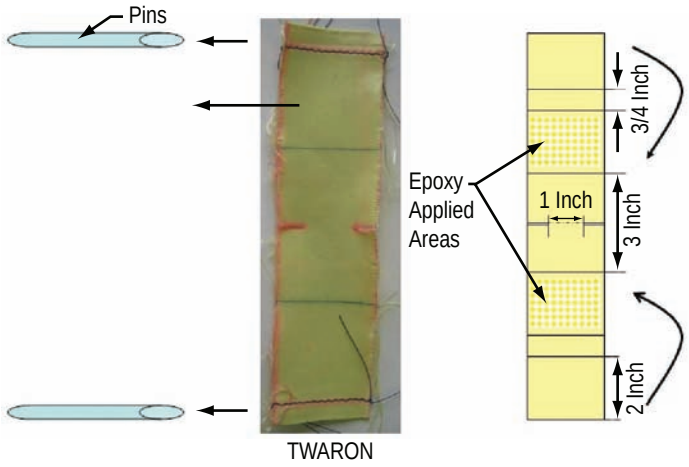

Figure 11. Tensile test samples.

Samples were mounted securely in the clamps, and extra attention was given to ensure that the samples were centrally located and that the long dimension was as nearly parallel as possible to the direction of force application. Since some of the samples cannot be satisfactorily held in clamps, they were placed around the pins and between the jaws as illustrated in figure 12, and jaw padding was also used when necessary. Even though the clamps were tightened just enough to avoid slippage but not too tight (to avoid breaks at the front), there were times when more modification (coating, padding, etc.) was required.

As stated earlier, fabric samples were cut 14 inches long and 2 inches wide. Since the fabrics were not breaking from the middle and the yarns near the edges were not breaking at the same time with the yarns in the middle, the samples were reduced 0.5 inch from each side (see fig. 11). Fabrics were marked across the samples at the front inner edge of each jaw to check for fabric slippage (fig. 11). Less than 0.05 percent pretension was applied to fabrics. This pretension was ≈2–3 N for Nextel, Nomex, and Gore PTFE and ≈8–10 N for Vectran, Twaron, and Zylon.

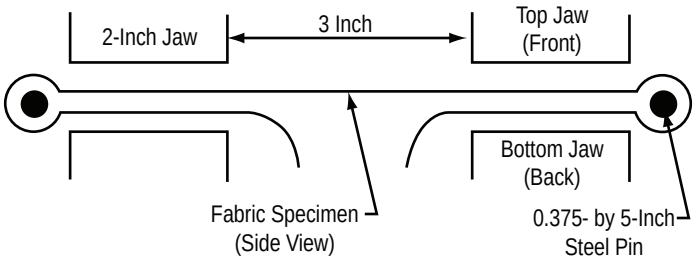

Figure 12. Mounting the tensile test samples in the jaws.[14]

2.2.2.2 Special Modifications. Fabrics clamped directly in the jaws produced problems with jaw breaks and yarn slippage in the fabric structure in the clamped area. A variety of techniques was used to minimize these problems including padding, coating, a fabric loop with pins located in the fold, and a glued fabric loop with pins in the fold. A cotton fabric used as a padding in the jaws proved successful for Nomex and Gore PTFE fabrics

A rubber coating was applied to several of the fabrics as an adhesive to pad the contact with the jaws, improve the jaw grip, and prevent yarn slippage in the test. This procedure worked well for the Nextel fabric and allowed compression in the jaws without the compression fracture caused by the brittleness of the fibers. The rubber coating also prevented yarn slippage in the jaws. Rubber (unvulcanized ethylene propylene rubber (EPR)) dissolved in hexane was painted on the fabric and the hexane was allowed to evaporate leaving the rubber coating on the Nextel fabric.

Since some of the yarns in the tested area of the high strength fabric samples (Twaron, Vectran, and Zylon) showed evidence of yarn slippage, had excessive breaking extension, and had lower than reported tensile strengths, an epoxy coating was applied to the clamped areas (see fig. 11). This treatment did not prevent yarn slippage, so pins were used in the manner depicted in figures 11 and 12. Even though the pins prevented the slippage, the results obtained were still significantly lower than reported values, so epoxy resin was also applied to the fabric samples just under the jaw area. As a result, for Twaron, Vectran, and Zylon fabric samples, pins and epoxy resin were used at the same time. Epoxy was prepared by mixing D.E.R.™ 331 (a Dow Chemical Company product) epoxy resin with EPIKURE™ curing agent (a Miller-Stephenson Chemical Company product) and acetone was added for easier application (14 g of curing agent, 100 g of epoxy resin, and 5 g of acetone). Modifications applied to the fabrics are listed in table 5.

Table 5. Modifications applied to the fabrics.

Fabric	**Modification**
Nextel	Rubber coating and padding
Nomex	Padding
Gore PTFE	Padding
Twaron	Epoxy resin and pins
Vectran	Epoxy resin and pins
Zylon	Epoxy resin and pins

2.2.2.3 Statistical Considerations. The coefficient of variations (CVs) of fabric tensile tests ranged from 2 to 6 percent for all tests at ambient conditions. This is in line with industry expectations. The results for hot and cold tests had increased CVs ranging up to 10 percent probably because of difficulties of controlling temperature and working in the environmental chamber under those conditions.

2.2.2.4. Fabric Tensile Testing at Ambient Conditions. Tensile tests of the fabrics were performed according to ASTM D-5035[14] (using five replicates of each fabric) at ambient conditions ≈22 °C, humidity uncontrolled). Tensile strength and elongation results are listed in table 6 and illustrated in figures 13 through 18.

Table 6. Fabric tensile strength and elongations in warp and filling directions at ambient conditions.

Fabric ID	Fabric Strength (kN/Inch) (W)	Fabric Strength (kN/Inch) (F)	Fabric Strength (MPa) (W)	Fabric Strength (MPa) (F)	Fabric Elongation **at Peak (%) (W)**	Fabric Elongation **at Peak (%) (F)**
Nextel	0.804	0.745	679	673	2.6	2.3
Nomex	0.462	0.425	522	505	16.4	15.2
Gore PTFE	1.335	1.37	736	801	17.1	10.6
Twaron	2.063	4.519	1,160	2,589	14.1	6.62
Vectran	2.293	4.264	1,308	2,535	19.6	8.9
Zylon	2.662	3.773	2,509	3,553	8.0	6.4

As shown in figure 13, strength values of fabrics are higher in the filling direction than in the warp direction as expected. Twaron fabric has the highest tensile strength (kN/inch) in the filling direction while Nomex has the lowest. Zylon fabric exhibited the highest strength in the warp direction and Nomex exhibited the lowest.

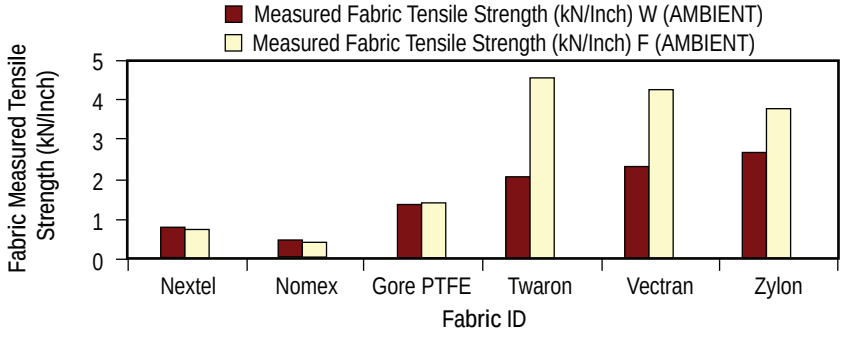

Figure 13. Tensile strength of fabrics in warp and filling direction (kN/inch).

Tensile strength values (MPa) obtained from the experiments in this study are illustrated in figures 15 and 16 compared to yarn measurements and reported values that were obtained from the producers.[8–13]

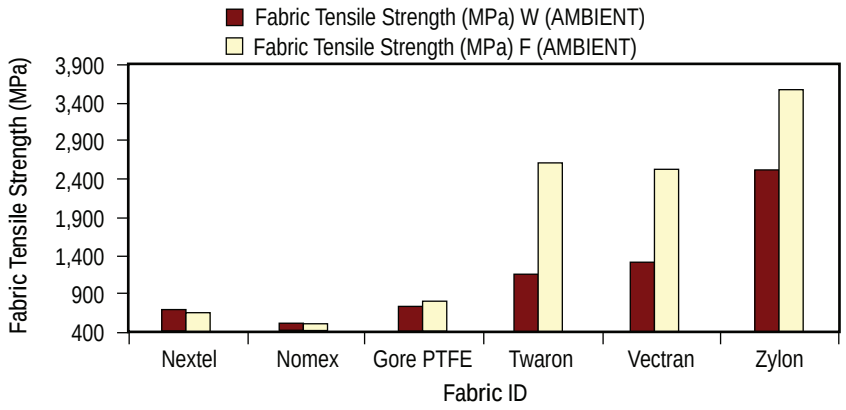

Figure 14. Tensile strength of fabrics in warp and filling direction (MPa).

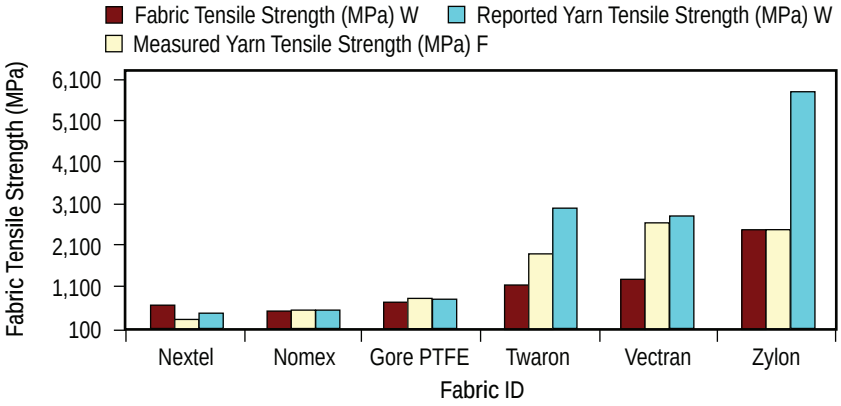

Figure 15. Comparison of measured tensile strength of fabrics with reported values —warp direction. (Reported values were obtained from producers.)

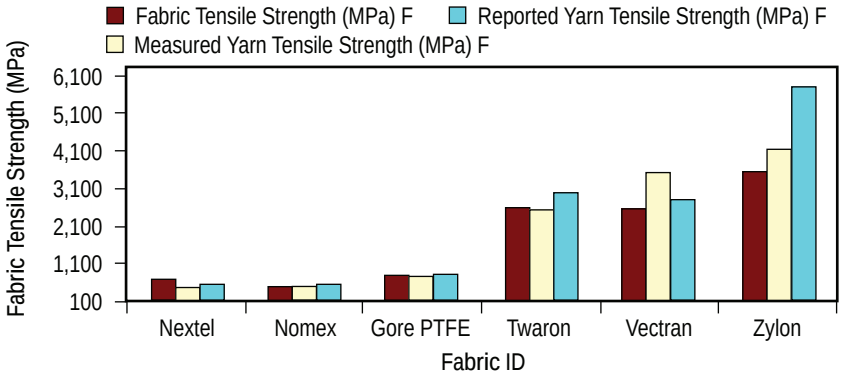

Figure 16. Comparison of measured tensile strength of fabrics with reported values —filling direction. (Reported values were obtained from producers.)

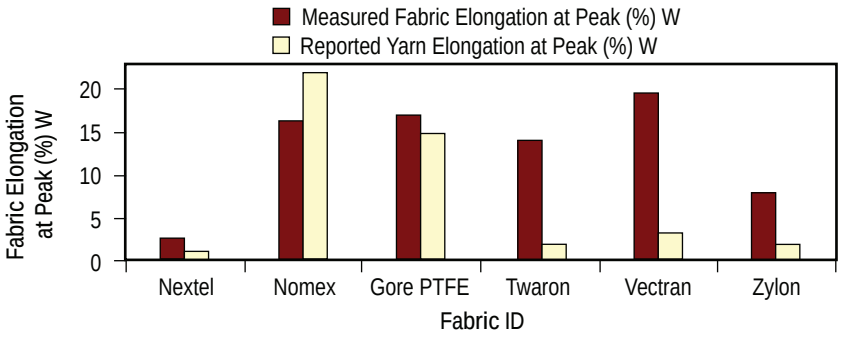

Figure 17. Fabric elongation at peak (percent) in warp direction.

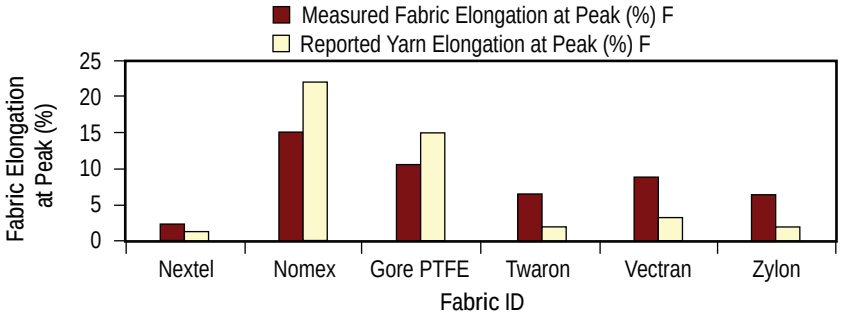

Figure 18. Fabric elongation at peak (percent) in filling direction.

Figures 17 and 18 show that elongation values of fabrics are generally lower in the filling direction.

2.2.2.5 Fabric Tensile Testing at Elevated Temperature. Tensile tests were performed on five samples of each fabric type according to ASTM D-5035[14] at elevated temperature. These tests were conducted in an oven (Instron Environmental Test Chamber Model 3119) that surrounds the test area. The sample was mounted on the tensile test machine, and oven heating was begun. The oven temperature reached 100 ºC in ≈2 min and after an additional 2-min wait, the test was run at 100 ºC. Tensile strength results at elevated temperature as compared to ambient conditions are listed in table 7 and illustrated in figures 19 through 22.

As shown in figures 21 and 22, the strength of fabrics (except Nextel) is decreased at elevated temperatures in both directions.

Tensile elongation results at elevated temperature compared to the ambient conditions are listed in table 8 and are illustrated in figures 23 and 24.

2.2.2.6 Fabric Tensile Testing at Cold Temperature. Tensile tests were performed on five samples of each fabric type according to ASTM D-5035[14] at cold temperature. Liquid nitrogen (LN_2)

Table 7. Fabric strength (kN/inch) at different conditions.

Fabric ID	Fabric Strength (kN/Inch) (COLD) (–100 °C) (W)	Fabric Strength (kN/Inch) (AMBIENT) (W)	Fabric Strength (kN/Inch) (HOT) (100 °C) (W)	Fabric Strength (kN/Inch) (COLD) (–100 °C) (F)	Fabric Strength (kN/Inch) (AMBIENT) (F)	Fabric Strength (kN/Inch) (HOT) (100 °C) (F)
Nextel	1.09	0.804	0.80	1.08	0.745	0.75
Nomex	0.56	0.462	0.41	0.55	0.425	0.40
Gore PTFE	1.09	1.335	0.84	1.40	1.37	0.74
Twaron	2.13	2.063	1.67	3.56	4.519	3.85
Vectran	2.54	2.293	1.26	5.11	4.264	2.95
Zylon	3.02	2.662	2.40	3.74	3.773	3.38

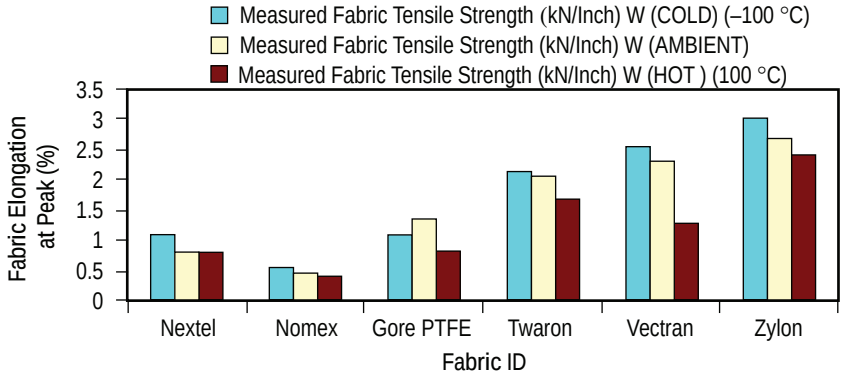

Figure 19. Fabric tensile strength (kN/inch) at different conditions—warp direction.

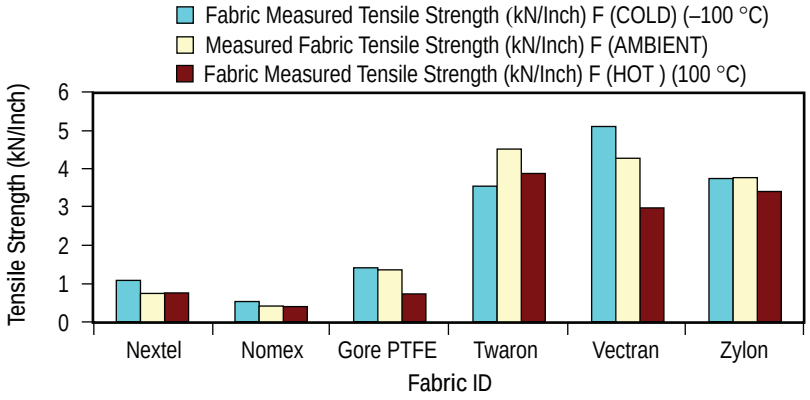

Figure 20. Fabric tensile strength (kN/inch) at different conditions—filling direction.

was used to cool the test chamber (the same environmental chamber used for elevated temperature testing) and although the boiling point is approximately –195 ºC, reaching a temperature that low proved impractical. The temperature that could be achieved in a reasonable time was approximately –100 ºC. A temperature control system was constructed as follows: A Dewar of LN_2 is fed by a submerged tube

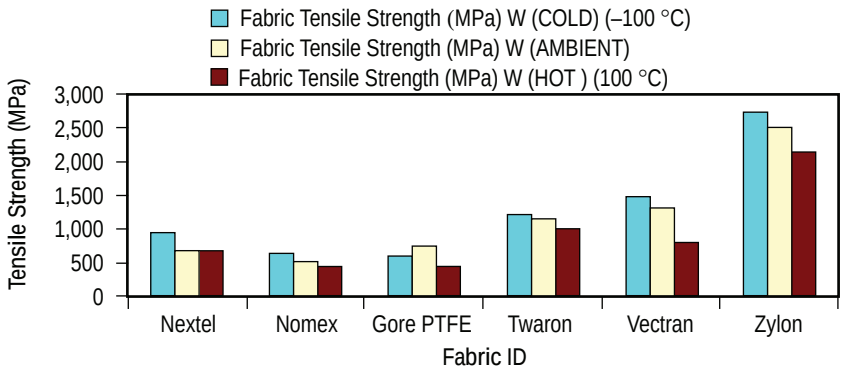

Figure 21. Fabric tensile strength (MPa) at different conditions—warp direction.

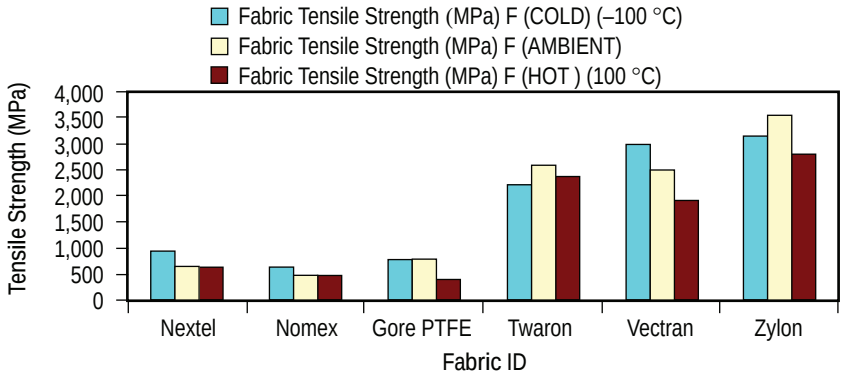

Figure 22. Fabric tensile strength (MPa) at different conditions—filling direction.

Table 8. Fabric elongation (percent) in different conditions.

Fabric	Fabric Elongation **(%) (COLD)** (–100 °C) (W)	Fabric Elongation **(%)** (AMBIENT) (W)	Fabric Elongation **(%) (HOT)** (100 °C) (W)	Fabric Elongation **(%) (COLD)** (–100 °C) (F)	Fabric Elongation **(%)** (AMBIENT) (F)	Fabric Elongation **(%) (HOT)** (100 °C) (F)
Nextel	4.2	2.6	2.7	3.8	2.3	3.2
Nomex	13.1	16.4	17.4	13.3	15.2	16.4
Gore PTFE	10.5	17.1	22.1	9.3	10.6	15.6
Twaron	10.96	14.1	15.3	5.3	6.6	8.03
Vectran	15.4	19.6	20.2	7.9	8.9	8.4
Zylon	9.4	8	8.9	7.9	6.4	7.5

piping dry gaseous nitrogen (GN_2) at a constant rate (fig. 25). The GN_2 was used to heat the LN_2 and cause it to boil. The cold vapor was then fed into the environmental chamber to cool it. At a constant flow rate, the chamber cooled to a constant cold temperature. The flow rate of the GN_2 was adjusted to achieve a chamber temperature of approximately –100 ºC within a reasonable time (≈3 min).

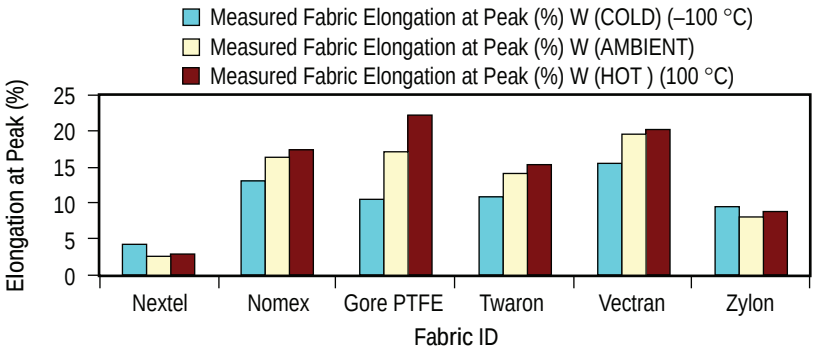

Figure 23. Fabric tensile elongation (percent) at different conditions—warp direction.

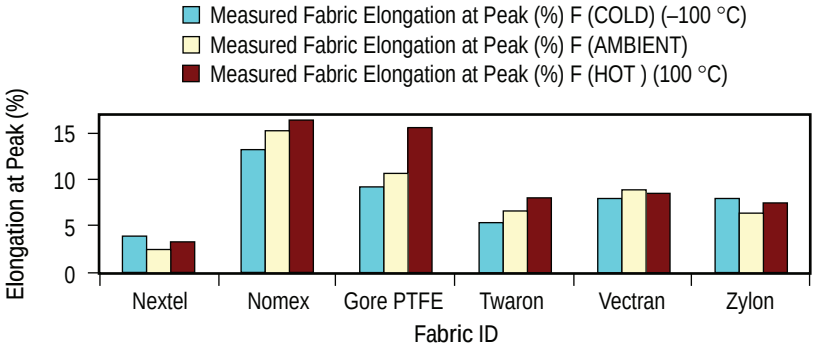

Figure 24. Fabric tensile elongation (percent) at different conditions—filling direction.

The equilibrium temperature under these conditions was approximately –105 ºC. So, by beginning a test ≈1 min after reaching –95 ºC, the sample was exposed and was equilibrated to a temperature within a narrow range of approximately –100 ºC at the time of testing. The procedure was to (a) load a sample, (b) close the chamber, (c) start the flow of nitrogen, (d) wait for the internal temperature to reach –95 ºC, (e) wait one additional minute, (f) test the sample, (g) open the door, (h) allow the interior to warm up, (i) remove the sample, and (j) start another test. Typical measured temperatures at the time of beginning a test were –105 ºC. Tensile results at cold temperature as compared to the ambient conditions as well as elevated temperature are listed in tables 7 and 8 and are illustrated in figures 19 through 24.

2.3 Fold Testing

2.3.1 General

Folding endurance is another measure of fabric strength and durability. In use, the fabric form is likely to remain folded for several weeks before being unfolded at cryogenic temperatures on the Moon and filled with regolith. The folding test was conducted using Massachusetts Institute of Technology (MIT) folding endurance tester (Tinius Olsen Testing Machines). Fabrics were cut 0.5 inch wide by 5 inches long only in the warp direction, mounted on the machine (see fig. 26), and 1.5-kg tension was applied. The folding test is performed with a device that folds the fabric samples at constant speed;

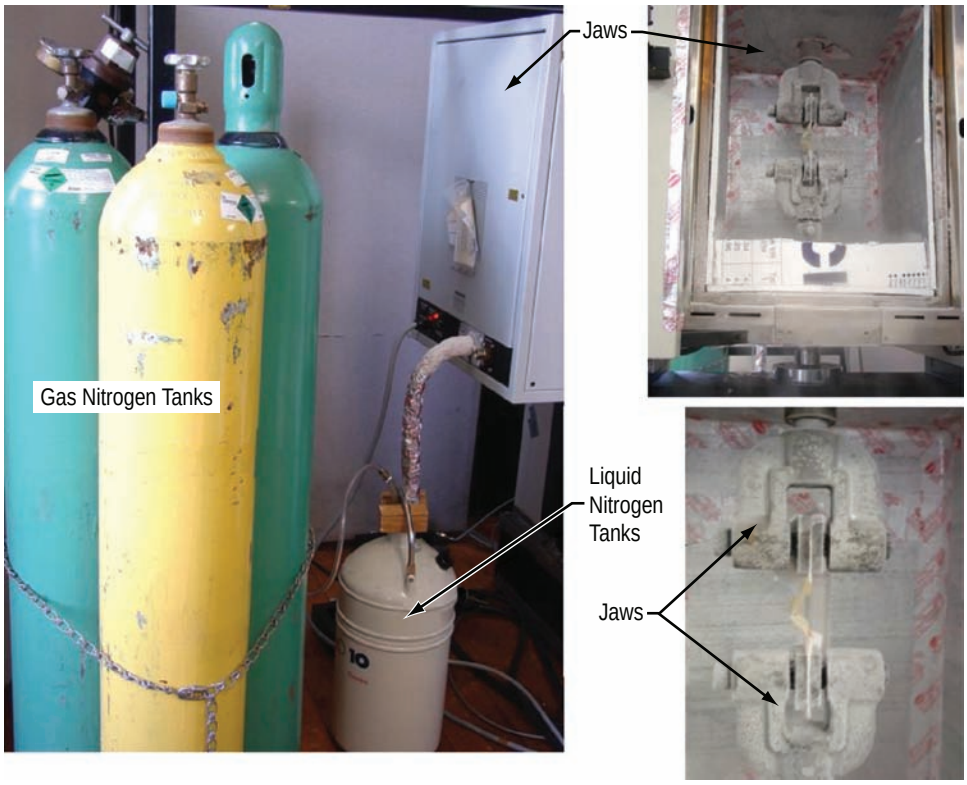

Figure 25. Tensile test system prepared for cold temperatures.

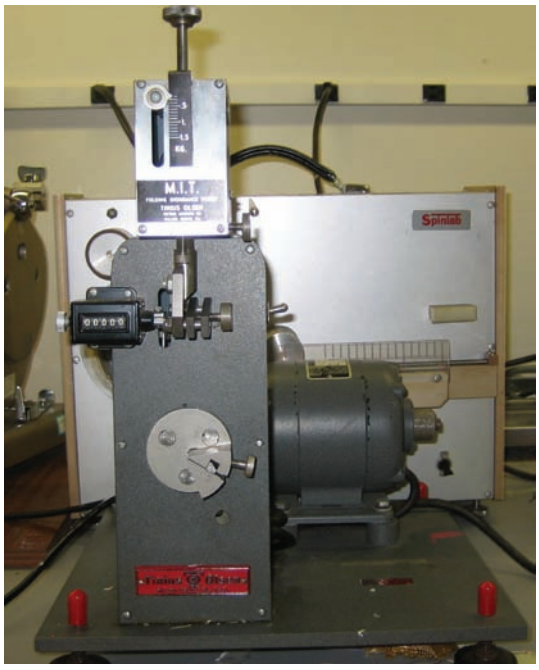

Figure 26. Folding test device.

the sample is removed after a specified number of cycles or just after the fabric sample has broken, whichever occurs first. Machine speed is ≈180 cycles/min. Three specimens were tested for each fabric at each temperature. All of the fabrics used in this study, except for Nextel, showed good folding resistance in the warp direction. Nextel was the only fabric with poor folding resistance (broken in <300 cycles at all temperature conditions). All fold testing was performed at Auburn University Department of Polymer and Fiber Engineering.

2.3.1 Ambient Conditions Fold Testing

The folding test was conducted at laboratory conditions (70 ºF, 65 percent humidity) and cycles to failure were recorded (or the test was stopped at 50,000 cycles because no failure was observed). The number of folding cycles for each fabric is shown in figure 27. Since the fabrics used in this study were high strength materials, all fabrics except Nextel were able to carry many folding cycles without any damage. Nextel fabric samples were broken in <1 min, after 100 cycles on average. Twaron fabrics started to show damage after 30,000 cycles and were broken at ≈40,000 cycles. For Nomex, Gore PTFE, Vectran, and Zylon, no significant damage was determined after 50,000 cycles. Figure 28(a) shows the damages on fabrics at ambient conditions.

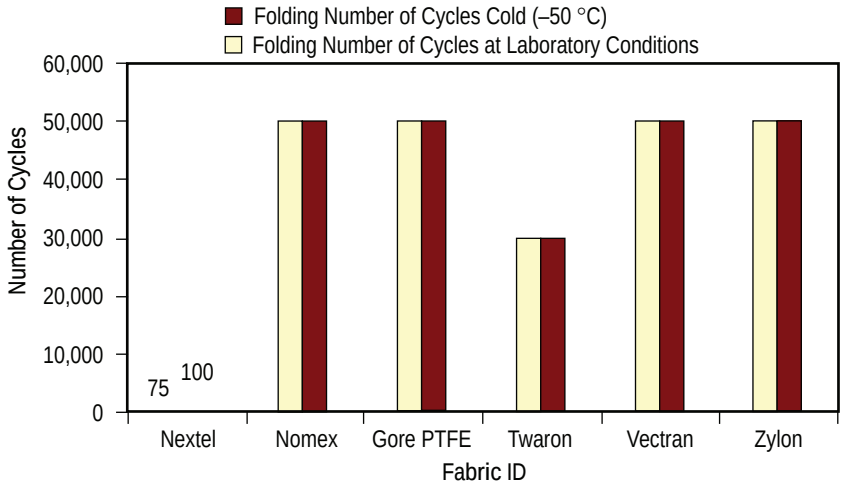

Figure 27. Number of folding cycles for fabrics—warp direction.

2.3.2. Cold Temperature Fold Testing

Folding tests were conducted at cold temperature (-50 ºC and lower) and readings were recorded. Dry ice was used to reach -50 ºC and lower. Dry ice is a solid form of carbon dioxide (CO_2) gas. Its sublimation temperature is -78.5 ºC. A Styrofoam™ (a Dow Chemical Company product) box was constructed around the area where the fabric folding takes place, and dry ice was placed in the box with a thermocouple to monitor the temperature inside the box (see fig. 29 and 30). There was no significant change in damage observed on the fabrics at cold temperature compared to ambient conditions. Nextel fabrics were broken after 75 cycles on average at cold temperature. The results at cold temperature are illustrated in figure 28(b).

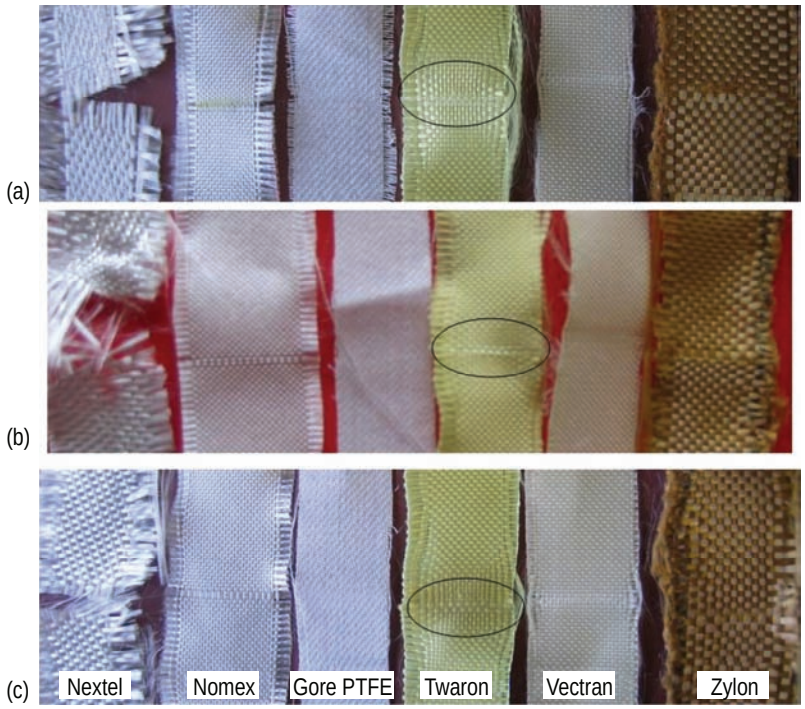

Figure 28. Photographs of fabrics after fold testing at (a) ambient conditions, (b) cold conditions, and (c) cryogenic conditions.

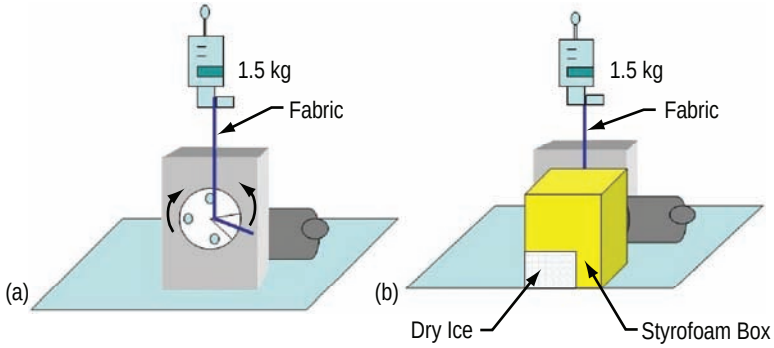

Figure 29. Folding device test for cold temperatures (a) before modification and (b) after modification.

2.3.3. Cryogenic Conditions Fold Testing

The Styrofoam box was again used around the area where the fabric folding takes place. LN_2 was poured over the fabric and the folding mechanism while concurrently running the machine. Since LN_2 was being poured onto the fabric while testing, the time for testing was restricted to ≈1 min or ≈100 cycles. After ≈100 cycles, fabrics were examined under the microscope. Photographs were taken of the fold area of all samples and are shown in figure 28(c). The precise temperature of the fabric during these folding tests was not monitored, but the temperature of the LN_2 is approximately –195 °C, so a temperature close to that value is expected.

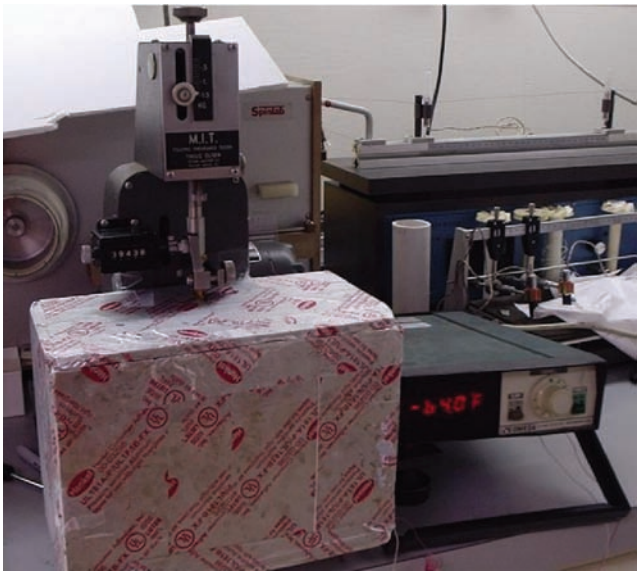

Figure 30. Folding test system for cold temperatures.

It was observed that the Nextel fabrics had less damage under cryogenic conditions than at ambient conditions, with ≈250 cycles before complete failure. None of the other fabrics showed any significant sign of filament breakage after 100 cycles of folding at cryogenic temperatures.

2.4 Radiation Exposure and Effects

2.4.1 Overview

Materials used for exploration must be capable of withstanding all components of the natural and induced environments to ensure survivability of the mission, and ultimately the survivability of the explorers themselves. An important component of any space environment is radiation produced naturally in our galaxy, or induced from sources such as nuclear power generators. As an initial look at materials that are potential candidates for use in developing structures on the lunar surface, a list of the pertinent components of the natural ionizing radiation environment was compiled to deduce the likely radiation dose caused by this environment. Candidate materials were subjected to environments equivalent to a 10-yr radiation exposure on the Moon at the NASA MSFC Space Environmental Effects Facility (SEEF). After exposure, the irradiated materials were returned to Auburn University for material strength testing as indicated in the following sections of this document. Additional testing incorporating a cobalt-60 (^{60}Co) gamma irradiation facility was performed at Auburn University.

2.4.1.1 Ionizing Radiation Environment. The major components of ionizing radiation in the natural lunar environment are from the solar wind, solar cosmic rays from solar particle events (SPE), galactic cosmic rays (GCR), and electromagnetic radiation from the Sun.[15] The solar wind is composed predominantly of low to mid energy (tens of keV/nucleon) protons, helium ions, and electrons. Generally, solar cosmic rays from an SPE consist of protons with energies >10 MeV. The galactic cosmic ray

spectrum consists of very high energy (GeV/nucleon) ions, and spans the range of nuclei up to about number 26 (iron). Ionizing solar electromagnetic radiation is the ultraviolet (UV) and vacuum UV (VUV) component of the solar spectrum, light that the atmosphere generally filters out on Earth. For the purposes of this investigation, the electromagnetic and particle radiation are treated separately, predominantly due to dissimilar test acceleration factors available for the two environmental components.

2.4.1.2 Radiation Transport Calculations. To predict anticipated radiation dose levels in the candidate materials, radiation transport calculations were performed to determine expected doses imparted during a 10-yr exposure on the lunar surface using available simulation programs. Electron transport calculations were conducted using the Integrated Tiger Series (ITS) 3.0 suite 2D TIGERP code,[16] and ion transport simulations using the "Stopping Range of Ions in Matter—(SRIM) 2003."[17] The details of the composition and abundance of components of the lunar radiation environment can be found in reference 15. Each component was analyzed separately for comparison, and for illustration, they are presented as they relate to the Vectran candidate material in figure 31.

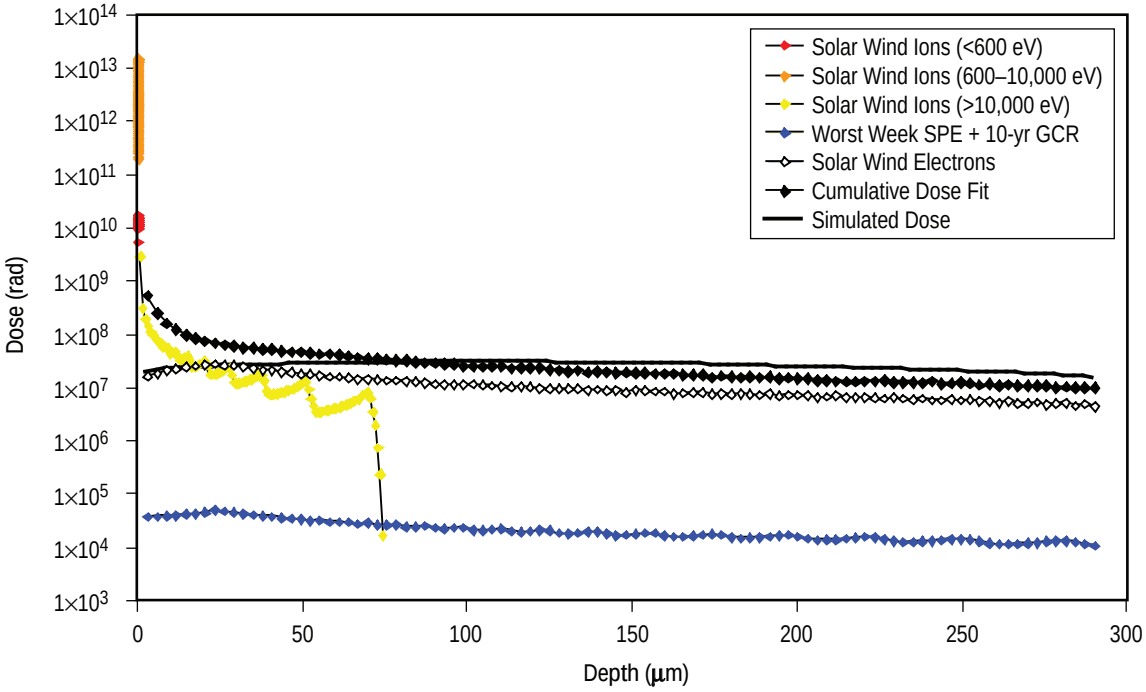

Figure 31. Comparison of individual components of the ionizing radiation environment on the lunar surface with the predicted total bulk dose absorbed in a sheet of Vectran fabric.

The ionizing particle components consist of solar wind ions, solar wind electrons, and galactic and solar cosmic ray ions. For analysis, the solar wind ions were grouped into the following energy ranges: <600 eV, 600–10,000 eV, and >10,000 eV. The solar wind electrons were modified using the parameters defined in reference 15. The GCR and SPE environments were combined for analysis, with the SPE environment being defined by a 180-hr recorded environment representing the highest radiation

level recorded for a solar event, referred to as the “worst week” environment. The expected radiation dose from each individual component in the Vectran candidate material is detailed in figure 31, alongside the expected cumulative dose from all components. As is apparent, while the solar wind ion component will supply an astonishing dose at the material surface, the depth of penetration of these components is on the order of a few microns and should not be expected to affect the bulk strength of the material. Additionally, the contributed 10-yr dose from the GCR and SPE environment is several krd. While penetrating into the bulk of the material, this is actually a low dose for material degradation, and is roughly three orders of magnitude lower than the anticipated solar wind electron dose. Therefore, the actual dose driver for material bulk damage in the lunar surface radiation environment is the solar wind electron component. Based on this analysis of individual contributions to the total dose, it was determined that the best method of simulating the total ionizing radiation dose for these materials was to use an appropriate single electron energy to simulate the expected dose profile. The damage imparted by a 250-keV electron beam passed through a 0.001-inch aluminum scattering foil is displayed as the “simulated dose” in figure 31, and provides an excellent simulation of the expected bulk damage for these materials. In order to impart a 10-yr equivalent dose into the material, a total fluence of 3.6×10^{14} electrons/cm² was supplied to each material sample, which is approximately equivalent to a 30 Mrd radiation dose.

2.4.1.3 Radiation Transport in Candidate Materials Comparison. Radiation transport calculations were performed, as outlined above, for each of the three candidate materials subjected to particle radiation exposure. The calculated and simulated 10-yr total ionizing dose for each material is shown in figure 32. The generated simulations are scaled to represent the damage induced by 3.6×10^{14} electrons /cm² at nominally 250 keV incident onto the sample.

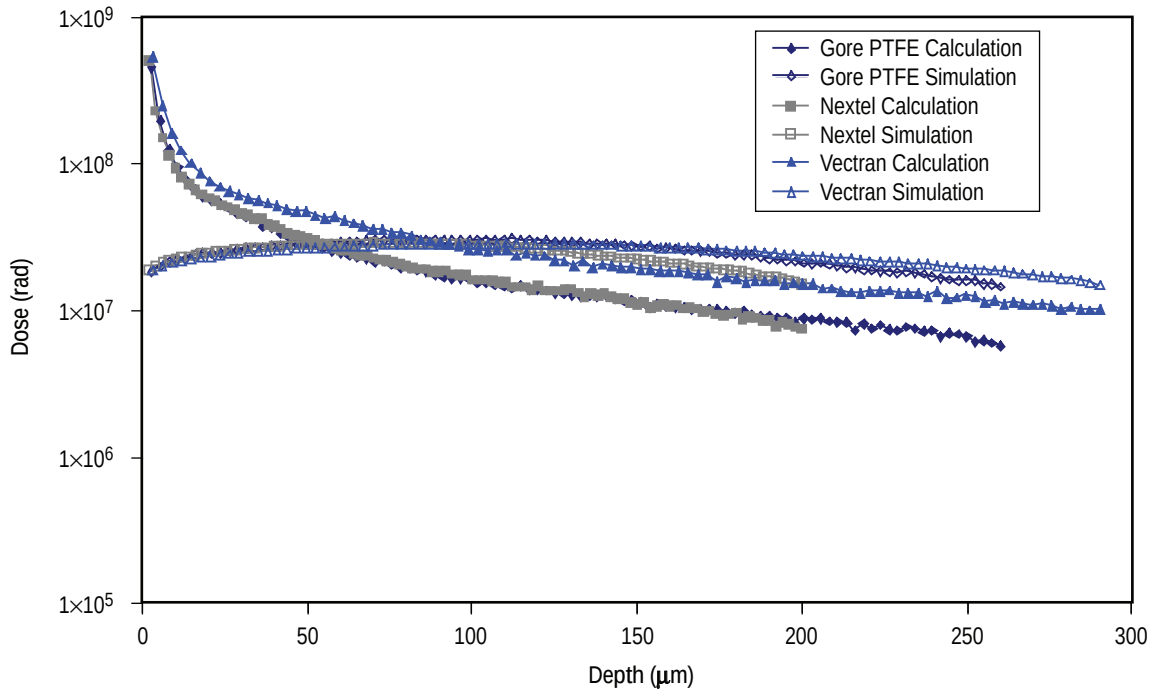

Figure 32. Calculated and simulated radiation doses in each of the three candidate materials (Gore PTFE, Nextel, and Vectran).

2.4.2 Charged Particle Exposure

The particulate radiation portion of these tests was performed using a National Electrostatics Corporation (NEC) Model 7.5SH Pelletron® accelerator-based system located in the MSFC SEEF. The accelerator produced the 250 keV electrons (fig.33). Electron beam currents were periodically monitored using a Faraday cup near the accelerator. The incident beam was directed through a 0.001-inch aluminum scattering foil, diffusing the beam over the desired sample area. This scattering process lowered and broadened the energy distribution of the electron beam, which was accounted for in the transport calculations. Particle flux at the samples was determined by calibrating with a Faraday cup at the sample location prior to introduction of the specimen. The signals from the Faraday cups were fed to an EG&G/ ORTEC Model 439 digital current integrator that generated an output pulse directly proportional to the number of particles incident on the Faraday cup. These pulses were in turn counted by an EG&G/ ORTEC Model 999 counter/timer.

Figure 33. NEC 7.5SH electron accelerator (left) and NEC 2SH positive ion accelerator (right) used to provide charged particle radiation.

The sample holder and configuration for the total ionizing dose irradiation are presented photographically in figures 34 and 35. Three candidate materials (Gore PTFE, Nextel, and Vectran) were subjected to electron irradiation, each represented by three replicate 2- by 10-inch samples. Each specimen was oriented such that it was directly irradiated at least 1 inch of the center of the width (fill direction), and at least 4 inches of the length (warp direction). Following exposure, each specimen was returned to Auburn

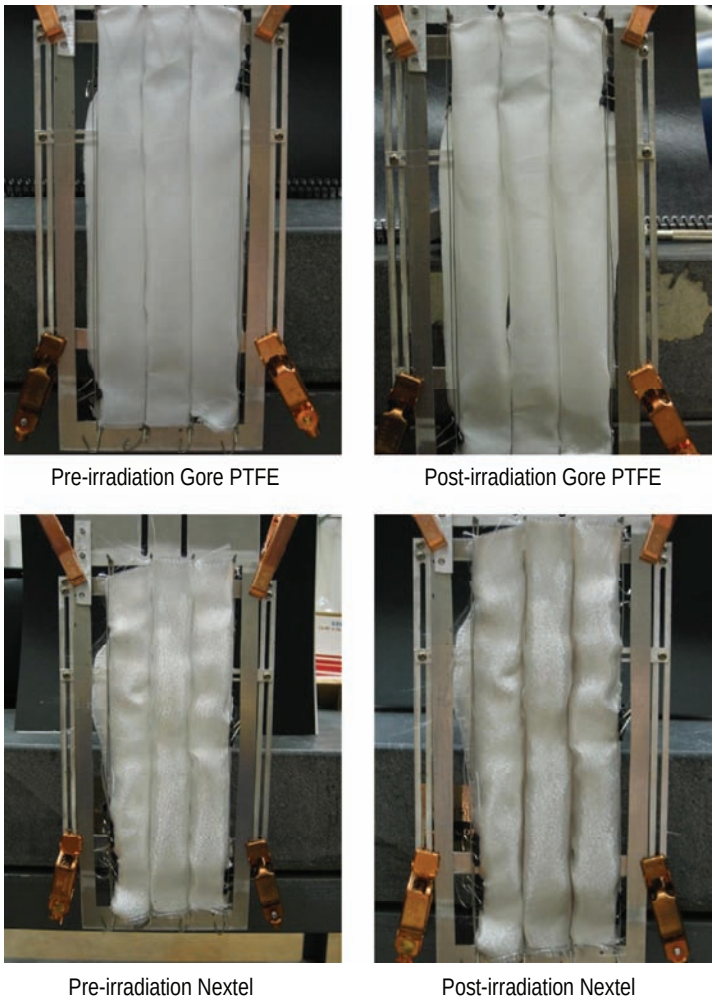

Figure 34. Particle radiation sample pictures for Gore PTFE and Nextel.

University for mechanical strength testing. A fourth test was run on a bag constructed from Vectran. One side of the nominally cubic bag was irradiated and sent to the MSFC Impact Test Facility where it was filled with material selected to simulate properties of lunar regolith and subjected to impact testing directed at the irradiated area of the bag. Details of the test are discussed in section 2.6.1.

Table 9 and figure 36 show the strength of fabrics before and after radiation exposure. Figure 37 shows the normalized strength before and after radiation exposure. Table 10 and figure 38 show the corresponding breaking elongation.

As the figures show, while Nextel fabrics gained a little strength after radiation, the strength of Gore PTFE decreased dramatically, and the Vectran strength decreased slightly.

Elongation of Nextel fabrics was essentially unaffected by radiation. The elongation of Gore PTFE decreased dramatically, and Vectran's decreased slightly.

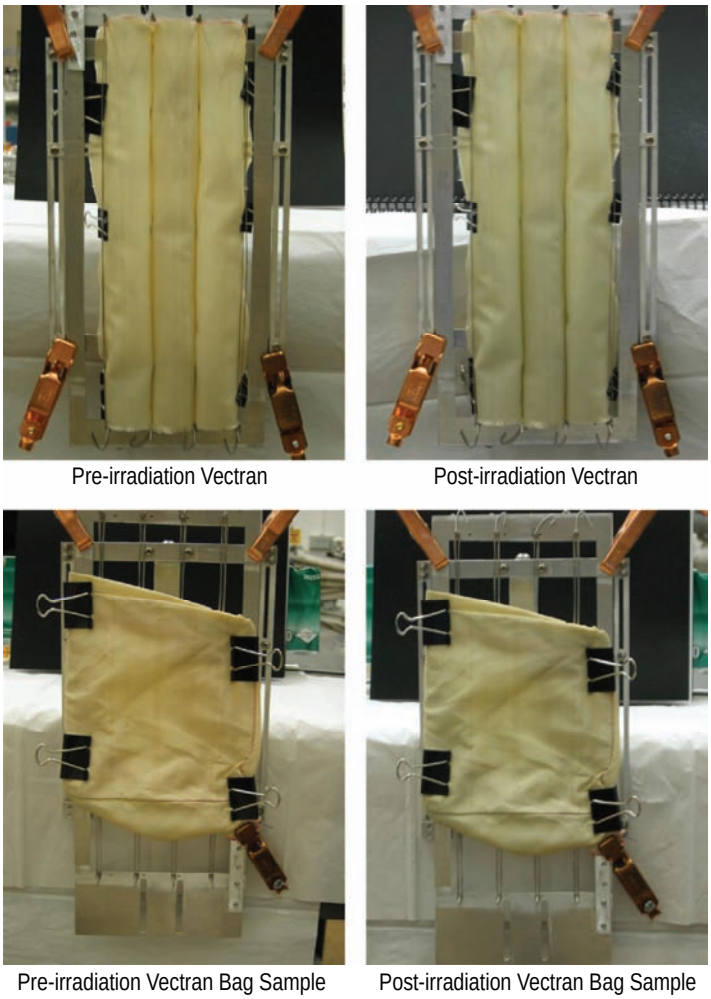

Figure 35. Particle radiation sample pictures for Vectran.

Table 9. Fabric strength before and after radiation (charged particle).

Fabric ID	Fabric Strength (kN/Inch) (Before Rad.) (W)	Fabric Strength (kN/Inch) (After Rad.) (Charged Particle) (W)	Fabric Strength (MPa) (Before Rad.) (W)	Fabric Strength (MPa) (After Rad.) (Charged Particle) (W)
Nextel	0.8	0.97	679	847
Gore PTFE	1.34	0.08	736	42
Vectran	2.3	2.1	1,308	1,222

2.4.3. Gamma Irradiation

Though not a major component of the natural space environment, gamma irradiation do mimic some aspects of material degradation due to radiation exposure. Gamma irradiation causes ionization damage within a material, and has a significant depth of penetration compared to massive particles

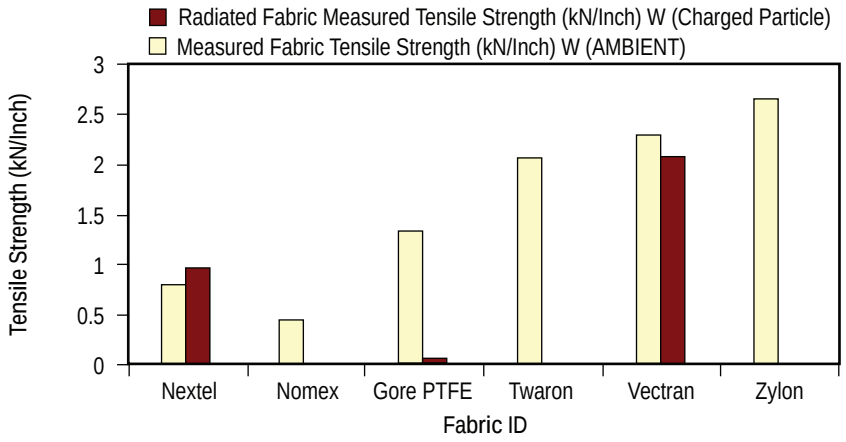

Figure 36. Comparison of fabric tensile strength (kN/inch) before and after radiation (charged particle)—warp direction.

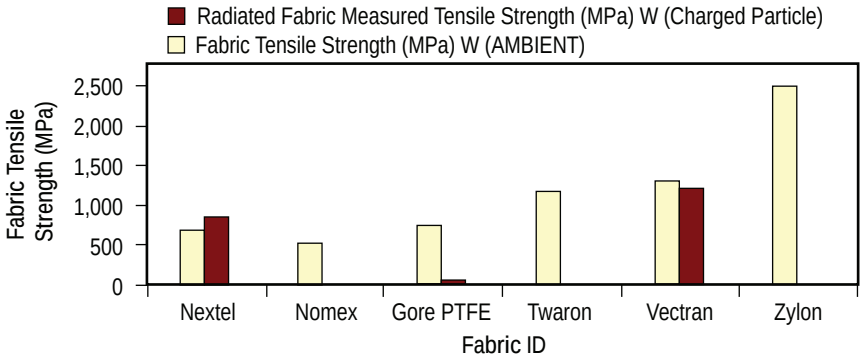

Figure 37. Comparison of fabric tensile strength (MPa) before and after radiation (charged particle)—warp direction.

Table 10. Fabric elongation (percent) before and after charged particle radiation.

Fabric ID	**Fabric Elongation at Peak (%)** (Before Rad.) (W)	**Fabric Elongation (%)** (After Rad.) (Charged Particle) (W)
Nextel	2.6	2.7
Gore PTFE	17.1	3
Vectran	19.6	15.9

such as electrons and especially solar wind ions. While they do not carry a charge and, therefore, do not directly simulate the particles responsible for the bulk material dose in the natural space radiation environment, gamma testing is a widely used technique due to cost and availability concerns compared to

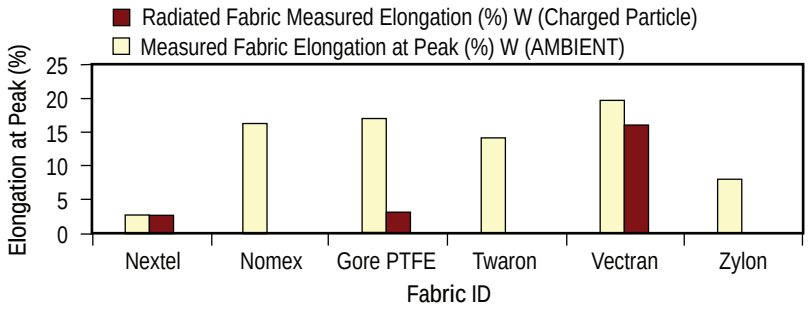

Figure 38. Comparison of fabric elongation (percent) before and after radiation (charged particle)—warp direction.

charged particle exposure. For these reasons, this method was included in the test regimen to allow a significant increase in material evaluation.

Five samples from the six different fabrics were exposed to gamma radiation in a ^{60}Co source to an estimated absorbed dose of 10 Mrd at 8.558 rd/min for 193.4 hr. Tensile strength properties were measured after exposure and results were compared to the un-irradiated samples. Radiation was performed in the Auburn University Leach Radiation Facility.

Table 11 shows the values obtained after fabrics were exposed to radiation using the same testing machine used to test the tensile properties at ambient conditions. Results are illustrated in figures 39 through 42.

Table 11. Fabric strength and elongation after gamma radiation (10 Mrd).

Fabric ID	Fabric Strength (kN/Inch) (W)	Fabric Strength (kN/Inch) (F)	Fabric Strength (MPa) (W)	Fabric Strength (MPa) (F)	Fabric Elongation (%) (W)	Fabric Elongation (%) (F)
Nextel	0.8	0.9	756	801	2.2	2.3
Nomex	0.4	0.4	500	488	16.4	16.8
Gore PTFE	0.2	0.2	95	114	6.3	4.5
Twaron	2.01	4.01	1,097	2,324	12.9	5.5
Vectran	2.2	4.1	1,274	2,415	17	7.2
Zylon	2.4	3.3	2,191	2,929	8.7	5.8

As shown in figures 39 and 40, the strength of all fabrics, except Nextel, is decreased after radiation both in warp and filling direction. As expected, Nextel was unaffected and perhaps had a slight increase in strength. Clearly, Gore PTFE had the poorest radiation resistance by far. It suffered a dramatic decrease in breaking strength after radiation. Other fabrics either increased or decreased only slightly.

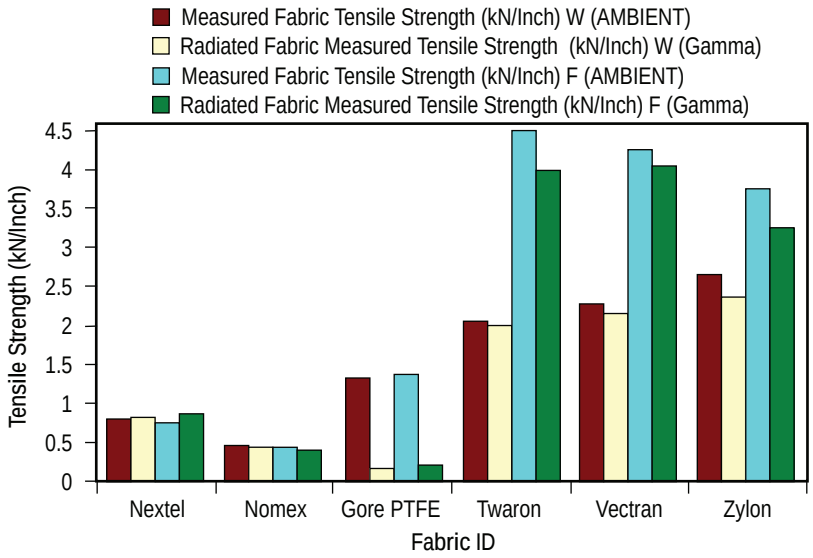

Figure 39. Comparison of fabric tensile strength (kN/inch) before and after radiation (gamma)—warp and filling direction.

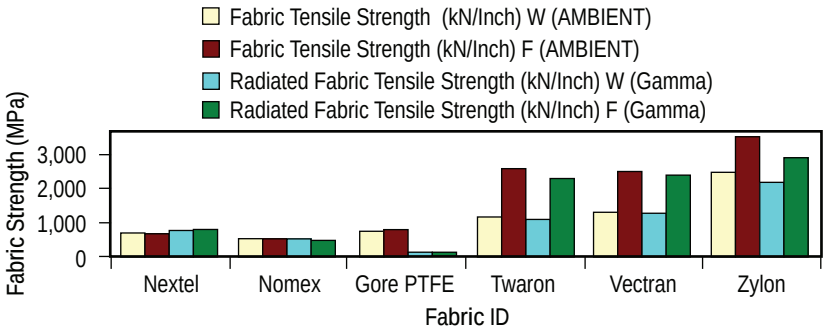

Figure 40. Comparison of fabric tensile strength (MPa) before and after radiation (gamma)—warp and filling direction.

Figures 41 and 42 show that the breaking elongation is dramatically affected by gamma irradiation only for Gore PTFE. The other fabrics remain relatively unchanged or slightly decreased by this level of exposure.

2.4.4. Vacuum Ultraviolet Testing

As mentioned above, the atmosphere largely filters electromagnetic solar radiation of sufficient energy to cause ionization prior to reaching the surface of the Earth. Because the Moon has no such atmosphere, materials on the lunar surface are subjected to this component of the electromagnetic spectrum, referred to as VUV radiation. A common method of simulating this component of the radiation environment is to use deuterium arc lamps housed in evacuated systems. A typical spectral output

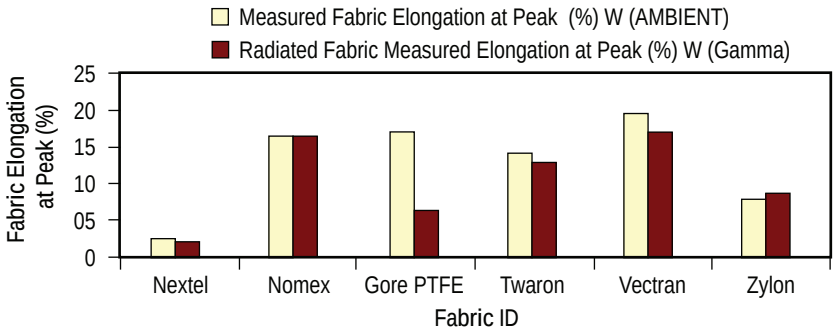

Figure 41. Comparison of fabric elongation (percent) before and after radiation (gamma)—warp direction.

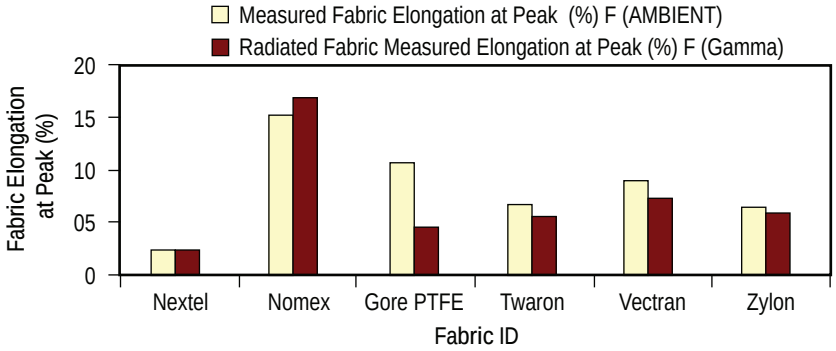

Figure 42. Comparison of fabric elongation (percent) before and after radiation (gamma)—filling direction.

of these sources as displayed in figure 43 spans the region from 110 to 170 Nm, correlating to ≈15 to 9.7 eV photon energies, respectively. These energies are sufficient to cause ionization damage in many materials, especially organics and polymers. Due to limited size and substantial costs associated with simulating this environment, the rate of accelerated testing of reasonably large sample areas is significantly lower than that of the available particle radiation facilities. It should be noted that solar electromagnetic acceleration factors are highly dependent on the spectral region used for integration and comparison. Typical methodologies integrate over a broad spectral region for comparison to the solar spectrum, and when compared to these methods, deuterium lamps display relatively low acceleration factors. In the current configuration, for irradiation at 39 inches from the source, a value of 2.5× is estimated as a minimum acceleration factor using a broad integration. However, if the integration region is stopped at short wavelengths, the acceleration factor can be more than two orders of magnitude greater than estimated.[17] Because the current effort is a comparative study, and all samples were subjected to the same VUV exposure, the actual acceleration factor is not critical. It is estimated that the acceleration is at least 2.5×, and likely, substantially higher. Therefore, for simplicity, the actual duration of exposure is stated as 1,246 hr of deuterium irradiation using a Hamamatsu L1835 deuterium lamp system at a distance of 39 inches under vacuum. Therefore, this is equivalent to at least 3,115 solar equivalent hours of irradiation.

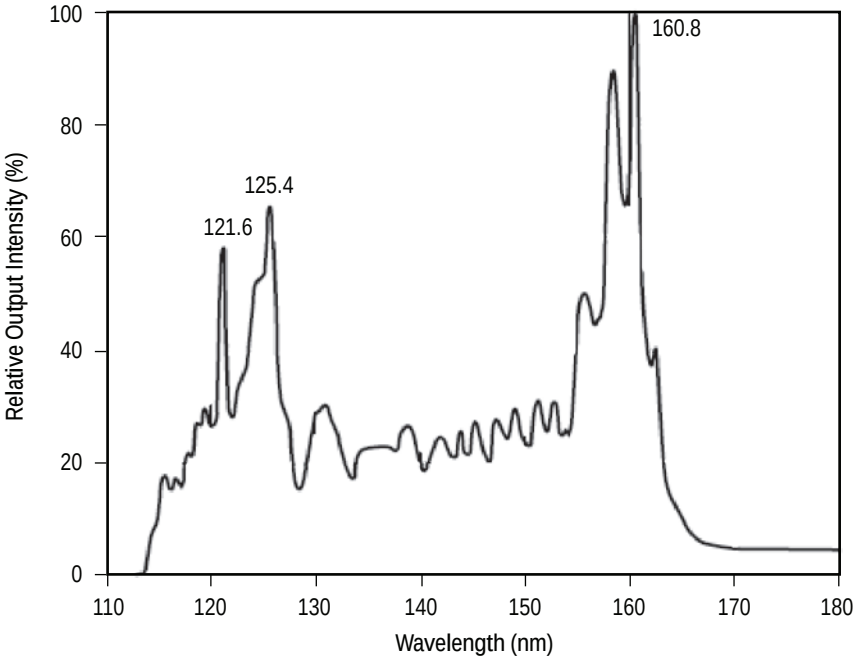

Figure 43. Relative spectral intensities for deuterium lamp emissions from 110 to 180 Nm.

The tensile specimens for each of the six candidate materials were mounted such that the warp direction of the specimen was directed radially outward from the center of the chamber. The 10-inch-long samples were exposed to VUV radiation on a 1-inch (fill direction) by 2-inch (warp direction) area in the center of each specimen. An aluminum mask, as depicted in figure 44, shielded the remainder of each sample. To enable simultaneous testing of replicate samples of each material, two separate pairs of sample holders and deuterium lamps (Hamamatsu model L1835) were used. On each sample holder, two sets of three replicate samples and one set of two replicate samples were mounted so that each lamp irradiated three candidate materials, and eight distinct specimens (fig. 44). Following irradiation, these samples were removed and returned to Auburn University for mechanical strength testing.

Table 12 shows the tensile test results obtained after fabrics were exposed to VUV radiation (testing done on the Instron 4505) and properties were measured at ambient conditions. Results are illustrated in figures 45 through 47.

Figures 45 and 46 show that Gore PTFE was the only fabric with a dramatic decrease in properties. While Nextel gained a little in strength, all others showed a slight to moderate decrease after VUV exposure.

Figure 47 shows that fabric elongation in warp direction increased slightly after VUV radiation in all fabrics except Gore PTFE.

Figures 48 and 49 illustrate the change in fabric strength and elongation before and after fabrics are exposed to different radiations in warp direction.

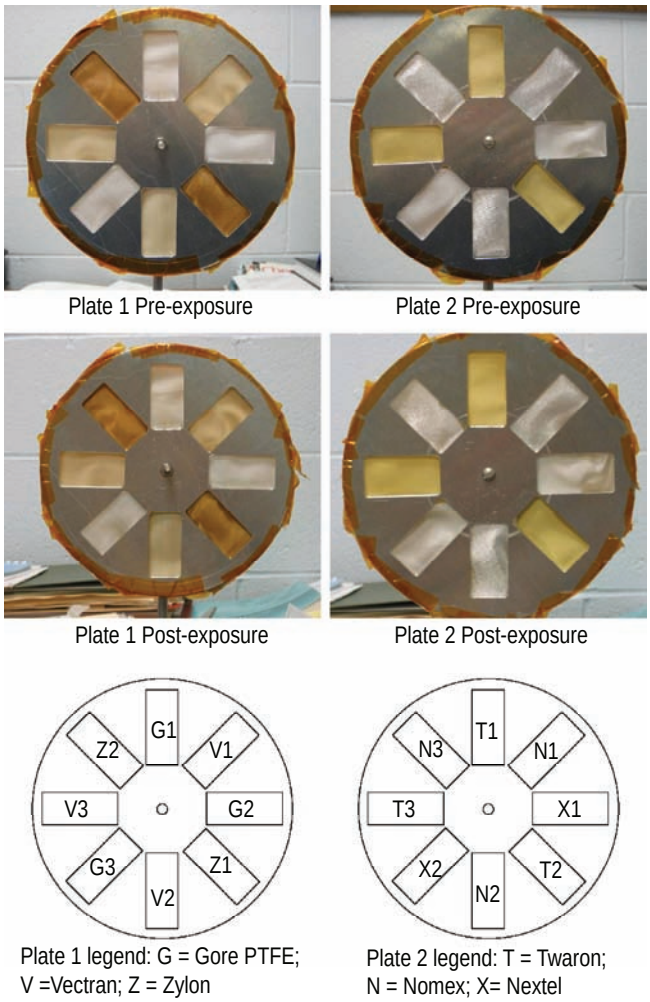

Figure 44. Sample photos.

Table 12. Fabric strength and elongation before and after radiation (VUV).

Fabric ID	Fabric Strength (kN/Inch) (Before Rad.) (W)	Fabric Strength (kN/Inch) (After Rad.) (VUV) (W)	**Fabric Elongation (%)** (Before Rad.) (W)	Fabric **Elongation (%)** (After Rad.) (VUV) (W)	Fabric Strength (MPa) (Before Rad (W)	Fabric Strength (MPa) (After Rad.) (VUV) (W)
Nextel	0.80	0.92	2.6	3.37	679	851.77
Nomex	0.46	0.42	16.4	18.72	522	496.36
Gore PTFE	1.34	0.29	17.1	9.52	736	168.18
Twaron	2.06	2.03	14.1	16.90	1,160	1,133.07
Vectran	2.29	1.88	19.6	23.04	1,308	1,185.87
Zylon	2.66	2.10	8	9.85	2,509	1,948.82

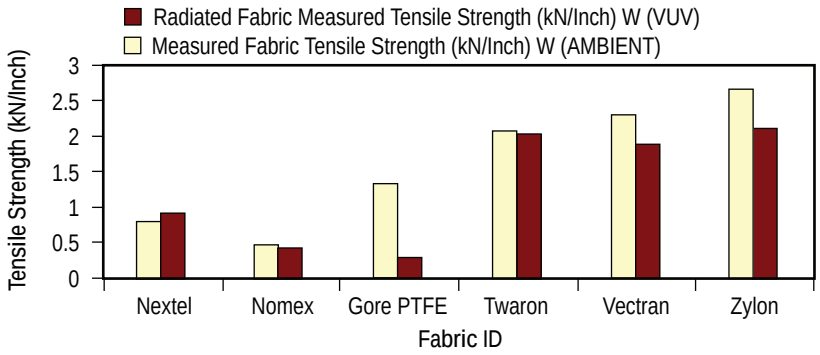

Figure 45. Comparison of fabric tensile strength (kN/inch) before and after radiation (VUV)—warp direction.

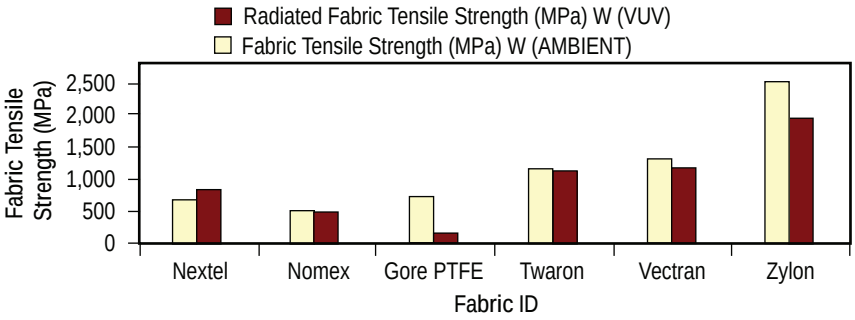

Figure 46. Comparison of fabric tensile strength (MPa) before and after radiation (VUV)—warp direction.

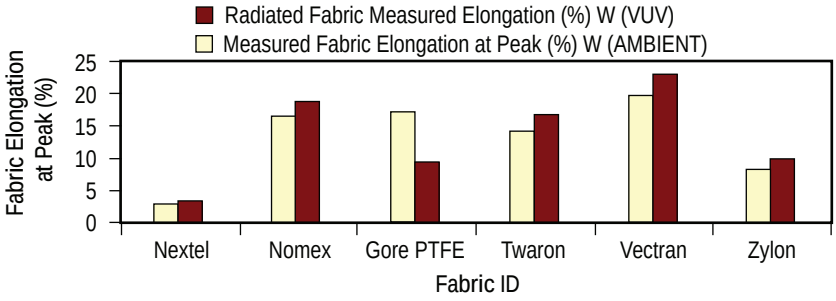

Figure 47. Comparison of fabric elongation (percent) before and after radiation (VUV)—warp direction.

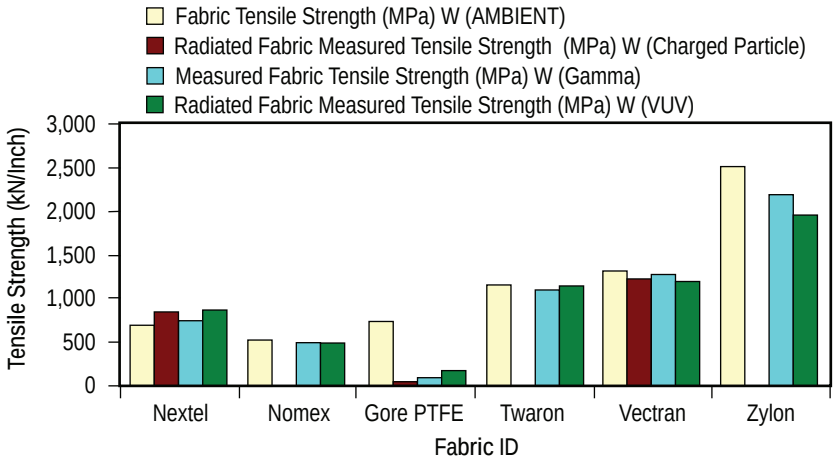

Figure 48. Comparison of fabric tensile strength (MPa) before and after radiation (VUV)—warp direction.

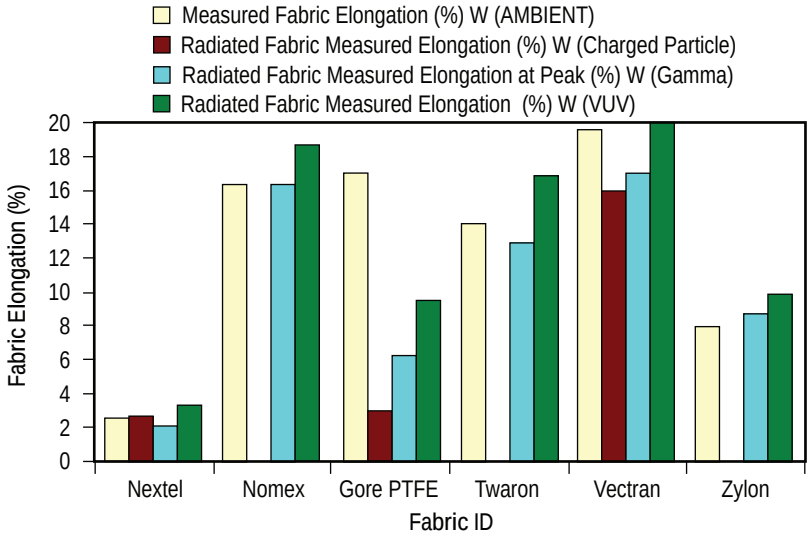

Figure 49. Comparison of fabric elongation (percent) before and after radiation (VUV)—warp direction.

2.5 Abrasion Testing

2.5.1 Standard Abrasion

The resistance of fabrics was determined by a Custom Scientific Instruments (CSI) Stoll Quartermaster universal wear tester according to the ASTM D-3885 standard test for abrasion resistance of textile fabrics (flexing and abrasion method).[14] The resistance to abrasion is affected by many factors, such as the inherent mechanical properties of the fibers, the dimensions of the fibers, the structure of the

yarns, the construction of fabrics and the finish type. The abrasion resistance of fabrics as measured by this method is generally only one of the several factors contributing to durability. In this test, three fabric samples, cut in 3- by 8-inch sections both warp and filling direction, are subjected to unidirectional reciprocal folding and rubbing over a bar, under 5 lb in weight. The sample is placed between the pressure (upper) plate and reciprocating (lower) plate. The upper plate moves forward and backward under pressure on the surface of the bottom plate, that is covered by sandpaper (grit size 220). Furthermore, 2.5-mm soft fabric padding is placed under the sample to give conformability to the sample. The number of cycles is recorded upon failure of the fabric, or after 1,000 cycles. The pictures of the fabrics taken after various numbers of abrasion cycles are shown in figures 50 through 58. Gore PTFE left some little particles on the sandpaper surface but the general surface was not damaged. Vectran and Twaron were in very good condition even after 1,000 cycles as seen in figures 55 and 56. Although the failure criteria are somewhat subjective, it can easily be seen from the photographs that Nextel samples had failed after 350 cycles, and Nomex and Zylon fabrics had failed after 500 cycles (see figs. 50, 52, and 57).

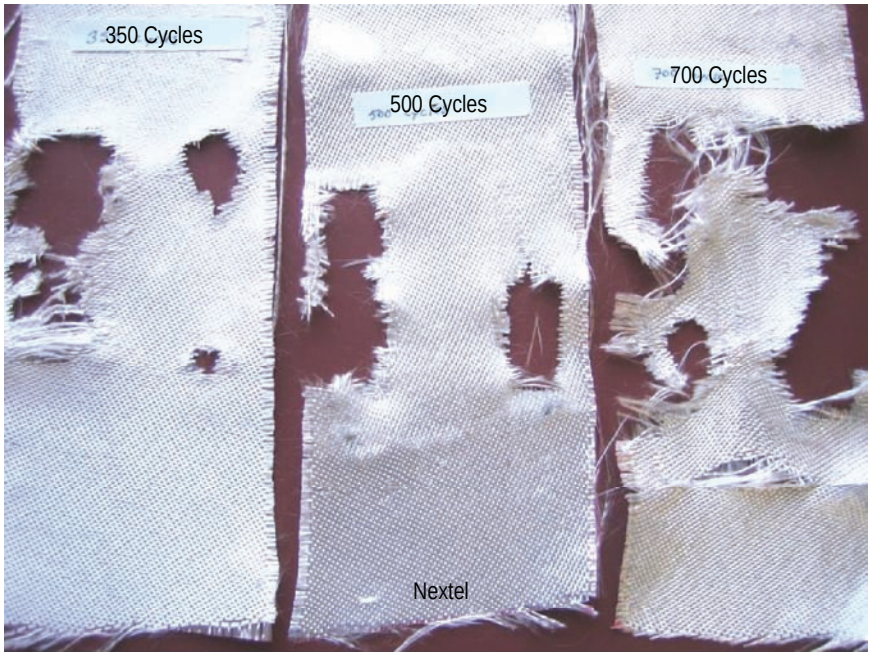

Figure 50. Damage on Nextel fabrics after various numbers of abrasion cycles.

2.5.2 Tumble Abrasion Testing with Regolith Simulant

Because lunar regolith is known to be extremely sharp and abrasive (due to meteor impact fracturing and lack of weathering), fabric samples were evaluated for abrasion with regolith simulant. Approximately 2-inch-diameter by 10-inch-long bags were sewn and seamed on three sides leaving ≈0.50-inch clearance from the cut edge. The bags were then reversed putting the seams on the inside and loosely filled with regolith simulant. An external seam then closed the narrow end of each bag. Three bags were made from each fabric type. The filled bags were shipped to Johnson Space Center (JSC), and tumble testing was performed by adapting a JSC procedure intended for abrasion testing

Figure 51. Sandpaper used in Nextel fabrics for abrasion.

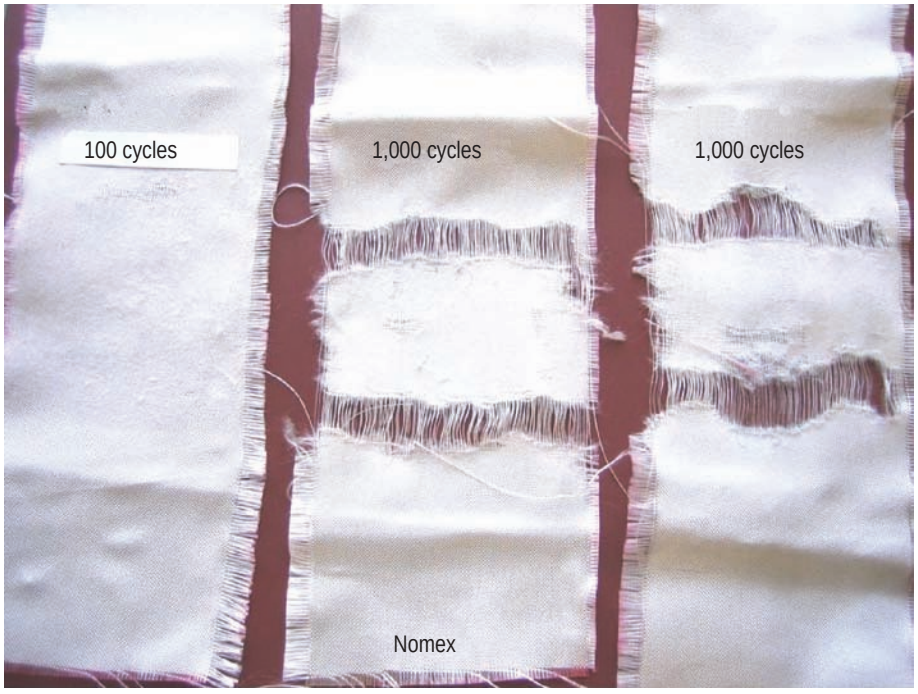

Figure 52. Damage on Nomex fabrics after various numbers of abrasion cycles.

Figure 53. Sandpaper used on Nomex fabrics for abrasion.

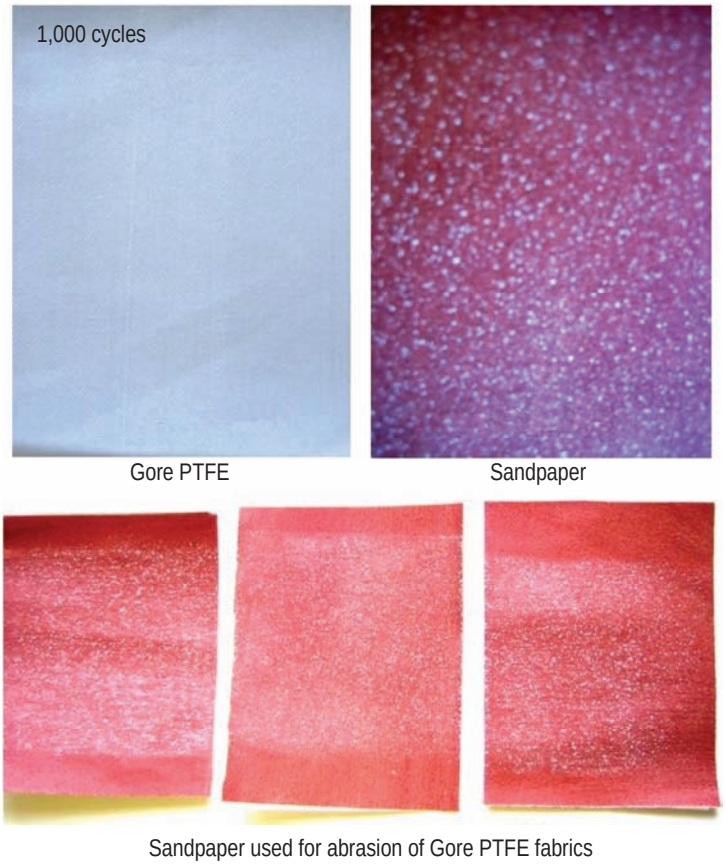

Figure 54. Damage on Gore PTFE fabrics (1,000 cycles) and used sandpaper.

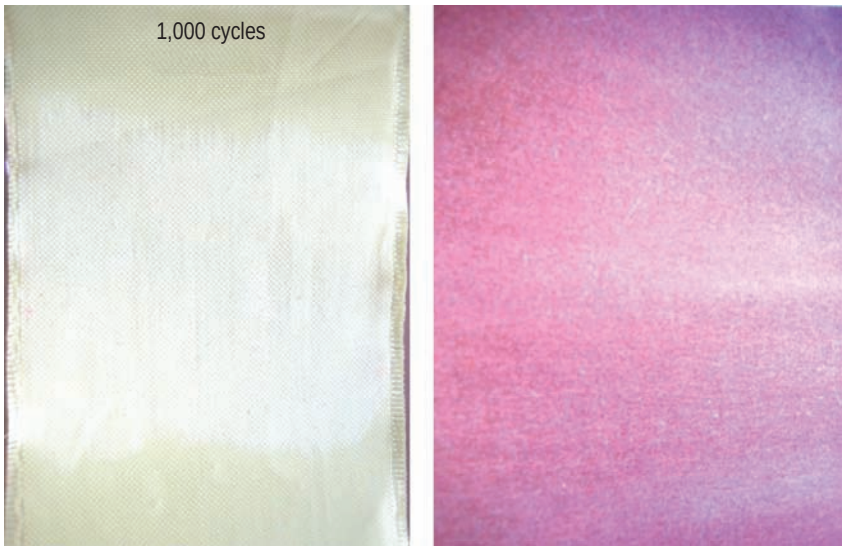

Figure 55. Damage on Twaron fabric (1,000 cycles) and used sandpaper.

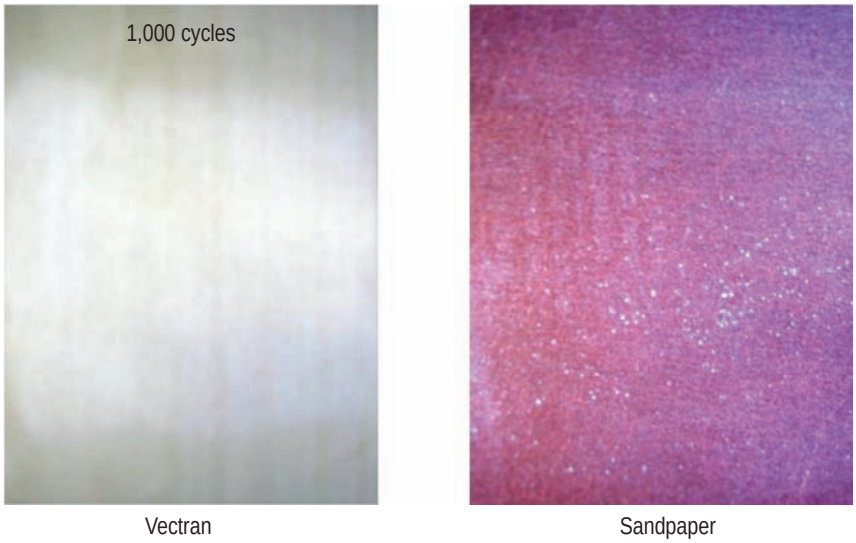

Figure 56. Damage on Vectran fabric (1,000 cycles) and used sandpaper.

of space suit fabric.[19] Pictures of the tumble tester are shown in figures 59 through 61. For the first test sequence, one bag of each fabric was placed in the tumbling drum along with regolith simulant on the outside of the bags, and the drum was rotated at 13 rpm for 1 hr. Subsequently, the remaining two bags were placed in the drum and were tumbled for 1 hr. The fabrics were examined for damage and the seams were carefully ripped out. The fabrics were then gently shaken in a pail of water to dislodge

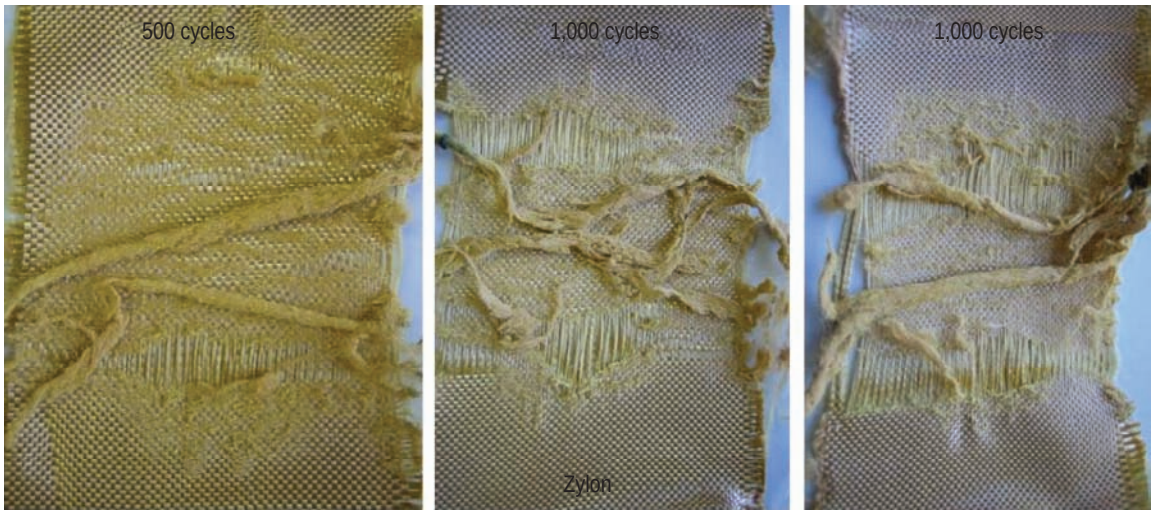

Figure 57. Damage on Zylon fabrics at various numbers of abrasion cycles.

Figure 58. Sandpaper used for Zylon abrasion.

the regolith simulant. After this gentle cleaning, the fabrics were allowed to dry, examined for damage, and photographed. As seen in figures 62 through 67, Nextel suffered the most damage and Gore PTFE suffered a little damage at one seam. The other fabrics showed little abrasion damage. With Zylon, there was some weave distortion and slight abrasion, but little significant damage.

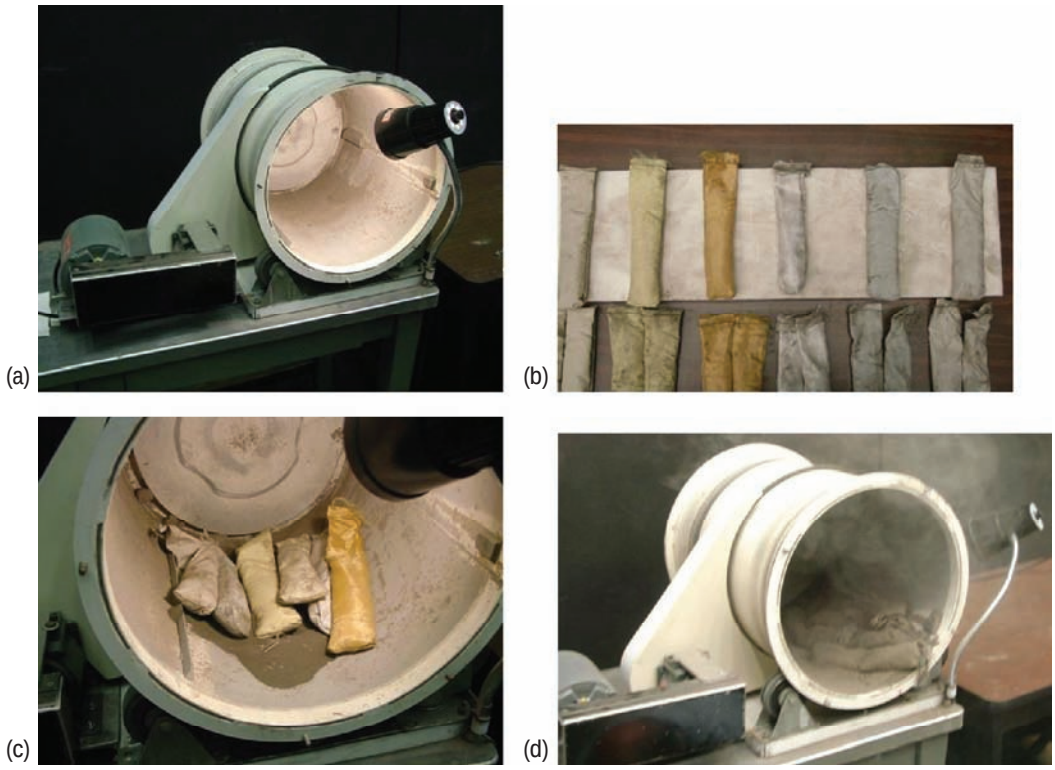

Figure 59. Tumble testing: (a) tester, (b) bags filled with regolith, (c) bags ready for testing, and (d) just opened tester after tumbling.

Figure 60. Bags in tester with regolith stimulant after tumbling.

Figure 61. Damage to Nextel caused by sewing and tumbling.

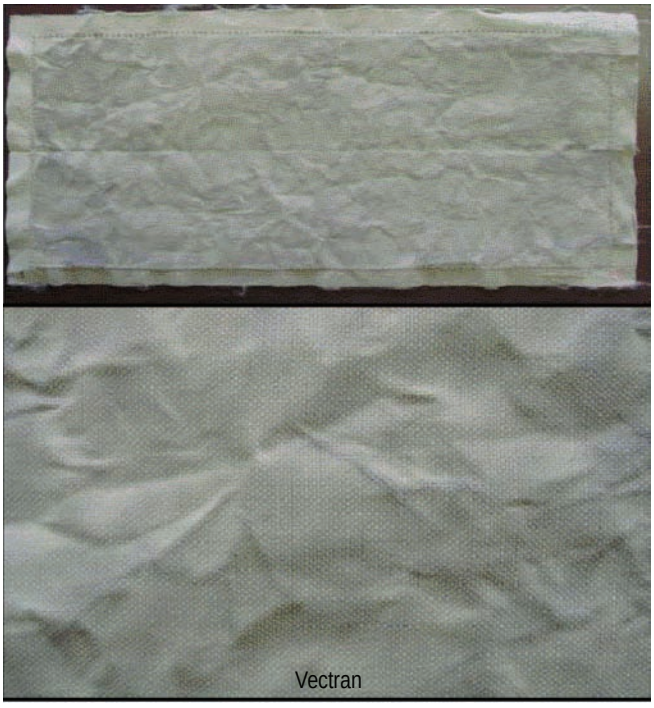

Figure 62. Tumble abraded Vectran sample.

Figure 63. Tumble abraded Gore PTFE sample.

Figure 64. Tumble abraded Nextel sample.

Figure 65. Tumble abraded Nomex sample.

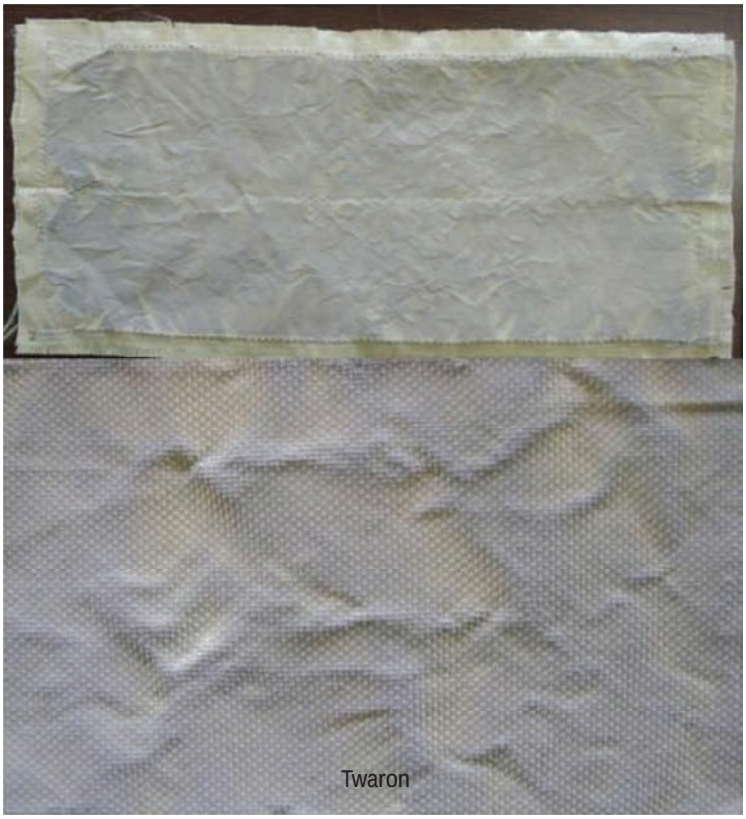

Figure 66. Tumble abraded Twaron sample.

Figure 67. Tumble abraded Zylon sample.

2.6 Hypervelocity Impact

2.6.1. Hypervelocity Impact Testing

Meteoroid and orbital debris impacts are a serious concern for spacecraft in orbit. More than 9,000 objects are being tracked, with millions of additional particles too small for radar or telescopes to track. These particles travel at hypervelocity speeds, with an average velocity of 10 km/s for orbital debris and up to 72 km/s for meteoroids. Meteoroids and space debris can puncture manned spacecraft, pit windows and telescope mirrors, and damage solar arrays and thermal radiators.

There are also risks on the lunar surface. Small particles, such as lunar dust up to slightly larger sized particles, can impact habitats that are on the lunar surface. These particle impacts must be studied and understood. The testing described below is a first look at the effects of these kinds of impacts on various candidate materials for proposed lunar habitat structures.

2.6.1.2 Test Equipment. To quantify the damage or to qualify debris protection systems against small particles, MSFC utilizes the micro light gas gun (MLGG). The MLGG (fig. 68) is capable of accelerating small particles (0.1- to 1.0-mm-diameter) to velocities of 3 to 10 km/s. The test chamber can handle targets on the order of 1-m in diameter. The average projectile velocity is measured with each test using photodiodes, but this method is being upgraded to ultra high-speed photographic technology.

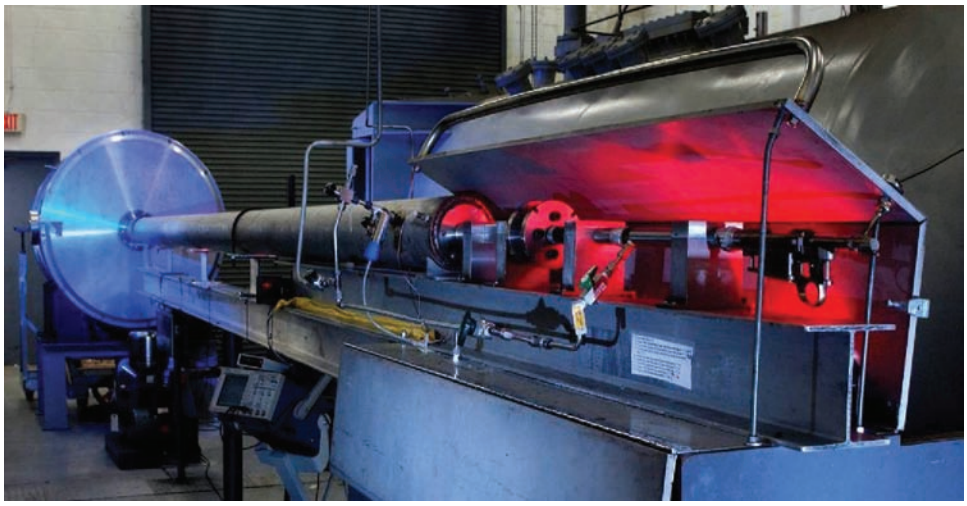

Figure 68. Two-stage micro light gas gun.

In this test series, 1-mm-diameter aluminum spheres were used as the projectiles. Each sphere was accelerated to an average velocity of 7 km/s.

2.6.1.3 Procedure. One bag was made from each candidate material. For Vectran only, an additional bag was made and irradiated (sec. 2.4.2) before testing, and was called Vectran-R. Each bag (6 by 6 by 4 inch), once filled with cement powder to represent lunar regolith, was sealed with heavy-duty tape. Then each bag was pressed down to be packed as tightly as possible. Extra fabric material, if any, was clipped to take any slack out of the material. The front face of the bag was, at that point, smooth. Each bag was put into the chamber for testing and aligned using a laser. Procedures for firing the MLGG can be found in EM50-OWI-029.[20]

2.6.1.4 Results. The raw data from the impact testing is shown in table 13. Each bag performed well when impacted. However, Nextel appeared to pull away at the seams even before the impact. Nextel, Nomex, and Zylon bag materials stretched while packing, which may make them difficult materials to use for this purpose. Gore PTFE did well, but seemed to have a problem with dust coming through the material even prior to testing. Twaron and Vectran materials did the best, with Twaron having the smallest impact penetration diameter on visual inspection. The exposed Vectran-R seemed to have a smaller penetration diameter after the radiation exposure compared to that of the unexposed Vectran. The reason for this is unclear. To understand the results seen in this testing and to verify the "first look" results found here, more testing is required.

Note in the photos below (figs. 69 through 75) that the impact penetration is circled in red. The other penetration sites are from the two halves of the fly away sabot used in the test system and small fragments of the pistons that extruded through the high pressure section. These impacts were at a distance far enough from the projectile impact as to not cause interference.

Table 13. Raw data from impact testing of bag materials.

Material	Velocity (km/s)	Penetration/ Damage Diameter (mm)	Notes
Vectran	6.1	6	Slight fraying on edges of penetration.
Vectran-R	7.16	4	Almost no fraying of edge of penetration. Very clean.
Zylon	7.16	9	Slack in material taken up with clips before testing. Some fraying. Material looks pulled and stretched post-test.
Twaron	6.8	5	Small penetration diameter. Lots of fraying right at edge of penetration.
Nextel	6.8	8	Regolith material coming out of bag at corners. Corners are pulling apart. Material appears very frayed and pulled, even torn, at penetration site.
Nomex	6.8	6	Slack in material had to be taken up with clips before testing. Material very pulled and torn at penetration site.
Gore PTFE	6.8	5	Regolith material everywhere even before testing. Penetration very clean but with a lot of dust leaking from bag.

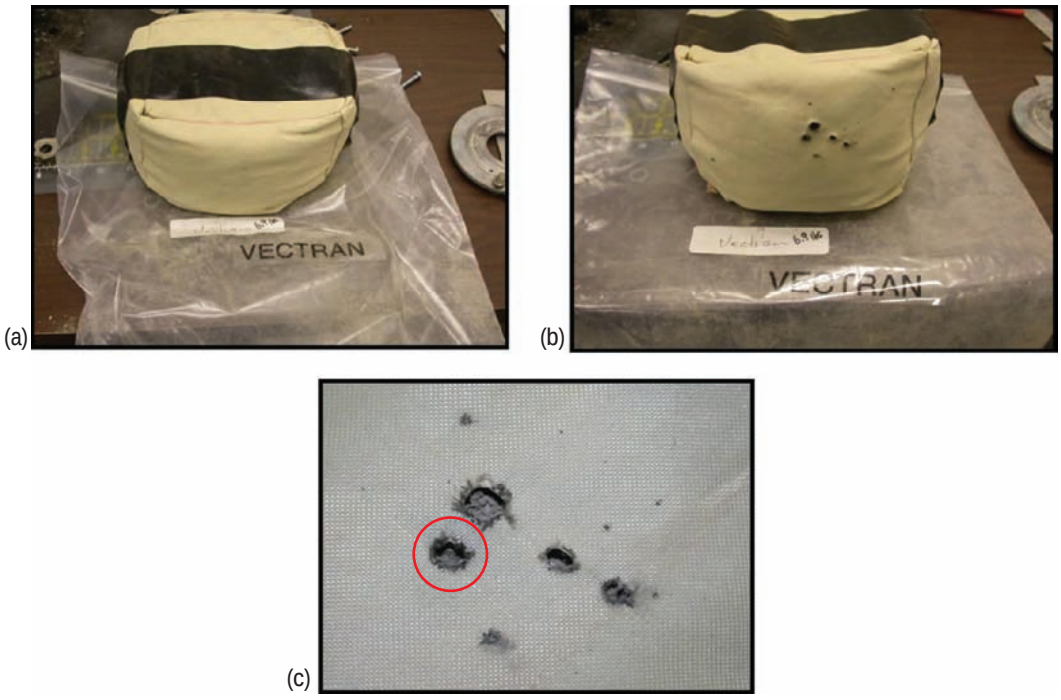

Figure 69. Vectran impact testing: (a) pre-test, (b) post-test, and (c) post-test close up.

2.6.2 High Velocity Impact Simulation

The smooth particle hydrodynamic code (SPHC) was used to simulate impacts of small particles on simplified models of regolith bags. The bag material was modeled by a 0.5-mm layer of Kevlar 49 and the regolith particles and impactor were modeled by a granite material in the SPHC material library.

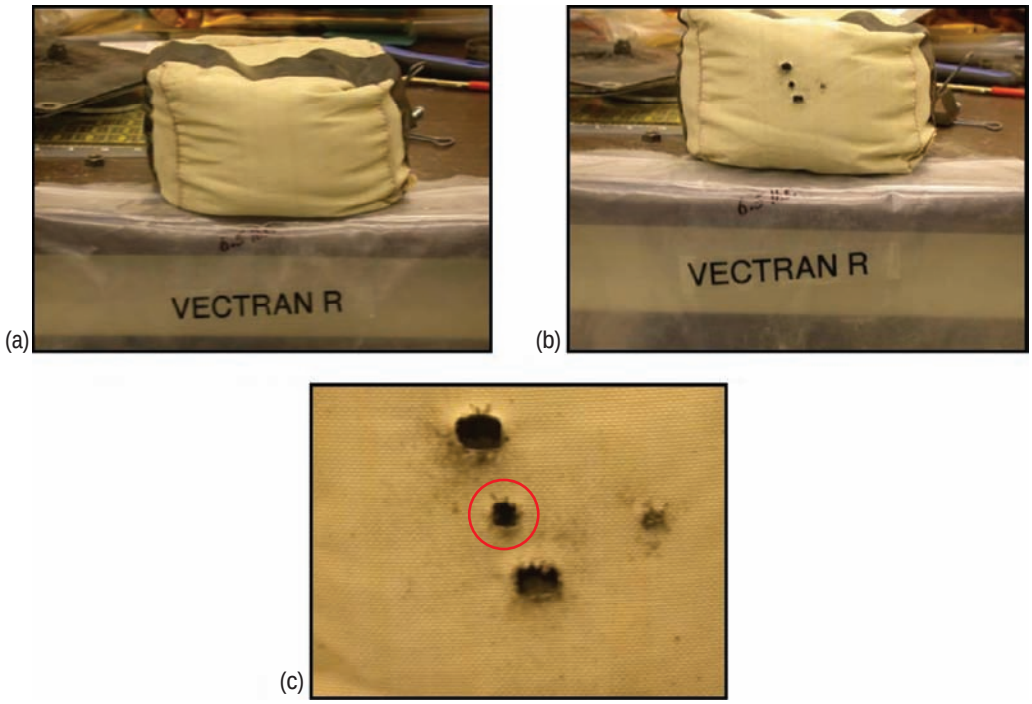

Figure 70. Irradiated Vectran impact testing: (a) pre-test, (b) post-test, and (c) post-test close up.

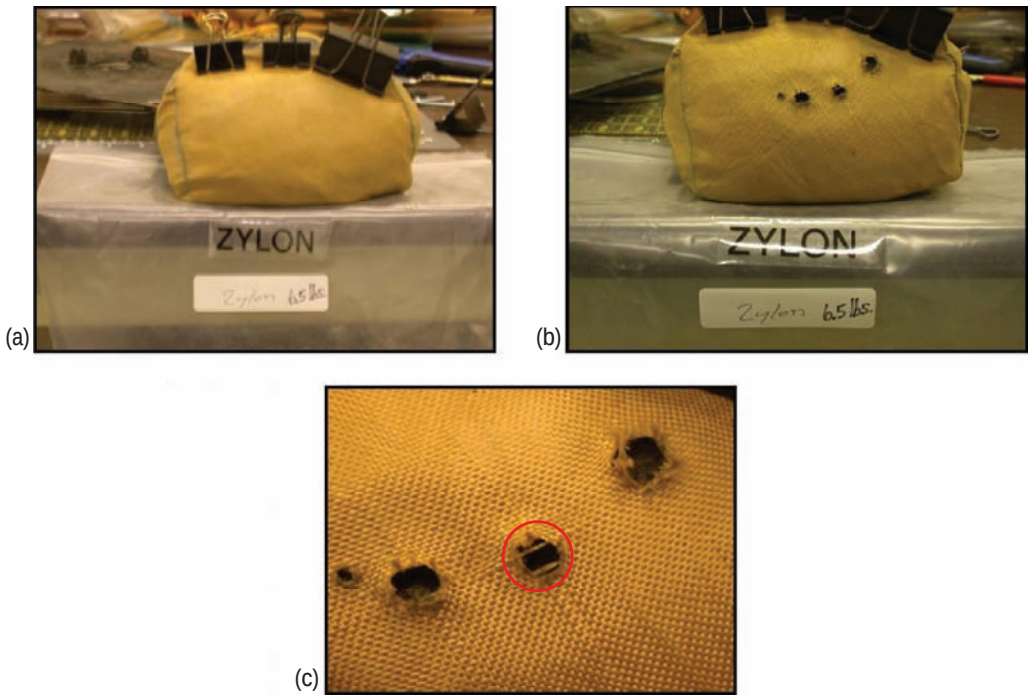

Figure 71. Zylon impact testing: (a) pre-test, (b) post-test, and (c) post-test close up.

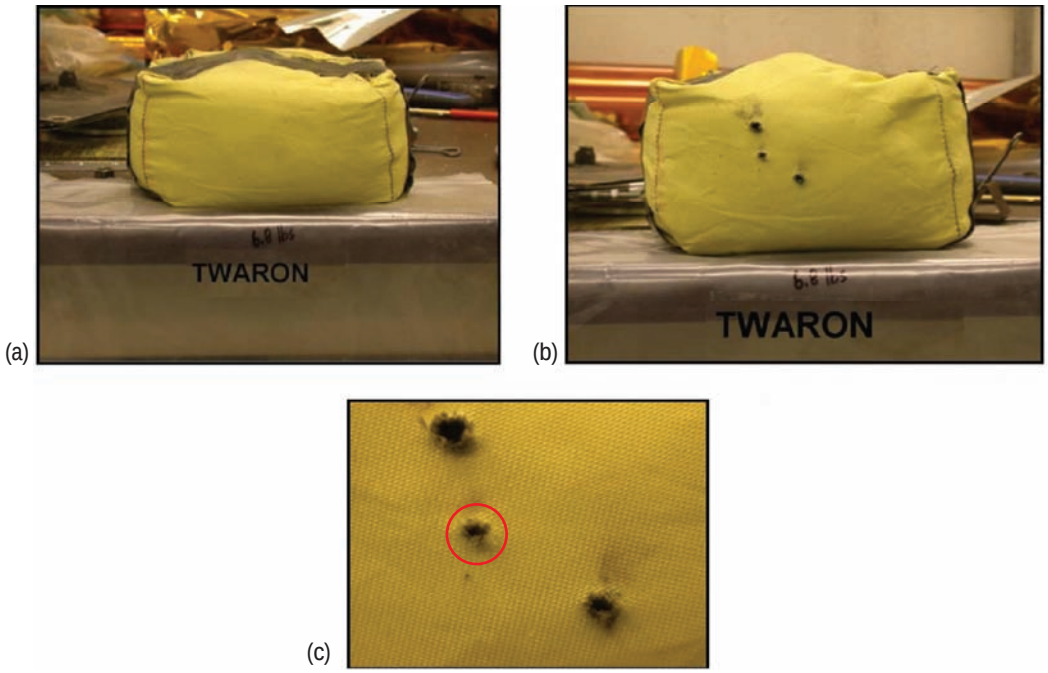

Figure 72. Twaron impact testing: (a) pre-test, (b) post-test, and (c) post-test close up.

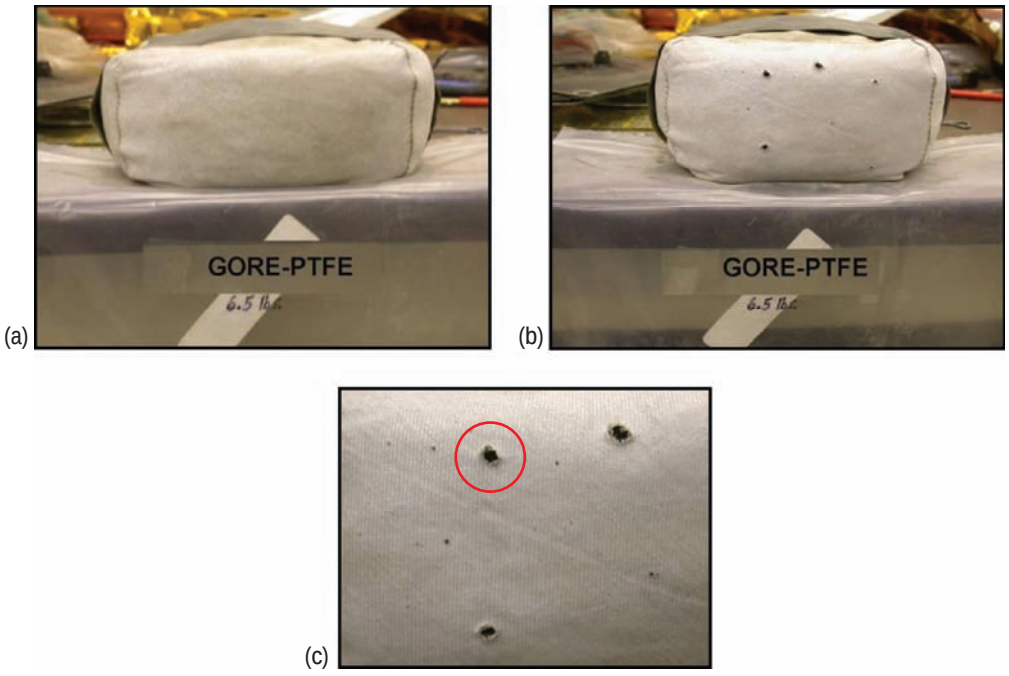

Figure 73. Gore PTFE impact testing: (a) pre-test, (b) post-test, and (c) post-test close up.

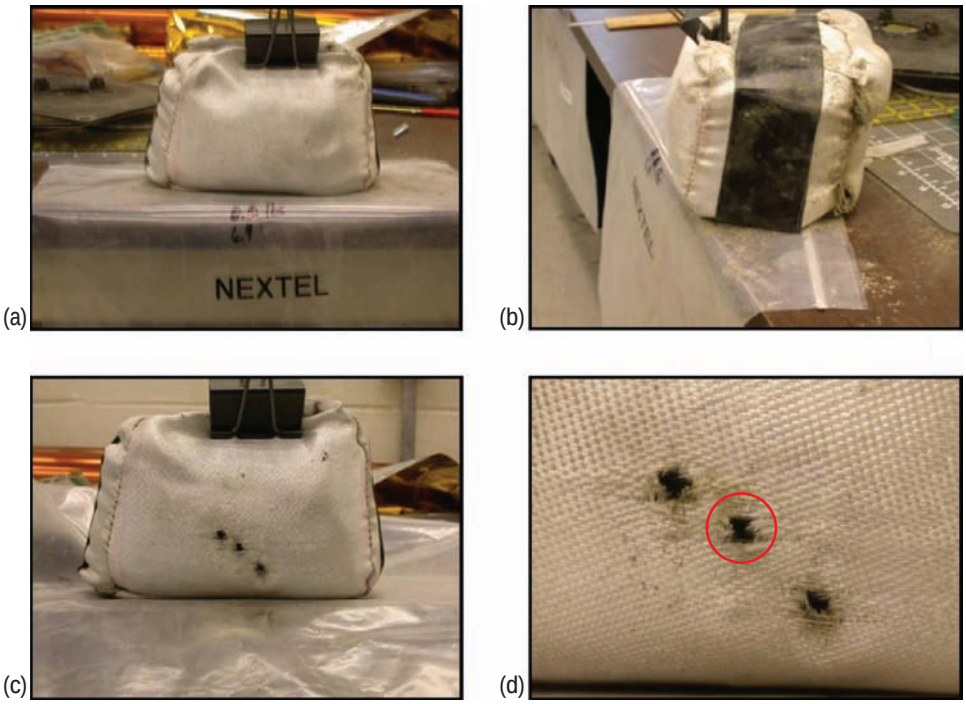

Figure 74. Nextel impact testing: (a) pre-test, (b) post-test seam split, (c) post-test, and (d) post-test close up.

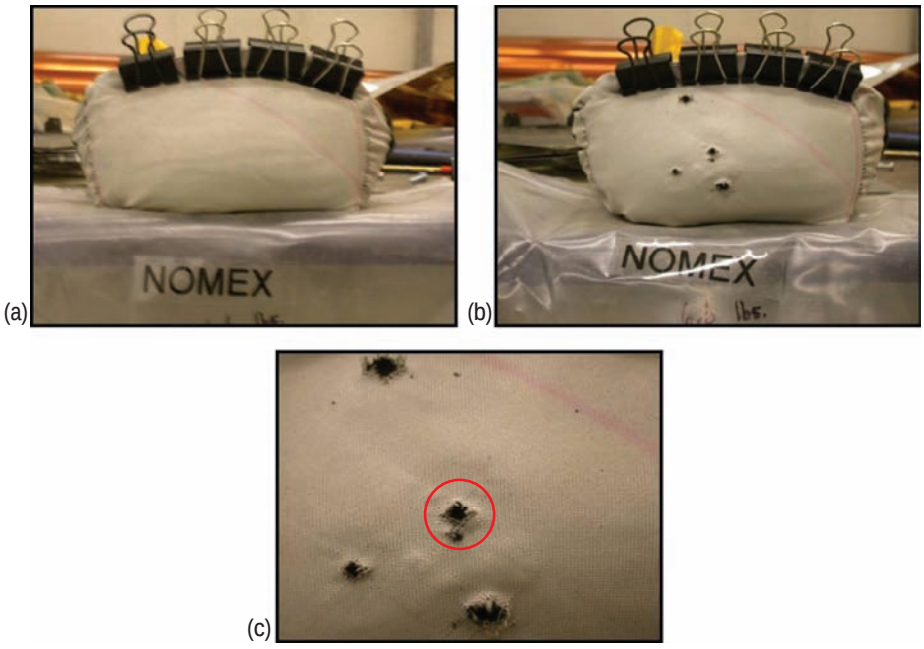

Figure 75. Nomex impact testing: (a) pre-test, (b) post-test, and (c) post-test close up.

Regolith particles were randomly oriented cubes, 0.1 mm on an edge, while the impactor was a 0.1-mm-diameter granite sphere traveling at 20 km/s (representative of the speeds of the ambient background meteoroid population). Figure 76(a) shows the setup prior to impact and figure 76(b) shows it at the 10 μs point. The color-coding indicates material phase, with red indicating vaporizing material. The simulation suggests that the hole caused by the impact will be surrounded by fractured matter, with a small portion of melted Kevlar; little if any regolith will melt, while much of it in the vicinity of the impact will be shattered into smaller fragments.[21,22] (M. D'Agostino, E-mail communication, January, 2006.)

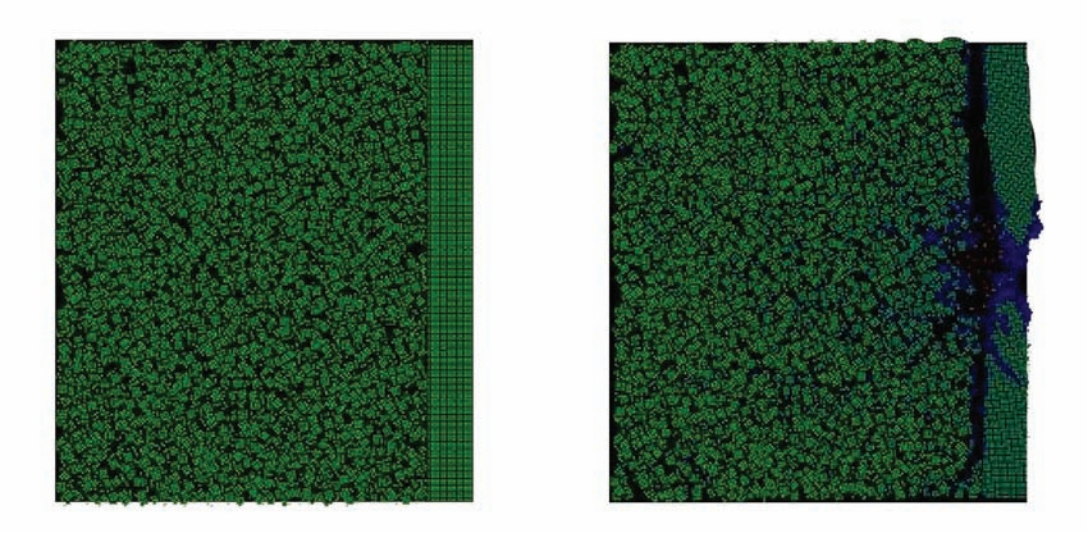

Figure 76. Simulation of meteoroid striking Kevlar bag filled with lunar regolith: (a) pre-impact and (b) post-impact.

3. DESIGN AND CONSTRUCTION OF GARAGE STRUCTURE

3.1 Introduction to Connected Fabric Bag Arches and Analogy to Masonry Arches

A lunar regolith bag arch can be erected very much like a masonry arch, as shown in figures 77[22] and 78. Masonry arches have been an important and much studied problem in the historical literature, and much can be learned from a review of masonry arch methods of design, analysis, and erecting. In this work each connected bag in figure 78 is filled with a soil-like material and packed so that it will act as a voussoir (or long brick shown in fig. 77).

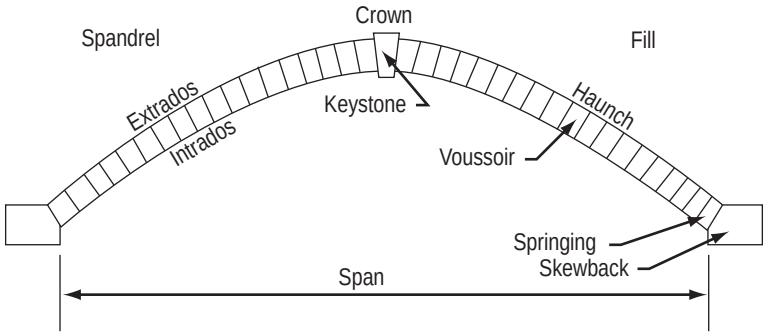

Figure 77. Form and terminology of a masonry arch.[22]

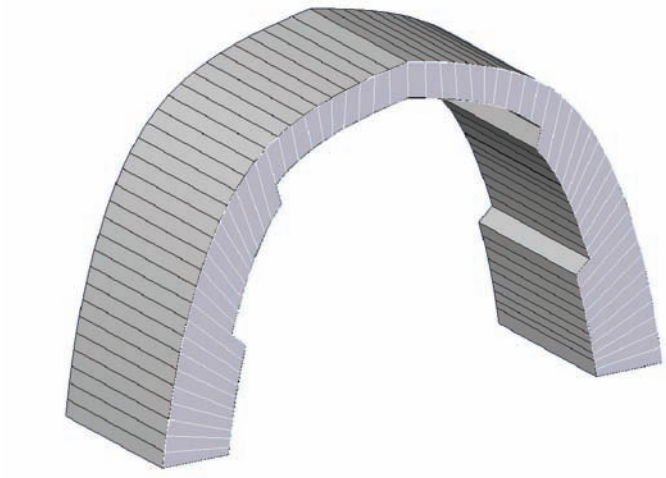

Figure 78. Arch formed from connected fabric bags filled with soil-like material (lunar regolith or vermiculite).

For any masonry arch to be stable, the line of compressive load or thrust (also known as a funicular polygon) should lie within the thickness of the arch (fig. 79). If the line of thrust lies outside the arch, then a joint will tend to open up or hinge (fig. 80) on the opposite side and area of contact between voussoirs (bricks) will be reduced. The failure of a masonry arch is due to the formation of hinges. The number of hinges (if any) and the location of hinges can be calculated, along with the compressive thrust loads, from basic equilibrium analysis. If a structure has three hinges, it becomes a statically determinate structure. If there are four hinges, the structure acts as a mechanism and the arch fails. It should be noted that masonry arches need to have strong foundations to support the horizontal and vertical loads at the bases.

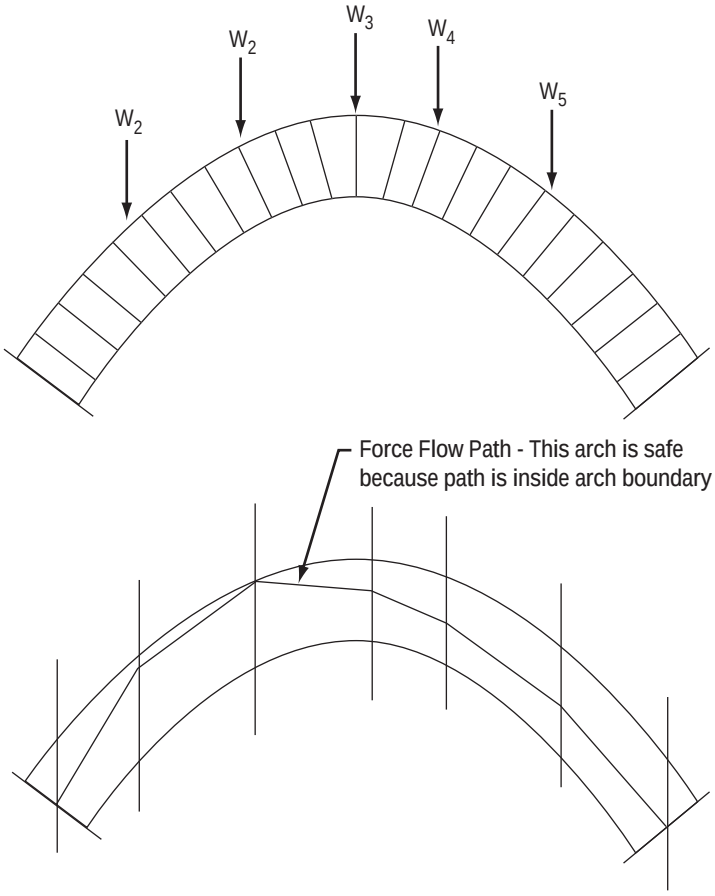

Figure 79. Masonry arch loading and compressive force flow path (aka line of thrust or funicular polygon).[22]

When calculating strength or designing a masonry arch, several important assumptions are made when performing a simple analysis:[22]

- Sliding failure between the bricks is assumed not to occur.
- Only compressive forces are transmitted across brick boundaries (bricks cannot transmit tensile loads).
- The bricks have infinite compressive strength.

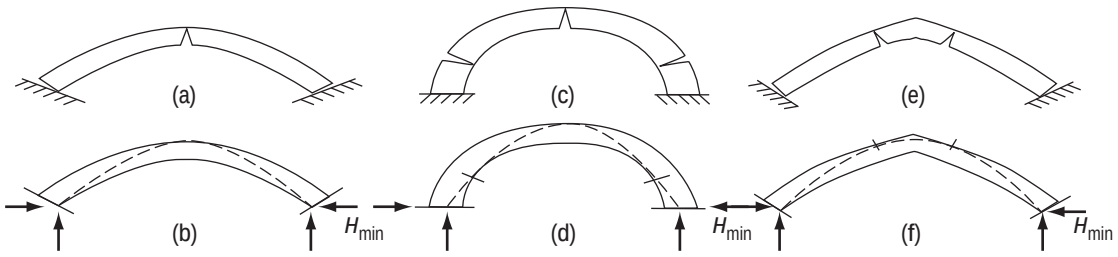

Figure 80. Masonry arches showing hinge formation where forces flow outside the arch boundary.

When extending these assumptions to the regolith bag structures shaped like masonry arches, the third assumption is the most critical. It is well known that for soil (such as regolith or vermiculite), strength depends on pressure to cause grains to interlock. If adequate soil pressure is not achieved, then the first assumption may be invalid as well. Even if the bags are tightly packed, the stuffed soil "bricks" may have a "spongy" character that may cause the arch to shrink under load. The approach in this study was to simply use the analytical techniques based on these assumptions, such as the funicular polygon,[23] as a design tool only, and to compensate with a relatively high factor of safety.

Masonry arches are erected following a standard procedure that has evolved over time. First, the arch is built on a temporary frame called the "centering." The last stone placed is the keystone. Then, the centering is removed, and the fill (dirt in the case of a bridge, or more masonry, in the case of an architectural feature) is very carefully placed and balanced on the arch. Similar erecting techniques are recommended here for connected bag arches.

3.2 Proof-of-Concept Preliminary Structures

3.2.1 Preliminary Considerations

A series of preliminary structures was designed and constructed at Auburn University as an insightful learning aid in the design of the garage prototype. Initially, sand was considered for filling the bags because it had bulk density similar to regolith. Bulk density is the mass of dry material per unit bulk volume. For sand, soil, and regolith, bulk density can be increased with pressure that reduces the void space between grains. Sand has a similar bulk density to lunar regolith ($\approx$1.5g/cm^3). Actual measured density for JSC-1 regolith simulant in the laboratory at Auburn was 1.59g/cm^3 and compression was $\approx$1 percent (to 1.61 g/cm^3).

On the Moon, gravity-induced loads from masses are one-sixth of what would be expected if the same structure were built on the Earth. Hence sand was judged to be excessively heavy and unwieldy for basic research on experimental lunar structures to be constructed on Earth. So alternative soil-like materials were sought that had a bulk density near one-sixth that of regolith. Vermiculite (an expanded clay mineral mined and manufactured by W.R. Grace Company) appeared to be the best alternative of the few available materials. Vermiculite has a specific gravity of 0.205, which is reasonably close to the

desired value of 0.27 based on one-sixth the density of regolith simulant. Vermiculite has the additional advantage that it is not a health hazard when wearing an efficient dust mask, and it is relatively inexpensive. It is not as abrasive as regolith, which may imply that it is a weaker soil because grains are less angular. So bags were filled with vermiculite (grade 5) instead of sand. The advertised bulk density is ≈10 lb/ft^3 (.16 g/cm^3). Vermiculite was measured in the lab at Auburn to have a density of 0.168 g/cm^3 and, when it was compressed, that value increased to 0.205 g/cm^3.

Filling the bags was a concern that is addressed below. A number of fill methods were considered, most of which are not recommended. A number of approaches from shovels, funnels and tubes, sandblasters, leaf blowers, etc. were tried with limited success. The best approach (selected and used only for the final prototype) was a hopper attached to a helical flexible screw conveyor system built by Hapman, Inc. The system is shown in figure 81, and consisted of a 12-ft-long Series 300 Hapman Helix™ conveyer (A Hapman Company product) with the following features:

- A stainless steel, flat wire helix (visible in fig. 82).
- An ultra high molecular weight (UHMW) polyethylene conveyor casing, 3-inch-diameter, complete with stainless couplings.
- A pusher drive/inlet assembly (fig. 82) fabricated of stainless steel. This includes a top access cover and a 2 hp, 208/230/460 V, 3-phase, 60 Hz, totally enclosed fan cooled (TEFC) drive motor operating through a gear reducer to provide a nominal auger rotational speed of ≈360 rpm.

Figure 81. Helical flexible screw conveyor system, with green hopper, black motor, and white tube, mounted on a jack stand for bag filling at different heights.

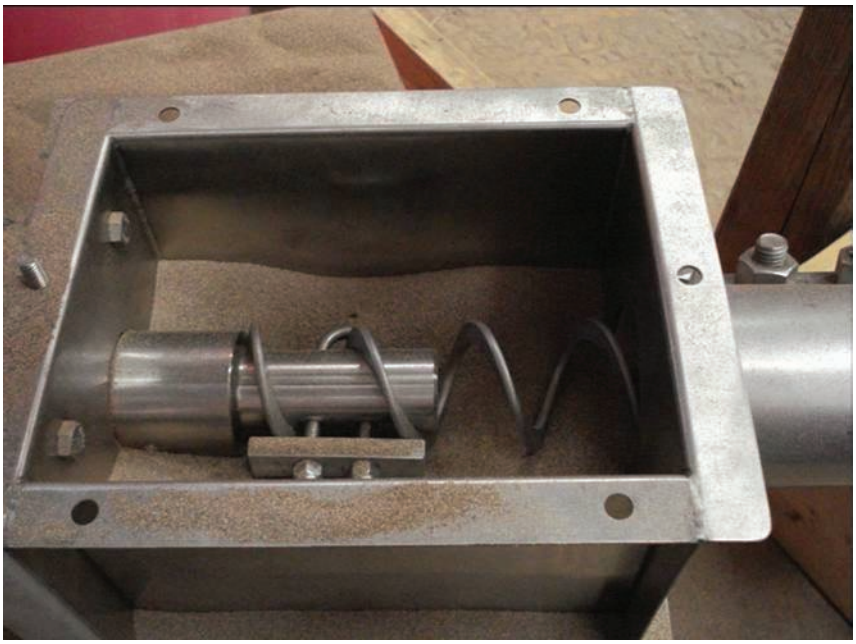

Figure 82. Opened receiving inlet, showing the helix.

- A stainless steel receiving inlet that is 6.5 by 9 inches with 0° pick-up, and a quick-release end clean-out cap.

The polyvinyl chloride conveyor tube that was selected is 12-ft long and somewhat flexible. It is inserted into the unzipped end of a bag, pushed all the way to the end of the bag, and withdrawn as the bag is filled with vermiculite.

Several constructions were evaluated before choosing the final design that was sewn by the subcontractor, Kappler Industries, and erected at MSFC. The first preliminary structure was the small center-connected bag arch that was cut and sewn from scrap fabric. The second was the large center-connected bag arch. The third was the top-connected beam.

3.2.2 Small Center-Connected Bag Arch

This simple structure, sewn from scrap fabric, consisted of eight bags each formed by two layers of fabric stitched together like an air mattress. On initial attempts, bags were filled with sand, but the sand was far too unwieldy and heavy to represent lunar gravitational loads. Hence all subsequent bags in this research project were filled with vermiculite. Bags were filled to capacity (causing them to round). A desired geometry for the bag arch was achieved by building on a catenary-shaped arch of aluminum (fig. 83). The legs of the bag arch rested on two tables, with sandbags acting as side foundations restricting horizontal motion. Once the aluminum arch was dropped, the bag arch maintained that shape.
The base length of the arch was 18 inches and the height was 16 inches. A total of 150 lb of sand were loaded on top of the structure as shown in figure 83 (only one sandbag is visible on top in the figure), and although the structure compressed, it did not collapse. It was noticed that the bags (also known as

Figure 83. Small center-connected bag arch (base length equals 18 inches, loaded with 150 lb).

voussoirs) bulged and stretched the fabric tight under load, and the voussoir contact width where neighboring voussoirs touched, increased with load, perhaps helping to improve the stability with increasing load. A funicular polygon (fig. 84) shows the structure to be stable based on the undeformed geometry and 150-lb load produced by three sandbags laid on top.

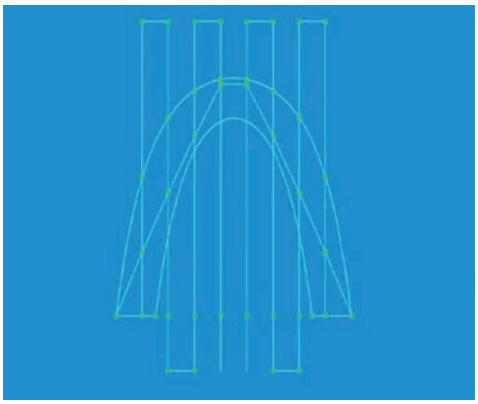

Figure 84. Funicular polygon of figure 83.

In figure 85 the base is widened to 20 inches and then the same 150-lb load is applied. The funicular polygon in figure 86 predicts hinging, that can be seen in the photograph in figure 85. Where a stretched seam is seen or felt with the hand, as in figure 83, there is a hinge opposite the seam. Fabric stretching and limiting the hinge opening prevent total collapse. The tensile strength of the fabric is preventing total collapse and adding stability. This geometry is called an “M-shaped configuration,” and it is stable because it stands, but it is less stable than the configuration of figure 83. This fabric and bag design could possibly be scaled up to make larger structures.

Figure 85. Small center-connected bag arch in "M-Shaped configuration" (base length equals 20 inches, loaded with 150 lb).

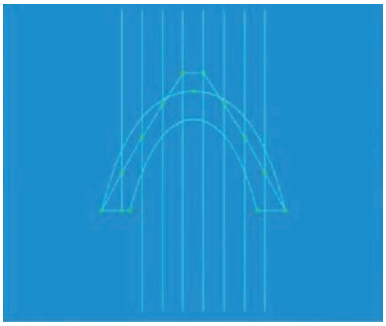

Figure 86. Funicular polygon of figure 85, predicting hinging.

3.2.3 Larger Center-Connected Bag Arch

The goal was to create a larger structure than the one shown in figure 83. The material used for this was surplus ballistic nylon, dimensioned and sewn as shown in figure 87. All but the top five bags were filled three-quarters full and positioned against a frame to provide shape. These bags served as the arch legs (fig. 88). The rest of the bags were fully packed by hand. Because the packing methods were not advanced at the time of erection, bags were loaded while laying flat on the ground, and then the entire structure was manually lifted onto the aluminum frame (needless to say this was very difficult). The bag arch collapsed shortly after removing the aluminum frame (figs. 89 and 90). It was difficult to achieve compression from one bag (voussoir) to the next across the top bags. This experiment showed that bag filling of large structures should probably take place as the bag arch is being built, and that there is a need for further investigation of better bag filling methods than hand filling in order to more tightly pack the bags, and of new techniques for erecting the structure. Even if these obstacles had been surmounted, analysis showed that the structure was close to being unstable under its own weight, because the arch was too wide at the base. The rounded shape of the center-connected bags may provide an easily hinged structure as well.

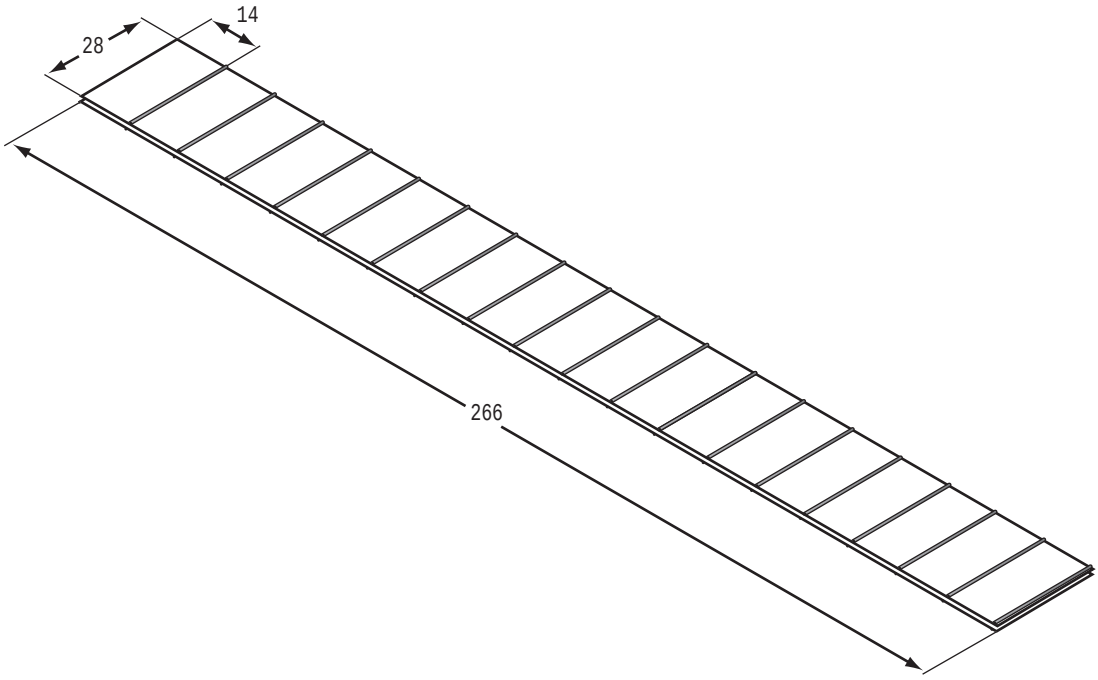

Figure 87. Center-connected bags geometry.

Figure 88. Erecting big center-connected bag structure.

3.2.4. The Top-Connected Bag Beam

The top-connected fabric configuration, constructed in this preliminary structure from ballistic nylon, offers advantages in both the erecting process and the strength of the structure. The unique feature of a top-connected configuration is a continuous layer of fabric that can resist tensile loads. The major advantage is during erecting, where a minimal frame is required, and secondly, the bag arch is more

Figure 89. Big center-connected bag arch with aluminum frame lowered prior to removal.

Figure 90. Big center-connected bag arch with aluminum frame removed.

forgiving of bags that are not completely filled. Some potential locations for hinges (on the intrados of the bag arch) are removed, making a stronger structure. To test this concept, a bag beam was constructed, shown as a computer-aided design (CAD) drawing in figure 91. In cross section, all bags were 6 by 12 inches. A plate was machined to cantilever the beam to ascertain if it could support its own weight, which it did, as shown in figure 92. Although much more analysis and testing could be performed here, this construction demonstrates the ability of the top-connected configuration to potentially

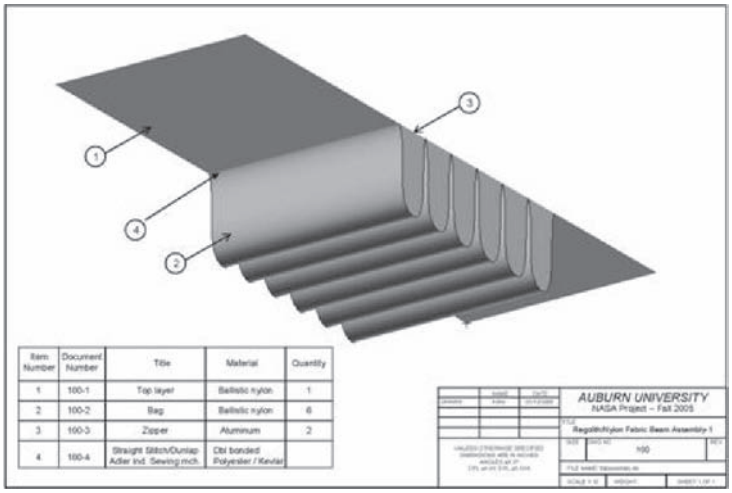

Figure 91. CAD drawing of top-connected bag beam.

Figure 92. Cantilevered top-connected bag beam held at one end and supporting its own weight.

support tensile loads and to maintain a bag arch geometry without a frame that may otherwise be impossible with the center-connected configuration.

3.3 Full-Scale Prototype and Erecting at MSFC

The full-scale prototype arch was sewn at Kappler, Inc. in Guntersville, AL according to the supplied design (figs. 93 and 94). The final structure was constructed from a coated Kevlar (type 159) fabric. The bag abrasion tests suggested that a tight weave was required to contain the fine particle-sized filler material, and that perhaps a coating would also be helpful. The fabric specification selected was

a 70 by 70 (220 Dtex) plain weave supplied by Lincoln Textiles (style 3041.062.02.000). It was coated with a layer of ethylene/vinyl acetate copolymer. This copolymer is often used as a hot melt adhesive for laminating. The uncoated fabric weight was 3.6 oz/yd^2 and the coating added about 3 oz/yd^2. The fabric proved to be impervious to the fine vermiculite and strong enough for this prototype. The seams were double stitched with a black polyester sewing thread (T 70 Anafil, 16-oz, bonded, from American and Efird, Mt. Holly, NC). The zippers were a standard urethane coated coil construction used for water repellent clothing and supplied by Kappler, Inc. During the construction and erection of the structure, there were no seam or zipper failures. Occasionally, loose threads became entangled in the zippers, but when these threads were removed, the zippers continued to function. The structure was erected at MSFC over several days, requiring the assistance of as many as five personnel at any one time. The purpose of this effort was two-fold: (1) to investigate methods of fabric construction and erection of a bag arch that may be able to serve as a standing lunar garage, and (2) to provide a standing structure at MSFC that could serve as a proof-of-concept and platform for test and observation. The prototype, with filled bags, was designed to stand on its own without external support (i.e., be stable), which it did, once the support system used for erecting was removed. A foundation support consisting of two 2- by 4-inch boards was left in place to guarantee support at the base and to prevent the legs from spreading. The prototype included 60 pockets in a top-connected configuration, which was envisioned, once erected, to look like figures 93 and 94, and included:

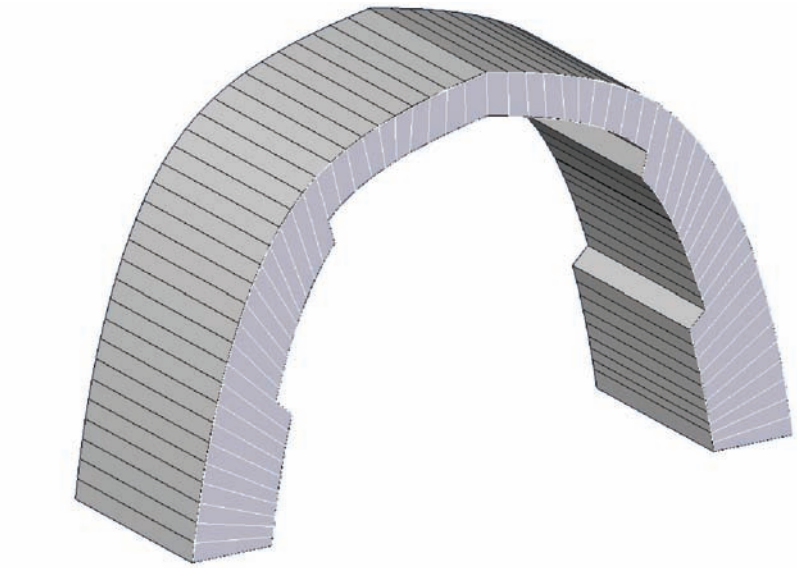

Figure 93. Concept drawing of arch.

- Twenty pockets at the bottom measuring 6 inches by 2 ft in cross section.
- Twenty pockets above the bottom pockets, measuring 6 inches by 1.5 ft in cross section.
- Twenty pockets that form the crest of the arch, measuring 6 inches by 1 ft in cross section.

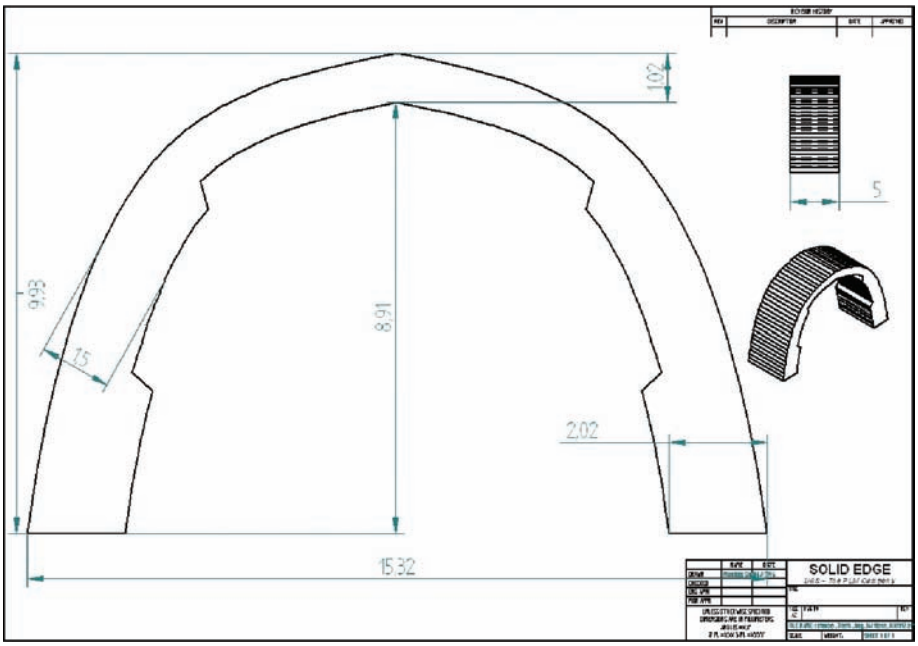

Figure 94. Front dimensioned view (dimensions in ft).

Prototype arch designs of a 60-bag catenary shape (see fig. 94) were analyzed using the funicular polygon technique. Under its own weight, the arch shown in figure 94 demonstrated that it could hinge (fig. 95). However, taller configurations were found to be stable (fig. 96), and should be able to support more weight.

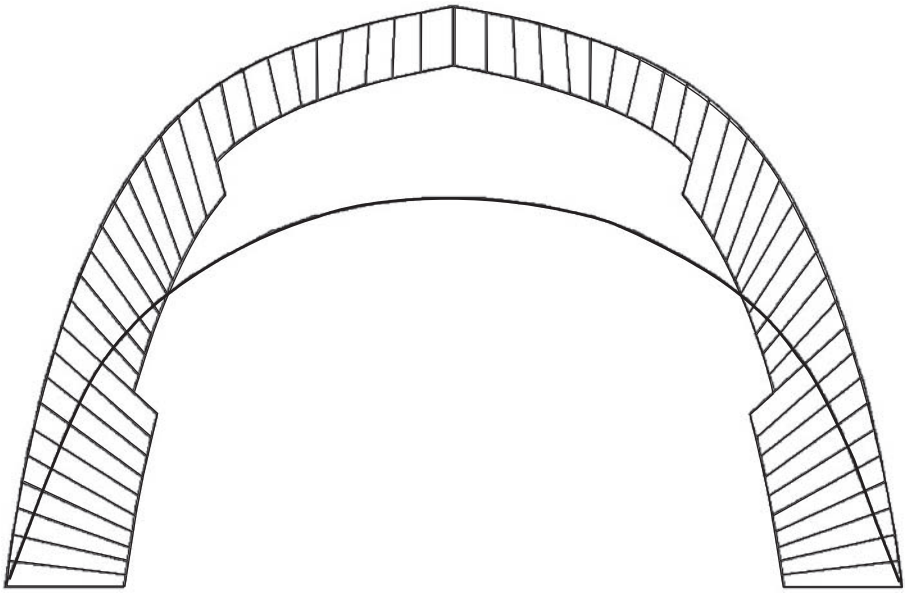

Figure 95. Funicular polygon showing possible hinging in arch design.

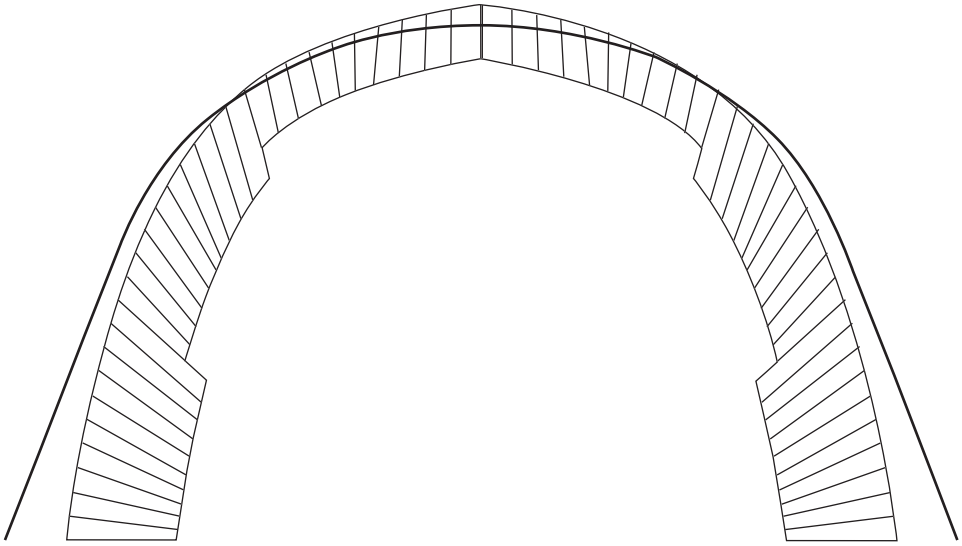

Figure 96. Another set of possible hinge locations.

Stability analysis using the funicular polygon (fig. 95) shows that the structure in figure 94 can possibly form hinges. The analysis assumed that no applied forces were acting on the system except vermiculite weight. One location was identified as lying between bags 15 and 16 starting from the left on the figure. Considering that this structure is symmetrical, the analysis indicates that hinges will form on the other side as well. Figure 95 shows that hinges appear to form around bags 15 and 16.

As can be seen in this figure, the hinges will tend to open towards the outside of the bags, but since these bags are top-connected by a stiff fabric layer, the fabric layer will prevent any opening, therefore not allowing a hinge to form. This shows that this configuration can be made stable using the top-connected bag construction. Another analysis for a wider base indicates that hinges can form near bags 20 and 21. This formation of hinges is shown in the figure 96. These hinges will open on the inside of the bags, where there is no connecting fabric layer.

Another configuration was analyzed to evaluate its stability. The height was increased and the width was decreased. The actual dimensions are shown in figure 97.

Analysis on this structure shows that the funicular polygon lies inside the structure, making the structure stable. Figure 98 shows the funicular polygon for this configuration. Increasing the arch height usually improves stability.

3.3.1 Erecting the MSFC Top-Connected Bag Arch

Only 46 of the 60 bags were required for building at MSFC. This size fitted within the available construction space, achieved a sufficiently large structure for presentation, shortened the time to erect, and also demonstrated how the extra 14 bags could potentially be used to serve as supplemental supports. Figure 99 shows a structure that is designed to be stable. Only three large bags were used as bottom bags. A wooden frame shown in figure 100 was constructed to serve as a guide for erecting toward

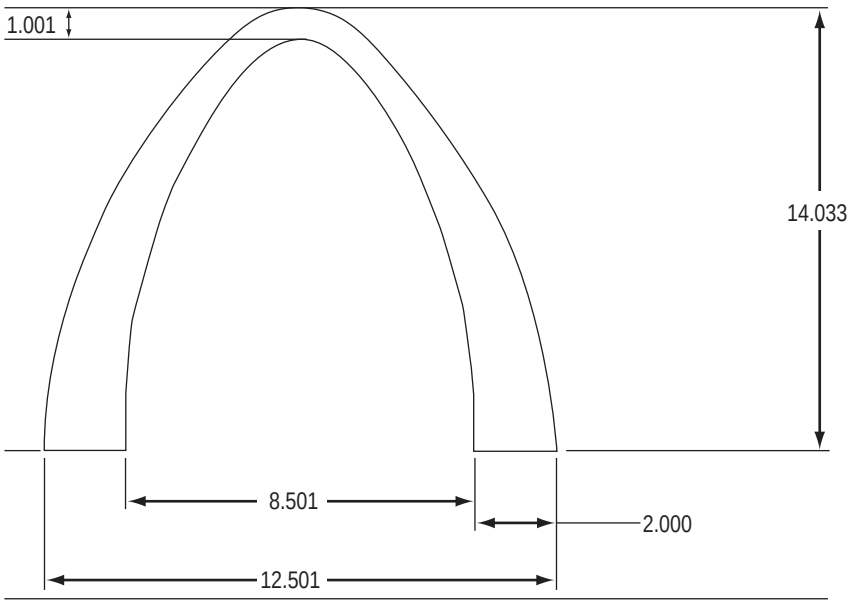

Figure 97. Taller design (dimensions in ft).

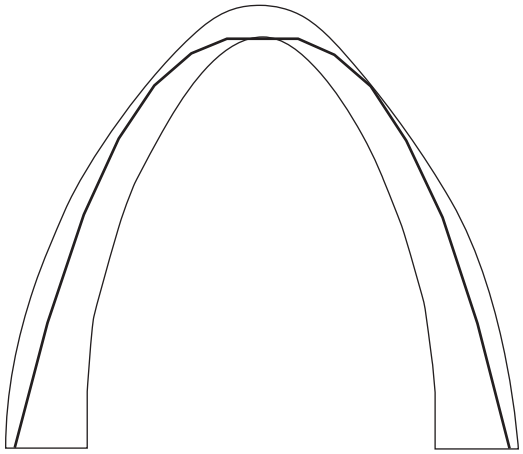

Figure 98. Funicular polygon of the 60-bag taller, more stable structure.

the approximate catenary shape at five points, where pipes were placed on the frame for the fabric to hang (note that in the top-connected bag arch, the pipes provide minimal support because of the bending stiffness that this construction offers). Two by fours attached to the bottom and sides of the frame (not visible) served as the foundation, preventing the bottom bags from slipping to the left or right. Actual pipe locations are compared to design dimensions in table 14.

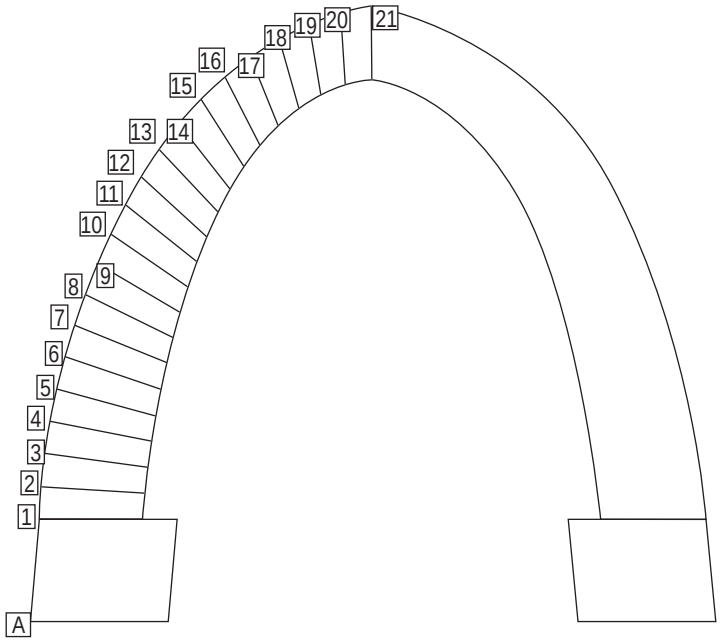

Figure 99. CAD model template to guide erecting.

Figure 100. Air-filled 46-bag structure (five pipes guiding bag filling).

Table 14. Construction coordinates of numbered points (inches).

Point	X	Y	Actual Pipe Locations
A	0	0	
1	1.45	18	
2	2.151	23.746	
3	2.985	29.475	
4	3.9	35.18	
5	5.1	40.857	
6	6.4	46.49	
7	7.9	52.08	
8	9.6	57.61	
9	11.59	63.06	
10	13.806	68.411	Lower Level Pipes: x = 14.5 Inch, y = 70 Inch
11	16.31	73.63	
12	19.129	78.687	
13	22.29	83.536	
14	25.817	88.127	2nd Level Pipes: x = 25.7 Inch, y = 88 Inch
15	29.724	92.399	
16	33.56	95.88	
17	38.66	99.73	
18	43.65	102.65	
19	48.913	105.087	
20	54.39	106.955	
21	60	108.287	Top Pipe: x = 60 Inch, y = 108 Inch

After air-filling the bags, the bags were filled with vermiculite from bottom bags up. Bags were filled using a Helix™ flexible screw conveyor system (a Hapman product), which can be seen in figure 100. The white pipe contains a helicoid screw (without a center core tube), rotated by a motor that feeds and forces vermiculite into the bags. This pipe was inserted into the bag to within ≈1 ft of the bag end, and the motor was turned on to rotate the screw. As vermiculite flowed out, the tube was slowly and incrementally pulled from the bag. This operation was labor-intensive, requiring human assistance to distribute the vermiculite as it came out of the tube into the bag (fig. 101).

Lower bags were filled and formed into a roughly rectangular shape (fig. 102), as personnel tried to provide bag angle (notice the black zippers) as the structure grew.

Filling the top 20 bags required a different technique. Unfilled bags hang down from the top fabric, and cannot be filled to a rectangular shape and maintain soil strength because of the looseness of the bag. Therefore, the top 20 bags must be filled to capacity with vermiculite, which causes them to round. With the top three bags unfilled, the topmost filled bags were nearly touching, making it difficult to fill the top three bags. The maximum amount of material that could be placed in a bag was restricted by the

Figure 101. Bag filling process.

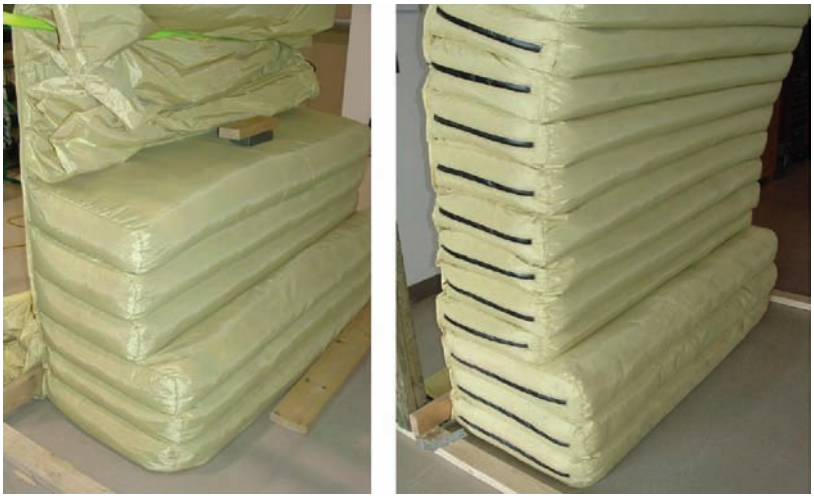

Figure 102. Rectangular packed bags.

Helix system, which was limited to relatively low compaction pressures due to the stiffness and strength limitations of the relatively flexible and shaftless helicoid. This low compaction pressure contributed to the top three bags not filling to the desired pressures and fullness. It was impossible to reach into the space and pack the bags by hand. The final erected prototype is shown in figure 103 (front view) and figure 104 (rear view). Note that in both views the pipes have been removed from their two by four supports, so the structure is standing without external support. The structure did settle ≈2 inch once the top three pipe supports were removed.

Figure 103. Front view (dimensions: 106-inches height, 118-inches external width at base, 65-inches internal width at base, 66-inches depth—front to back/zipper side to non-zipper side).

Figure 104. Rear view (note the zippers).

Review of the standing structure and the process of erecting showed the following:

(1) The left side of the structure in figure 103 (right side in fig. 104) is the "good side." It was built and maintained the catenary shape very closely to the design specifications, except for the top-most bags.

(2) The right side of the structure in figure 103 (left side in fig. 104) is the "bad side." Several flaws were found that were a result of bags not being filled to capacity.

(3) Figure 105(a) shows several bags on the bad side with a flattened profile that lost the catenary-shape curvature. Bags slipped downward despite best attempts to erect the structure with a catenary shape; bag slippage was visible and occurred over a several second interval. Slippage is attributed to a shortage of vermiculite due to incomplete packing, which did not occur on the good side; the vermiculite grains may slide (shear) with respect to each other inside the bags. This situation is correctable (but difficult, given that zippers are only on one end) by hand-loading more vermiculite through an open zipper and forcing material into the bag with a plunger. Using an auger-type system that deposits vermiculite under higher pressure than the Helix would have been a simpler fix.

(4) Figure 105(b) shows a tightly filled bag; it bulges and exhibits a hardness that can be felt by applying finger pressure. Tightly filled bags are necessary to create bags with sufficient vermiculite strength. Part of the internal bag pressure is a result of loading from the bags above.

(5) Figure 105(c) shows another characteristic of a well-built structure with tight bags. Here it is difficult to insert a finger between the bags, implying that the bags are tightly packed with respect to each other. Compressive and shearing loads are transmitted without failure across the fabric boundary, from bag to bag.

(6) Figure 105(d) shows a characteristic of inadequately packed bags. Here it is easy to insert a finger between the bags—this may imply the beginnings of hinge formation. The bags themselves are loosely packed and are easily indented by applying finger pressure to them. The dark patch seen in the figure represents glue that was placed in between the bags as an experiment. If the glue had affected the structure, the glued fabric would have been in tension, and this was not the case.

In summary, the top-connected bag structure is stable if erected correctly—by filling the bags with sufficient pressure and using the masonry arch structural design principles. Recommendations and comments for future work are as follows:

- The auger system used in this study did not fill the bags to sufficient pressure. An auger with a central shaft would have provided higher pressure and a more stable structure. It would have been convenient to have a method for easily "topping off" bags with vermiculite once the auger was removed and filling was thought to have been complete. The top three bags were not filled completely.

- Other possible methods of erecting the structure could be simpler and more appropriate for erecting on the Moon. Sensors could be used to measure bag pressure and shape deviations during erecting, so adjustments can be made. Shaping of bags during and after filling was a challenging manual task.

- Analysis could be greatly improved by incorporating both fabric and regolith materials and their characteristics in the analysis, perhaps using nonlinear finite element analysis. Improved analytical methods could be used to optimize the design. Regolith and vermiculite soil strength parameters (determined by standard soil mechanics tests or the Lunar Sourcebook[7]) should be incorporated into the modeling, along with fabric strength parameters.

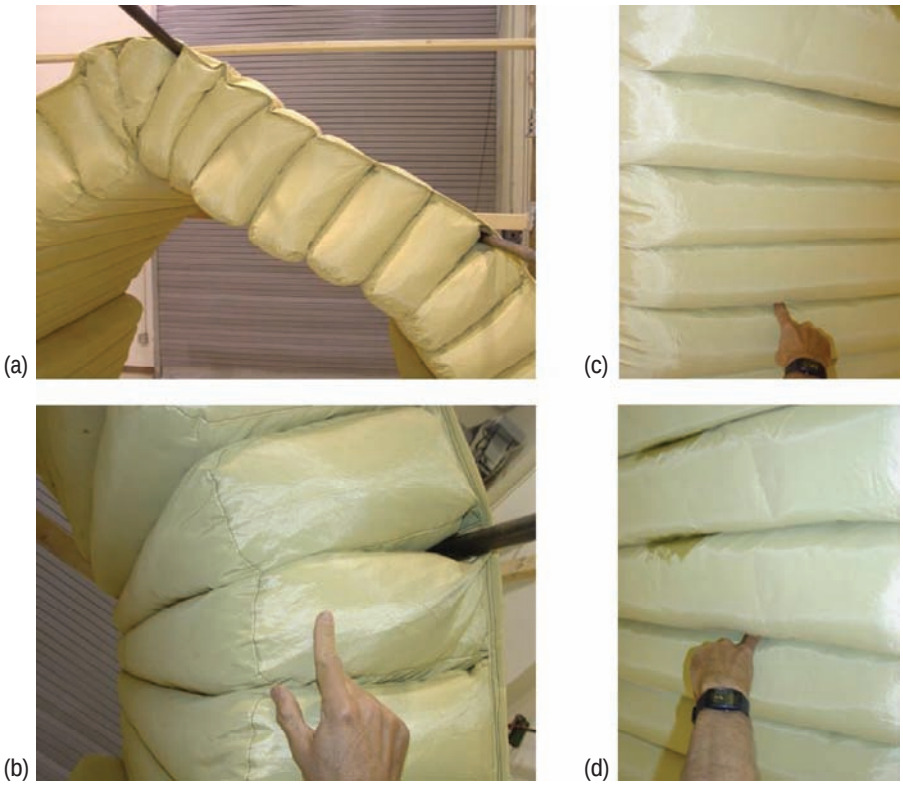

Figure 105. (a) Bags in a straight line, deviating from a caternary shape, (b) tightly packed, bulging bag, (c) tightly packed 1-ft bags on the good side—it is difficult to insert a finger between the bags, and (d) loosely packed bags on the bad side—the finger is easily inserted between the bags.

3.4 Berms and Blanketing

The center-connected bags can be easily maneuvered to create berms of various shapes. Of course, it is not as technically challenging to design and erect a berm from connected bags as it is for a garage or living space. Tightly filled or shaped bags are not required as they are for the freestanding arch. The 19 center-connected bags were all partially and loosely filled (as sandbags are), lined up end-to-end on the ground, and then stacked by pulling and then lifting the connected bags into various shapes for berms and blankets.

3.4.1 Berms

By partially filling the bags, berms can be constructed into many configurations, a few of which are: (a) a berm shaped like a wall, (b) a berm with a triangular cross section, and (c) a conical berm where construction proceeds by coiling the bags in stacked circles with radii that decrease with height, and bags following a path like the wire of a conical spring.

3.4.2 Blanketing

Blanketing is placing partially filled or unfilled bags on top of or around an existing structure for protection from radiation or impacting debris. A barrel laying lengthwise on the ground was wrapped by rolling it up in a blanket of 19 partially filled center-connected bags Then, a barrel laying lengthwise on the ground was blanketed on the top only with the 19 center-connected bags—one bag layer thick and later, two bag layers thick.

3.4.3 Cylindrical "Exhaust Plume" Berm

By tailoring the fabric geometry and stitch orientation, it is envisioned that a cylindrical berm, as drawn in figure 106, could be constructed. Two fabric layers could be cut with different inner and outer radii, stacked on top of one another, and stitched, with between bag stitches running radially toward the center. Bags would be filled one at a time, proceeding circumferentially, making one layer at a time. Bag filling could be automated and done simultaneously while erecting the berm. Figure 107 shows that it was still possible to create a cylindrical berm using the 19 center-connected bags. This was accomplished by vertically orienting the seams between the bags so the seams could act as hinges.

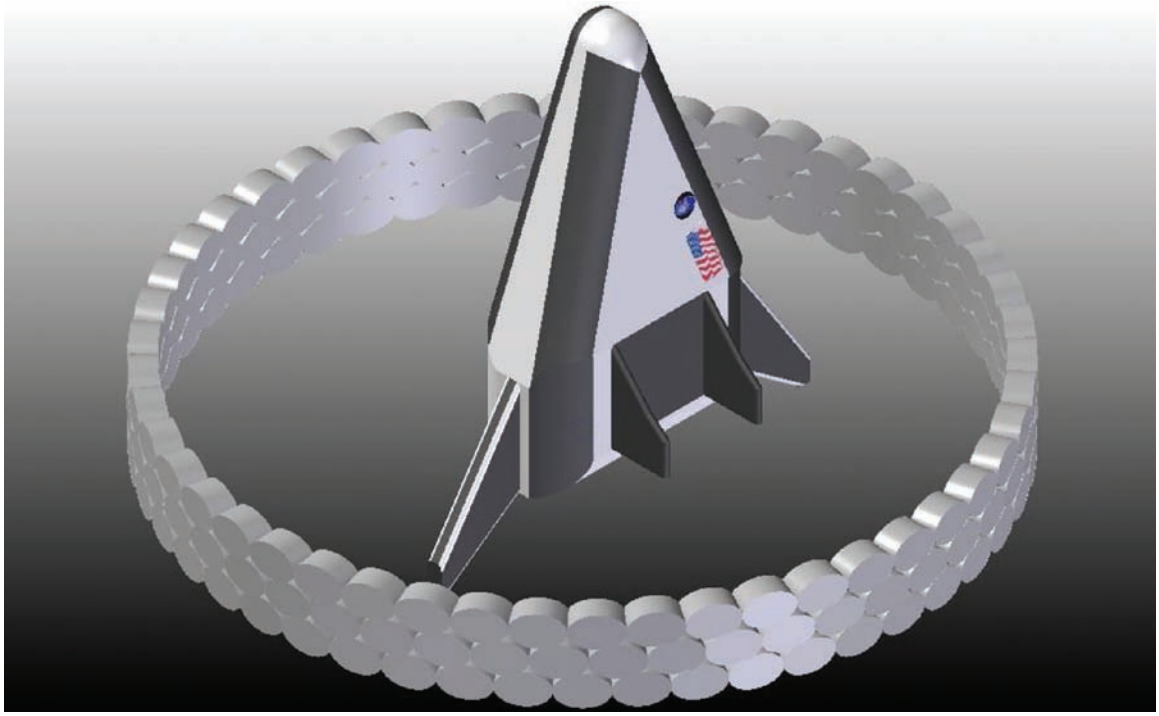

Figure 106. Rendered CAD conceptualization.

Figure 107. Berm configuration using 19 partially filled center-connected bags.

4. CONCLUSIONS AND RECOMMENDATIONS

Upon completion of this initial materials testing and prototype development program, the following conclusions and recommendations are offered:

(1) Vectran (which tested best overall) should be carried into the next stage of study. Kevlar or Twaron could also be considered for additional study, but Gore PTFE, Zylon, and Nomex should be dropped as base material candidates. If Gore PTFE is considered as an auxiliary material, a higher strength type of Gore PTFE should be tested. Nextel should be dropped as a candidate, with the possible exception of considering it for limited use in any rigid area where it is sandwiched between other materials. If some type of coating could be developed for Nextel that would make it more flex and abrasion resistant, its radiation resistance could be utilized.

(2) The simulated 10-yr total ionizing dose used for radiation exposure in this testing worked well, since it showed sensitivity differences in fabric candidates. In future radiation exposure testing, Vectran should be tested at a 30-yr total ionizing dose, if possible.

(3) Vectran and Twaron tested best in the standard abrasion test and should be tested to failure in the test. They also tested well in the JSC regolith simulant tumble abrasion test, but the duration was not long enough to draw final conclusions, so another tumble test of longer duration is recommended. Also, there is a question about the ability of the simulant (JSC-1) to behave as harshly as the actual material.

(4) Although Zylon showed superior tensile strength in general, it is not recommended for further consideration because of its inferior abrasion testing performance.

(5) Vectran appears to have high folding endurance; however, a higher number of cycles are recommended for the cryogenic folding test.

(6) More extensive hypervelocity impact testing is recommended for Vectran, the highest overall performer.

(7) At this point, a “demonstration article,” the one-piece lunar regolith bag garage prototype, is standing, on its own, in building 4493 at MSFC. The Project Office will decide whether it should remain as a demo, or whether to perform structural testing consisting of loading the structure with weights in certain locations to test its strength/integrity. Work to date indicates the validity of the theory that a regolith bag arch can behave in much the same manner as the classic masonry arch; however, only the first step has been taken to prove this theory; other steps are required.

(8) Before any continued laboratory work in this area, any high-level goal changes since this work began should be considered and the high-level schedule/plans should be studied to determine the timeframe during which a garage or habitat might be constructed on the lunar surface. There are many questions to be considered, such as, should early-on habitats be sub-surface?

(9) The merits/feasibility of various lunar habitat concepts should be considered and overall considerations should be examined to determine if it makes sense to pursue regolith bag garages or habitats.

(10) There should be discussion on what a "next phase" might look like—there are many possible approaches. Should this proceed in small increments or should several "angles" be considered at once?

(11) A materials testing program that investigates using multiple layers of fabric for the regolith bag pockets should be considered. For example, a two-layered structure, using Vectran and Twaron, or Kevlar might prove worthwhile. Or, a three-layered structure using Nextel sandwiched between two layers of Vectran could be considered.

(12) A materials testing program looking at Vectran as a single layer with various coatings should be considered.

(13) A materials testing program investigating the materials used in the sample prototype section that was produced by Techsphere, Inc. (fig.108) should be considered. This material consisted of Vectran laminated with a thin layer of aluminum foil. This was the material originally planned for constructing the prototype for this study, but the cost and lead-time were prohibitive.

Figure 108. Sample (foil over Vectran) prototype section produced by Techsphere, Inc.

(14) Types of customized blended fiber should be studied to determine what could be used to make a fabric tailored for this application.

(15) There should be further discussion about the simulated lunar environment to be used for testing materials and structures and ways to improve on procedures used in this work. Ideas for future testing environments should be discussed with personnel from the Project Office, the Natural Environments Branch, the Space Environmental Effects Team, the Environmental Test Facility, and others. The aim should be for increasingly higher fidelity lunar environment simulation.

(16) Before follow-on investigations, considerations for robotic construction of a regolith bag structure on the Moon should be discussed. Several issues to consider include:

(a) Should a regolith bag structure be composed of connected bags/pockets or of individual, separate bags? The connected bags provide stability to the structure that would be difficult to obtain using individual bags. On the other hand, handling the connected bags requires more effort and is perhaps less versatile as to what kind of structure that can be fabricated—particularly if the type of structure to build is changed on-site.

(b) As discussed in section 3 of this Technical Manual, the prototype was constructed by a sizable team of individuals. Construction of the fabric form (the part which would be done on Earth) is certainly doable. Filling the fabric form (the part which would be done on the Moon) required a team of about six persons working for about 15 hours, using the previously described equipment. Filling the bags with air before filling with vermiculite greatly facilitated assembly; however, if this technique is used on the lunar surface, the air would have to be brought from Earth. Refinements to the equipment and techniques used in this test will improve manufacturability; however, robotic assembly of this structure on the Moon will present challenges, although it is doable.

(17) Additional materials testing should be performed before a larger prototype is constructed.

(18) At some point in materials testing, either actual lunar regolith samples or a simulant, which provides the harshness/abrasiveness equivalent to the actual material, should be used.

(19) Regolith bag “blankets” which, in layers, could be used as temporary radiation shields should be considered.

(20) What equipment must be carried from Earth to the Moon to facilitate automated filling?

(21) Future prototypes on Earth should use a filling material that simulates both the texture and sharpness of regolith as well as its weight under lunar gravity. One suggestion would be a simulant made from something like JSC-1, combined with crushed, jagged glass, plus some other material to reach an overall lower weight.

(22) Using connected regolith bags as a component in a radiation protection system which rises above and covers a habitat system should be considered.

APPENDIX

MCP Award Winners
Environmental Design Requirements
September 9, 2005

Requirements and Assumptions:

Assume the mission will be in South Pole region of the Moon:

Exterior temperature range: -60° to -220°C

Exterior atmosphere: 10^{-12} torr vacuum

Assume radiation: See attached paper entitled "Lunar Radiation Environments for characterization of ISFR/Habitat Structures Materials," by J. I. Minow and R.L. Altstatt for further definition of radiation environment.

1. Ultraviolet
2. Ionizing radiation

Lifetime of habitat: 30 years

Table 15. Lunar Meteoroid Environment.

Diameter (cm)***	Mass (g)*	Flux (#/m^2*hr)**
0.01	5.24E-07	0.000150685
0.03	1.41E-05	5.70776E-06
0.05	6.55E-05	9.80251E-07
0.07	1.80E-04	2.90297E-07
0.1	5.24E-04	7.70548E-08
0.3	0.014	1.11621E-09
0.5	0.065	1.48973E-10
0.7	0.18	3.92237E-11
1	0.524	9.47831E-12
3	14.137	1.17009E-13
5	65.45	1.50799E-14
7	179.594	3.90639E-15

*Masses are computed assuming a meteoroid density of 1 g/cm^3
**Average velocity = 20 km/sec
***It should also be noted that even though the fluxes of the larger particles are quite small, many of them strike the lunar surface over the course of a year. For example, there are over 1200 lunar impacts by 7 cm diameter meteoroids each year.

REFERENCES

1. Brown, Sebrina; Kundberg, Kimberly; et al.: “Lunar Regolith Bagging System,” NASA—CR–86652; Georgia Institute of Technology and Universities Space Research Association; Atlanta, GA, March 1990.

2. Pope, Regina: “Regolithbag Report,” Qualis Corporation, Huntsville, AL, August 2005.

3. Kearney, Mark; and Meyers, Charles: “Regolith Bag Structures Analysis,” NASA Marshall Space-Flight Center Dynamics, Loads, and Strength Branch, Marshall Space Flight Center, AL, October 2005.

4. Schunk, Greg: “Preliminary Regolith Bag Lunar Habitat Thermal Study and Deliverable,” NASA Marshall Space Flight Center Spacecraft Thermal Team, Marshall Space Flight Center, November 2005.

5. Kaul, Raj; and Smithers, Gweneth: “Bagging Material Trade Study for Lunar Sandbag Habitat,” NASA Marshall Space Flight Center Nonmetals Engineering Branch, Marshall Space Flight Center, AL, June 2005.

6. Minow, J.I.; and Alstatt, R.L.; “Lunar Radiation Environments for Characterization of ISFR/Habit Structures Materials,” Unpublished Manuscript, 2005.

7. Heiken, G.H.; Vaniman, D.T.; and French, B.M. (eds.): *The Lunar Sourcebook: A User’s Guide to the Moon*, Cambridge University Press, Cambridge, England, 1991.

8. “3M Nextel Ceramic Textiles Technical Notebook.” <http://www.3m.com/ceramics/pdfs/Nextel_Tech_Notebook_11.04.pdf>, May, 2006.

9. Goodfellow Corporation Online Catalog. <http://www.goodfellow.com/csp/active/STATIC/A/Polyaramid_.HTML>, May, 2006.

10. W.L. Gore and Associates Online Catalog. <http://www.gore.com/MungoBlobs/rastex_weave_data-sheet.pdf>, May, 2006.

11. Azom.com, “The A to Z of Materials Supplier Data,” <http://www.azom.com/details.asp?Article ID=1992%20#_Background>, May, 2006.

12. “Vectra A®–Liquid Crystal Polyester,” <http://www.goodfellow.com/csp/active/gfMaterialInfo.csp?MATID=ES31#>, May, 2006.

13. Toyobo Company, LTD. Product Technical Information," <http://www.toyobo.co.jp/e/seihin/kc/pbo/technical.pdf>, May, 2006.

14. *1998 Annual Book of ASTM Standards: Section 7: Textiles*, American Society for Testing and Materials, Philadelphia, PA, 1998.

15. Minow, J.L.; Altstatt, R.L.; Blackwell, W.C., Jr.; and Harine, K.J.: "Radiation Environments for Lunar Programs," Science and Technology Applications Forum 2007, Albuquerque, NM, February 11–15, 2007.

16. Halbleib, J.A.; Kensek, R.P.; Valdez, G.D.; et al.: "ITS Version 3.0: The Integrated TIGER Series of Coupled Electron/Photon Monte Carlo Transport Codes," Technical Report SAND91–1634, Sandia National Laboratories, Albuquerque, NM, August 1993.

17. Zeigler, J.F.; et al.: "Stopping Range of Ions in Matter–SRIM 2003, <http://www.srim.org/#SRIM>, May, 2006.

18. Finckenor, M.M.; Edwards, D.L.; Vaughn, J.A.; et al.: "Test and Analysis Capabilities of the Space Environment Effects Team at Marshall Space Flight Center," NASA—TP–2002–212076, Marshall Space Flight Center, AL, November 2002.

19. Kosmo, J.J.: "Resistance Screening of Candidate Materials by Tumbler Test," NASA, Johnson Space Center, Houston, TX, July 2005.

20. Hovater, M.: "Micro Light Gas Gun," NASA-SOP-EM50-OWI-029, Marshall Space Flight Center, AL, February 2005.

21. Stellingwerf, R.F.: "SPHC Smooth Particle Hydrodynamics Code–Version 7.64: Problem Setup Guide: Input File Setup," Stellingwerf Consulting–Complex Systems Analysis, Huntsville, AL, October 2005.

22. Stellingwerf, R.F.: "SPHC Smooth Particle Hydrodynamics Code–Version 7.64: User Guide," Stellingwerf Consulting–Complex Systems Analysis, Huntsville, AL, November 2005.

23 Heyman, J.: *The Masonry Arch*, 118 pp., Halsted Press, New York, NY, 1982.

REPORT DOCUMENTATION PAGE

Form Approved
OMB No. 0704-0188

1. AGENCY USE ONLY *(Leave Blank)*	2. REPORT DATE	3. REPORT TYPE AND DATES COVERED
	September 2007	Technical Memoradum

4. TITLE AND SUBTITLE

A One-Piece Lunar Regolith Bag Garage Prototype

5. FUNDING NUMBERS

6. AUTHORS

G.A. Smithers, M.K. Nehls, M.A. Hovater, S.W. Evans, *J.S. Miller, **R.M. Broughton, Jr., **D. Beale, and **F. Kilinc-Balci

7. PERFORMING ORGANIZATION NAME(S) AND ADDRESS(ES)

George C. Marshall Space Flight Center
Marshall Space Flight Center, AL 35812

8. PERFORMING ORGANIZATION REPORT NUMBER

M–1199

9. SPONSORING/MONITORING AGENCY NAME(S) AND ADDRESS(ES)

National Aeronautics and Space Administration
Washington, DC 20546–0001

10. SPONSORING/MONITORING AGENCY REPORT NUMBER

NASA/TM—2007–215073

11. SUPPLEMENTARY NOTES

Prepared by the Materials and Processes Laboratory, *Qualis Corporation, Huntsville, AL, and **Auburn University, Auburn, AL

12a. DISTRIBUTION/AVAILABILITY STATEMENT

Unclassified-Unlimited
Subject Category 14
Availability: NASA CASI 301–621–0390

12b. DISTRIBUTION CODE

13. ABSTRACT *(Maximum 200 words)*

Shelter structures on the moon, even in early phases of exploration, should incorporate lunar materials as much as possible. This Technical Memorandum details the design and construction of a prototype for a one-piece regolith bag unpressurized garage concept and a materials testing program to investigate six candidate fabrics to learn how they might perform in the lunar environment. The conceptualization was that a lightweight fabric form be launched from Earth and landed on the lunar surface to be robotically filled with raw lunar regolith. Regolith bag fabric candidates included: Vectran™, Nextel™, Gore PTFE Fabric™, Zylon™, Twaron™, and Nomex™. Tensile (including post radiation exposure), fold, abrasion, and hypervelocity impact testing were performed under ambient conditions, and also performed under cold and elevated temperatures. In some cases, Johnson Space Center lunar simulant (JSC-1) was used in conjunction with testing.

A series of preliminary structures was constructed during final prototype design based on the principles of the classic masonry arch. The prototype was constructed of Kevlar™ and filled with vermiculite. The structure is free-standing, but has not yet been load tested. Future plans would be to construct higher fidelity prototyes and to conduct appropriate tests of the structure.

14. SUBJECT TERMS

lunar structures/construction, lunar regolith utilization, materials resistance to lunar environment, in situ materials for lunar base construction, regolith bags, lunar sand bags, materials testing for the lunar environment, lunar garage prototype

15. NUMBER OF PAGES

92

16. PRICE CODE

17. SECURITY CLASSIFICATION OF REPORT	18. SECURITY CLASSIFICATION OF THIS PAGE	19. SECURITY CLASSIFICATION OF ABSTRACT	20. LIMITATION OF ABSTRACT
Unclassified	Unclassified	Unclassified	Unlimited

National Aeronautics and
Space Administration
IS20
George C. Marshall Space Flight Center
Marshall Space Flight Center, Alabama
35812